UNIVERSITÉ DU QUÉBEC

MÉMOIRE PRÉSENTÉ À
L'UNIVERSITÉ DU QUÉBEC À TROIS-RIVIÈRES

COMME EXIGENCE PARTIELLE DE LA
MAÎTRISE EN GÉNIE ÉLECTRIQUE

PAR
DANIEL FELIPE HERRERA VEGA

ANALYSE ÉLECTROTHERMIQUE EFFICACE, ESTIMATION DE L'ÉNERGIE RÉSIDUELLE ET DU TEMPS DE DÉCHARGE POUR UNE BATTERIE LI-ION À DES TEMPÉRATURES INFÉRIEURES À ZÉRO DEGRÉ CELSIUS

NOVEMBRE 2016

UNIVERSITY OF QUEBEC

MEMORY PRESENTED AT
UNIVERSITY OF QUEBEC AT TROIS-RIVIERES

AS PARTIAL FULFILLMENT OF THE
MASTER IN ELECTRICAL ENGINEERING

BY
DANIEL FELIPE HERRERA VEGA

EFFICIENT ELECTROTHERMAL ANALYSIS, RESIDUAL ENERGY AND DISCHARGE TIME ESTIMATION FOR A LI-ION BATTERY IN TEMPERATURES BELOW ZERO DEGREE CELSIUS

NOVEMBER 2016

Résumé

L'électrification des transports présente notamment des avantages en termes d'émissions polluantes (gaz à effet de serre et particules) vis-à-vis des véhicules conventionnels, mus uniquement par un moteur à combustion interne. Cependant, la localisation des véhicules électriques hybrides (Hybrid Electric Vehicles - HEVs) et des véhicules électriques à batterie (Battery Electric Vehicles - BEVs) dans les systèmes de transport, pour les zones géographiques où la saison d'hiver est extrêmement longue et froide, nécessite le développement de méthodes d'estimation fiables et efficaces de l'énergie et du temps de décharge.

La température d'opération est un facteur clef pour les performances de tous dispositifs électrochimiques. La quantité d'énergie servant à propulser le BEV dépend directement de leur température d'opération (en particulier à températures inférieures à 0°C). De plus, les basses températures ont une influence sur la variation de la résistance ohmique de la batterie, du telles variations conduisent à une réduction de la puissance délivrée, ainsi que de l'énergie disponible. Dans les environnements où la température est très faible, les batteries doivent atteindre leurs conditions de fonctionnement normal dans le plus bref délai afin de maintenir ses performances optimales.

Avant de penser à la façon de prévenir la formation de glace sur la batterie lorsque la batterie est exposée à des températures négatives, il est important, dans un premier temps, de bien comprendre le comportement de la batterie et de déterminer, d'une façon fiable, la quantité d'énergie disponible lors de son utilisation. Dans les applications réelles, les constructeurs automobiles prennent des mesures préventives en actionnant les mécanismes de démarrage du véhicule : généralement, il s'agit d'un système de chauffage de la batterie qui

minimise sa dégradation. Toutefois, cette solution ne fournit pas une possibilité d'estimer la quantité d'énergie consommée dans la phase de démarrage ni la quantité d'énergie disponible à la propulsion du véhicule. Dans la plupart des cas, telle estimation se fait en utilisant des tables de consultation. Nous soulignons la nécessité d'étudier le comportement thermique des batteries Li-ion dans des conditions hivernales. Des techniques, à la fois simples et efficaces, capables d'estimer l'énergie résiduelle devraient être considérées pour augmenter ainsi la capacité et la durée de vie de la batterie. Il est également nécessaire de développer du méthodes servant à une meilleure estimation du temps de décharge de la batterie ; cette valeur servira comme référence à l'utilisateur sur la quantité d'énergie qui peut être extraite.

À partir de la problématique identifiée précédemment, l'objectif principal de ce travail de recherche est d'accroître l'efficacité énergétique d'une batterie Li-ion et de permettre au système et à l'utilisateur d'avoir une prise en compte de la consommation d'énergie de la batterie lorsque le véhicule électrique est exposé à des conditions de basse température (allant de 0 °C à -40 °C), ce qui se traduira par une augmentation de la durée de vie de la batterie. Dans ce contexte, les contributions apportées s'articulent autour des points suivants :

- L'instrumentation et la mise en œuvre d'une stratégie pour l'étude des performances des batteries en conditions hivernales : cette stratégie prévoit une méthode qui combine les équations thermiques et électriques régissant le modèle, l'impact de la température extérieure sur les performances de l'ensemble de cellules, et les contraintes opérationnelles imposées par le système de gestion de l'énergie de la batterie au Li-ion. Par ailleurs, les phénomènes d'échange de chaleur qui se produisent au niveau des cellules du batterie seront pris en compte pour augmenter la performance de l'algorithme d'estimation d'énergie ;

- Le développement d'une méthode simple qui favorise l'identification des paramètres du modèle de la batterie au Li-ion (résistance interne, chaleur spécifique, capacité calorifique massique) à partir de la mesure de la tension en circuit ouvert tout au long du cycle de fonctionnement. L'intérêt d'une telle méthode réside dans la possibilité d'effectuer

une gestion de l'énergie dans la batterie lors du démarrage à froid du véhicule électrique ;

- La conception de deux méthodes permettant l'estimation de l'énergie résiduelle de la batterie. Il est à souligner qu'une méthode doit faciliter le traitement des données en temps réel ;

- Le développement d'un algorithme qui permet l'estimation en ligne du temps de décharge de la batterie. Ceci prend une importance particulière au moment où le courant de décharge n'est pas constant et l'amplitude du courant moyen varie au fil du temps.

La méthodologie suivie tout au long de ce travail se déroulera en six étapes de la façon suivante :

Configuration du banc d'essai :

Le banc d'essai est composé d'une charge électronique pilotable permettant la décharge de la batterie sur plusieurs profils de conduite ; une source d'alimentation permettant la charge de la batterie ; une chambre de refroidissement dédiée à la régulation en température de la batterie (de 0 °C à -40 °C) ; un système d'acquisition "National Instruments DAQ system" et un logiciel de commande développé sous "LabVIEW". Ce logiciel permet aussi de contrôler la charge électronique et d'afficher et enregistrer les paramètres tels que la température, le courant et la tension.

L'ensemble des cellules de la batterie Li-ion est construit par CrossChasm pour sa motoneige électrique et utilisé pour des études de recherche sur l'environnement à la Fondation nationale pour la science des États-Unis "Summit Station" au Groenland. L'ensemble comprend dix cellules raccordées électriquement en série fabriquées par la société allemande "GAIA Advanced Battery Systems" et les cellules sont classifiées en Amérique du Nord comme "MIL SPEC" (grade militaire).

Caractérisation de la batterie Li-ion :

La caractérisation a été étudiée en décharge et un profil spécifique a été fixé pour la charge avec son correspondant de température ambiante optimale. Des essais à différents courants constants (50 A, 125 A et 200 A) et à différentes températures (24 °C et de 0 à -30 °C) ont été menés pour décharger la batterie. L'estimation de l'énergie résiduelle au cours de la décharge et à très basse température constitue une originalité majeure de ce projet de recherche. Cet aspect est souvent négligé, mais s'avère crucial pour l'autonomie des véhicules électriques. En outre, la décharge sous cette température constitue un défi technologique clairement identifié par le Département de l'Énergie des États-Unis. Toutes ces expériences ont été réalisées au niveau de l'ensemble de cellules. Cette étape de la méthodologie nous a permis de cartographier l'énergie de la batterie au Li-ion dans des conditions hivernales tout en permettant de comprendre la sévérité des dégradations de performances jusqu'à la fin de l'estimation du temps de décharge.

Conception du modèle électrothermique :

L'étude d'un modèle électrothermique, présenté au troisième chapitre, comprend les contraintes du projet. À ce stade, toute représentation mathématique contenant les principes électriques et thermodynamiques a été exprimée afin de définir les équations et leurs variables. Le lien entre les équations électriques et thermiques issues des paramètres tels que la tension de circuit ouvert, la masse thermique, la chaleur spécifique, la capacité calorifique de la batterie sera établi.

Estimation de l'énergie résiduelle :

Cette phase a eu pour objectif principal d'identifier la quantité d'énergie résiduelle dans la batterie au Li-ion en utilisant deux méthodes d'estimation : d'une part en appliquant un algorithme d'apprentissage par réseaux de neurones artificiels (Artificial Neural Networks - ANN) et d'autre part en appliquant une méthode directe qui permet l'estimation en temps

réel. La méthode directe a été utilisée comme une base pour l'apprentissage du réseau de neurones. L'ANN a eu en entrée les valeurs de la tension et de la température et en sortie les courbes d'énergie prises lors de la caractérisation de la batterie.

Estimation du temps de décharge final :

À partir du modèle électrothermique précédemment défini et de l'estimation de l'énergie résiduelle de la batterie, un algorithme pour estimer le temps de décharge a été mis en œuvre. En effet, cela nous a permis de savoir combien de temps de conduite reste avant que la batterie soit complètement déchargée. L'algorithme développé doit être capable de fonctionner en temps réel en tenant compte les paramètres de fonctionnement du véhicule électrique (tels que le voltage, le courant, la température, l'estimation de l'énergie résiduelle) et en utilisant un minimum de ressources informatiques pour exécuter chaque tâche. En sus de ce qui précède, il convient de prendre en considération les restrictions suivantes : (i) la quantité d'énergie disponible déterminée par la méthode d'estimation de l'énergie résiduelle doit être respectée ; (ii) la durée pendant laquelle le véhicule électrique est arrêté et hors tension sera préalablement défini par l'utilisateur et doit être respectée ; et (iii) le système de contrôle thermique doit s'adapter en permanence à la valeur de la température ambiante.

Validation expérimentale :

Chaque étape de la méthodologie proposée a été évaluée expérimentalement au sein de l'Institut de Recherche sur l'Hydrogène afin de vérifier les résultats du calcul et de valider l'exactitude des algorithmes quant à l'estimation du temps de décharge.

Après avoir exposé la méthodologie de ce travail de recherche, nous listons les résultats obtenus comme suit :

La Figure 2.5 présente les résultats obtenus lors de la caractérisation de la décharge de la batterie. À partir de ces résultats, nous pouvons observer une tendance similaire dans le

comportement de la tension et de la température des cellules, et pourtant, il a été possible de présenter la valeur de la température d'une cellule et la tension totale de la batterie comme référence pour tous les résultats obtenus au cours de ce travail.

La Figure 2.8 nous présente le comportement de la batterie lors de sa caractérisation dans des conditions de basse température. Une chambre de refroidissement a été mise en place pour simuler les différentes conditions de température ambiante. Des essais expérimentaux, à trois valeurs différentes de courant constant, ont été menés pour comparer l'effet de la température ambiante par rapport à l'effet de l'augmentation du courant sur la batterie, voir Figure 2.9. Nous pouvons observer qu'il existe une forte influence de l'amplitude de courant sur le temps de décharge de la batterie, cependant l'effet de la température s'avère négligeable. En outre, la Figure 2.9 nous montre une chute de tension, ceci est provoqué par le comportement de la résistance interne de la batterie, qui a subi une forte augmentation de sa valeur due aux basses températures. Également, les tensions de fonctionnement sont réduites du fait qu'un environnement froid allonge la diffusivité de Li+ dans la cellule.

La comparaison du delta de température (ΔT) devient un point fort, car il permet de comprendre le comportement de la température dans la batterie, ce qui pourrait être utile pour résoudre le problème du démarrage à froid. Par exemple, une amplitude de courant de décharge élevée peut être appliquée pour réchauffer les cellules. Cependant, l'étude du comportement au courant de grande amplitude doit être prise en considération vis-a-vis d'une accélération de la dégradation des cellules et une réduction de la durée de vie de la batterie.

La Figure 3.2 présente le modèle électrothermique. L'estimation des paramètres telles que la résistance interne, la chaleur spécifique et le coefficient de chaleur convective de la batterie se font grâce à la mesure de la tension en circuit ouvert au fil du temps. La tension en circuit ouvert a été présentée sur la Figure 3.5 et le tableau 3.2 regroupe les résultats de chaleur convective multiplié par la surface de la batterie.

La Figure 3.6 nous présente l'estimation de la chaleur spécifique et la résistance interne de la batterie. Après avoir estimé ces paramètres, nous avons obtenu des résultats semblables

à la littérature.

Une méthode a été présentée pour obtenir l'énergie résiduelle de la batterie. Pour ce faire, nous avons pris en considération les pertes thermiques lorsqu'on effectue l'estimation de l'énergie, voir le Tableau 3.3 et la Figure 3.8. Cela nous a permis d'avoir une approximation plus précise de l'énergie résiduelle par rapport à l'estimation obtenue par un simple comptage de Coulomb.

Un réseau de neurones artificiels a été développé en fonction de la température et de la tension. L'énergie résiduelle estimée précédemment pour certaines températures ambiantes a été utilisée comme sortie du réseau de neurones. Comme prévu, l'ANN nous a permis de généraliser et de calculer l'énergie résiduelle de la batterie pour chaque entrée de données de tension et de température, voir la Figure 3.12. Les résultats nous montrent une bonne convergence, la marge d'erreur quadratique moyenne est acceptable, aussi bien que les régresseurs qui s'approximent vers 1, voir la Figure 3.13.

L'algorithme d'estimation du temps de décharge final (End Of Discharge - EOD) a été présenté et mis en œuvre. Ceci en reliant la variation du courant et de l'énergie résiduelle finale. Les résultats obtenus grâce à la méthode proposée ont été satisfaisants, l'erreur relative est faible entre la mesure réelle et l'estimation du temps EOD, voir la Figure 3.18.

Pour conclure, dans ce travail nous avons proposé une méthode servant à augmenter l'efficacité énergétique d'une batterie au Li-ion lorsque le véhicule électrique est exposé à des conditions de basse température. Plus précisément, cette méthode permet au système et à l'utilisateur d'avoir une meilleure prise en compte de la quantité d'énergie consommée et du temps restant avant que la batterie se décharge complètement, ce qui à la fin se reflète dans une amélioration de sa durée de vie.

En résumé, les principales contributions peuvent être énumérées comme suit : (i) afin de déterminer la résistance interne, la chaleur spécifique et la capacité calorifique de la batterie au Li-ion, un modèle simple intégrant les équations thermiques et électriques régissant son comportement a été développé et analysé, tout en mesurant la tension de circuit ouvert au fil

du temps ; (ii) deux méthodes permettant d'estimer la quantité d'énergie résiduelle dans la batterie ont été développées. L'impact de la température ambiante sur l'évolution thermique de l'ensemble des batteries a été considéré, aussi bien que les contraintes d'opération imposée pour le système de gestion ; et (iii) la conception d'un algorithme qui permet l'estimation en ligne du temps restant avant la décharge totale de la batterie a été mise en œuvre.

Mots clés : Batteries au lithium, analyse thermique, stockage d'énergie, gestion d'énergie, estimation de l'énergie résiduelle, réseaux de neurones artificiels, temps final de décharge.

Abstract

The electrification of transportation presents particular benefits in terms of emissions (greenhouse gases and particles) compared to conventional vehicles powered by internal combustion engines.

The operating temperature is a key factor for the performance of all electrochemical devices. The amount of energy that can be extracted from batteries depends directly on their operating temperature (especially in extremely low temperatures) and it becomes necessary to provide an electrothermal model that do not requires a huge quantity of computational resources to run. In addition, it is also necessary to provide a method that allows to estimate the amount of energy extracted from the battery and the quantity of time left before the battery is fully discharged. This helps to seek a better understanding of the battery's degradation under low temperature conditions.

The project itself will be divided into six phases: first, the instrumentation of a battery pack and its test bench; second, the characterization and study of the battery's performance in winter conditions with different discharge currents; third, the identification of an electrothermal model of the battery with its corresponding parameters estimation; fourth, the estimation of the residual energy in the battery by using a direct method and a trained method; fifth, the end of discharge time estimation by relating the variance of the current and the final residual energy in the battery; and sixth, the experimental validation.

The characterization will be studied in discharge and will be set a specific profile for the charge with its correspondent optimal ambient temperature. Tests at different currents (50A, 125A and 200A) and different temperatures (+24 °C to -30 °C) will be carried out to

discharge the battery. The estimation of residual energy during the discharge in very low temperatures is a major originality of the project. This aspect is often overlooked but is crucial for electric vehicles' autonomy. The consideration of these multi-physical interactions represents a major technological challenge. Furthermore, discharging under this temperatures is a technological challenge clearly identified by the US Department Of Energy. All these experiments will be performed with a pack and not a single cell. In conclusion, this work will map the battery's energy in winter conditions while helping to understand the severity of the degradation through the end of discharge time estimation.

Keywords: Lithium batteries, Energy management, Energy storage, Energy consumption, Residual Energy, Artificial neural networks, Feedforward neural networks, Thermal analysis, Resistance, Thermal resistance, Temperature, End Of Discharge time.

Acknowledgments

First, I would like to thank my director, Professor Loïc Boulon, for his comments and constructive criticisms at different stages of my research, they helped me focus my ideas and I am grateful to him for holding me to a high research standard and enforcing strict validations for each research result.

I want to thank my co-director, Professor Sousso Kelouwani, for his priceless contributions to make this work possible. He encourages and guides his students to meet high standards. I am indebted to him for his continuous encouragement and guidance. His patience and support helped me overcome many crisis situations and allowed me to finish this work.

I am grateful to Professors Y. Dubé, D. Massicotte, M. Doumbia and A. Skorek for their encouragement and practical advice. I also want to thank to all my colleagues at the Hydrogen Research Institute for the nice working environment and all the different good times shared.

Thanks to my friends during my master studies at Trois-Rivières, for the tons of fun during this years, special thanks to my friends Julien, his family and Antonella for the movies, drinks, dinners, the night time deep talks and all great times they shared with me, and huge thanks to Elvira for your patience, the several contributions to my work and overall thank you for the million of great times during this years.

Last but not the least, I would like to thank my family: my parents Hugo and Judith, my brother Sebastian and my cousin Bibiana. Mom, as many battles we have fought side by side, this is one that I dedicate you completely and for what I want to thank you greatly, thanks for never let me down.

Contents

List of Tables

List of Figures

List of Symbols

Abbreviations

Description	Symbol
Artificial Neural Network	ANN
Battery Electric Vehicle	BEV
Battery Management System	BMS
Data Acquisition	DAQ
Dynamic Electronic Load	DL
Electric Vehicle	EV
End of Discharge	EOD
Feed-foeward back-propagation network	FBN
Final Residual Energy	FRE
Gasoline Vehicle	GV
Greenhouse Gas	GHG
High amplitude current	HAC
Hybrid Electric Vehicle	HEV
Internal Combustion Engine	ICE
Levenberg-Marquardt Algorithm	LMA
Low amplitude current	LAC
Mean Squared Error	MSE
Medium amplitude current	MAC
Particle Filtering	PF
Plug-in Hybrid Electric Vehicle	PHEV
Power Electronic Source	PS
Residual Energy	RE
Snowmobile Current Profile	SCP
State of Charge	SOC
State of Health	SOH

Greek Letters

Description	Symbol
Characteristic length of the geometry	α
Coefficient of volume expansion	β
Kinematics viscosity of the fluid	υ
Mean value	μ
Thermal relation	τ

List of Symbols (Continued...)
Roman Letters

Description	Symbol
Ampere	A
Capacity	C
Carbon Dioxide	CO_2
Cents of a U.S. Dollar	¢
Degrees Celsius	°C
Degrees Fahrenheit	°F
Degrees Kelvin	K
Energy	*W*
Kilogram	kg
Kilometer	km
Lead-Acid	Pb-acid
Lithium	Li
Lithium-ion	Li-ion
Minutes	min
Nickel-Cadmium	NiCd
Nickel-Metal Hydride	NiMH
Prandtl number	Pr
Seconds	s
Sodium	Na
Volt	V
Watt	W

Chapter 1

Introduction

Low temperatures always have been a big challenge for any type of electrical and electronic equipment. The exposure of electric vehicles to this harsh condition is not an exception, especially in the Canadian weather. The components of vehicles tend to change their normal behavior in relation with optimal temperature conditions[1]. One important component that is basically the heart of electric vehicles is the battery. This component goes through huge chemical reactions in order to provide the energy requested by the vehicle. But, how important is the effect of the temperature in this component? Is it possible to know when is it going to be discharged after being exposed to low temperatures? This last question gets high importance due to constant problematic of cold start of electric vehicles.

In order to solve this questions, it is necessary to have a solid and well defined basis for the entire project. All work covered in this document is conveniently presented in chapters and its corresponding subsections. This first Chapter will determine the general basis of the research subject, the problematic, objectives and methodology on which the main work is supported.

[1] In this document, the optimal or ideal temperature condition is defined by the manufacturer of each component. It is usually a temperature between 15°C and 30°C.

1.1 Context

Human being activities largely causes climate change to occur, which is a significant risk for a board range of human and natural systems. Over the past several decades research efforts have being increasing to provide a wealth of information to decision makers about the known problems and potential risks posed by climate change. It is not just necessary to have enough research to support strategies for limiting climate change, but also, effective information and decision-support systems that can contribute to improved understanding and more effective decision making flexible enough to identify and pursue emerging research challenges [10].

Currently, the transportation sector represents a very significant percentage of the total greenhouse gas (GHG) that is emitted globally. As can be seen in Table 1.1, just in Canada for 2012 transportation sector represents almost 24 % of total GHG emissions. Also, almost 28 % of U.S. GHG emissions can be attributed to the transportation sector, with the overwhelming share in the form of CO_2 emitted from combustion of petroleum-based fuels. The transportation sector also emits other pollutants that endanger human health. The transportation sector thus stands at the nexus of climate change, human health and economic

Table 1.1: Canada GHG emissions 1990-2012, by economic sector [1]

Greenhouse Gases	**1990**	**2000**	**2005**	**2008**	**2009**	**2010**	**2011**	**2012**
				Mt CO_2 **equivalent§**				
NATIONAL GHG TOTAL	**591**	**721**	**736**	**731**	**689**	**699**	**701**	**699**
Oil and Gas	101	151	159	162	161	163	164	173
Electricity	94	129	121	113	97	99	92	86
Transportation	128	155	168	166	163	167	166	165
Emissions Intensive and Trade Exposed Industries†	95	92	89	88	75	76	80	78
Buildings	70	82	84	84	82	79	85	80
Agriculture	54	66	68	71	66	68	67	69
Waste and Others‡	48	46	47	48	45	46	47	47

† The Emissions Intensive and Trade Exposed Industries represent emissions arising from non oil and gas mining activities, smelting and refining, and the production and processing of industrial goods such as paper or cement.

‡ "Others" includes coal production, light manufacturing, construction and forest resources.

Note: Totals may not add up due to rounding.

Estimates presented here are under continual improvement. Historical emissions may be changed in future publications as new data become available and methods and models are refined and improved.

§ *Mt* CO_2 equivalent, i.e. Million metric tons of carbon dioxide equivalent is a measure used to compare the emissions from various greenhouse gases based upon their global warming potential.

growth [11].

In order to electrify transportation it is necessary to understand the types of existent technologies that are being currently in use or in research state and briefly understand what is the difference between them and in that way to start seeking what could be the technical or economical problematic to be solved. Two big technology alternatives to petroleum-fueled internal combustion vehicles are the biofuel vehicles and electrical vehicles. The second technology is the one in which this document is going to be focused.

Biofuel vehicles are basically vehicles that uses bioethanol or biodiesel as a fuel and this fuel is produced from plant materials or other forms of biomass. Despite that this technology is already widely used in nations worldwide, there are two big reasons why it can be said that this technology is not a really good option for replacing the petroleum-fuels: First, analysis that looks at GHG levels emitted along the biofuel production chain reveals that CO_2 emission has no reduction relative to petrol and diesel production and actually emissions levels will rise; Second, in land matters biofuel crop growth spells economic and environmental disaster, because not only will the earth run out of food to eat, but cutting down forests that act as carbon purifiers will exacerbate climate change [12].

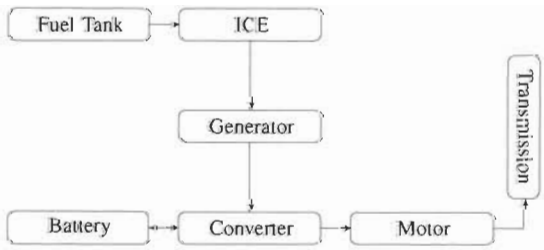

(a) Series HEVs

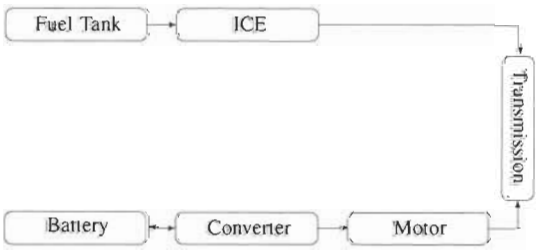

(b) Parallel HEVs

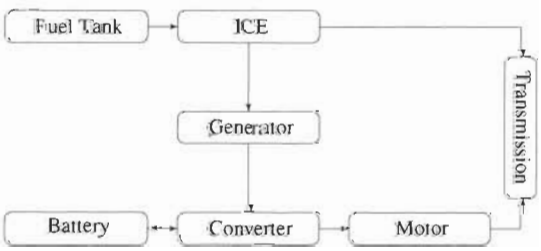

(c) Complex HEVs

Figure 1.1: HEVs configurations [6]

In the other hand, electric vehicles (EVs) are a really good alternative when it comes to CO_2 reductions since they consume a little bit of fuels or in some cases nothing, depending in the type of electric vehicle. EVs use electric motors to obtain propulsion and there are three main different types of EVs: First, there are Hybrid Electric Vehicles (HEVs) that have both an internal combustion engine (ICE) and an electric motor for propulsion, which can be configured in series, parallel or both series/parallel, as it can be seen in Figures 1.1a, 1.1b and 1.1c respectively. In this vehicles the battery is recharged by conversion of breaking energy; Second, there are Plug-in Hybrid Electric Vehicles (PHEVs) that are like the HEVs but the only difference is that the battery can be recharged by external power sources; and Third, Battery Electric Vehicles (BEVs) that have only electric propulsion and a rechargeable battery pack [13] that can be recharged by conversion of breaking energy and/or by external power sources.

To understand more deeply the BEVs, in [2] can be found an introduction of how BEVs work and it explains their basic configuration as shown in Figure 1.2. Through that article are also explained the four types of batteries commonly used in EVs with some of its technical specifications, like the ones shown in Table 1.2 and a deeper overview of the four types of Lithium-ion (Li-ion) batteries that exists.

The use of EVs brings a lot more advantages than just GHG emissions reduction, for instance money expenses reduction due to lower or zero fuel consumption through time.

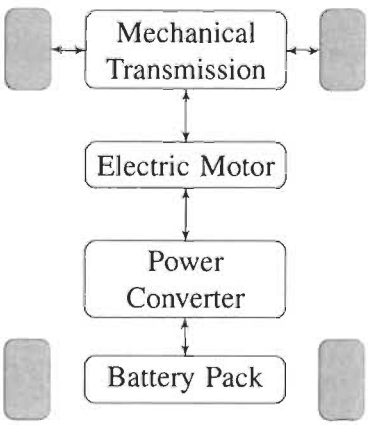

Figure 1.2: BEVs configuration [2]

Table 1.2: Basic technical performance of batteries used in EVs [2]

Battery Type	Lead-acid	Ni-Cd	Ni-MH	Li-ion
Energy Density† ($W \cdot kg^{-1}$)	30-50	45-80	60-120	110-160
Power Density‡	180	150	250-1000	1800
Nominal Voltage	2 V	1.25 V	1.25 V	3.6 V
Overcharge Tolerance	High	Moderate	Low	Very Low
Self Discharge	Low	Moderate	High	Very Low
Operating Temperature	-20 °C to 60 °C	-40 °C to 60 °C	-20 °C to 60 °C	-20 °C to 60 °C
Cycle Life§	200-300	1500	300-500	500-1000

† Chargeable electric energy per weight of battery pack
‡ Proportion of dischargeable electric energy to charged energy
§ The number of charging/discharging cycles in battery's entire life

With this kind of advantages it is necessary to have a huge support from companies to start spreading EVs into the market and a clear view of this are research and development companies. At beginning of 2014 the company FleetCarma took it a few steps further. They made an analysis focused not on the differences within electric vehicle models, but the differences between electric and gasoline vehicles as ambient temperature drops. They looked through FleetCarma's real world database to find out how much the fuel economy of each vehicle changes under freezing temperatures [3].

Figure 1.3 shows the average range reduction for electric and gasoline vehicles due to temperature decrease. When ambient temperature decreases the actively heating components

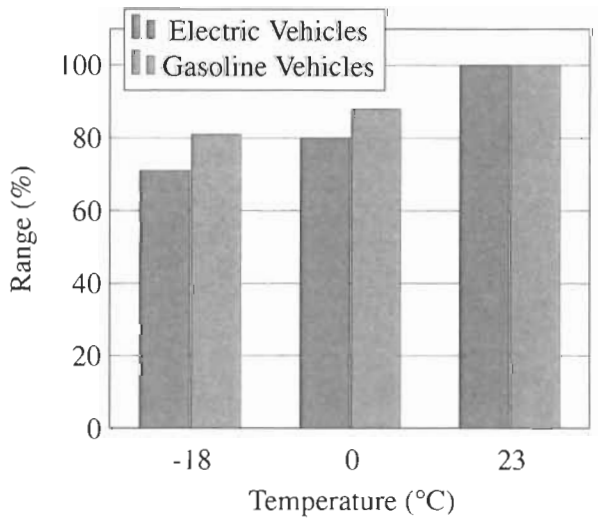

Figure 1.3: Average range reduction - FleetCarma [3]

Table 1.3: Energy cost savings - FleetCarma [3]

	ELECTRICITY COST PER MILE	GASOLINE COST PER MILE	ELECTRIC SAVINGS†
73 °F / 23 °C	2.6¢	15.0¢	12.4¢
32 °F / 0 °C	3.3¢	17.2¢	13.9¢
0 °F / -18 °C	3.8¢	18.6¢	14.8¢

† Per mile averages

are started, like the battery heater for instance, which produces more energy expenditure and hence there is a reduce of range for the vehicles. This figure shows an average range reduction of 19 % for gasoline vehicles (GVs) and 29 % for EVs when ambient temperature drops from 23 °C to -18 °C and when it drops from 23 °C to 0 °C there is an average range reduction of 12 % for GVs and 20 % for EVs. The big gain for electric vehicles can be seen in energy costs savings, for instance, in Table 1.3 is emphasized how EVs payback improves at lower temperatures, making of it very attractive for the market.

Other companies like Hydro Quebec had a major initiative in the roll out of charging infrastructure needed to support the arrival of plug-in vehicles with the project "The Electric Circuit", the largest public charging network for EVs in Quebec. Also, they announced the addition of Quebec's first 400 V fast charge station. The charging station is installed at a restaurant on Rue Albanel, Boucherville, is accessible to drivers of all-electric vehicles with quick-charging capability. With ideal charging conditions[2], a fast charge to 80 % of battery capacity will take only about 30 minutes for each one of the BEVs. With cold temperatures during the winter, it can take significantly longer to charge an EV at a charging station of 400 V, unlike a 240 V station, which is not affected by ambient temperature.

Hydro-Quebec's Boucherville pilot project was Canada's largest field test of BEVs. It was conducted in collaboration with the City of Boucherville and Mitsubishi Canada. As a result of this project they find out that the range is strongly related to ambient temperature and it can be 40 % less in winter. So it can be said that energy consumption depends greatly

[2] Ideal charging conditions are: a mild temperature of 15 °C to 25 °C and a low initial charge.

on ambient temperature[3] [14–16].

To have a wider view of the huge effort that companies are making to spread EVs is necessary to show a qualitative idea of how popular EVs have become and how EVs have been spreading through the market, the Table B.1 in the Annexe B shows a survey of EVs on the market. This table is organized by the year in which the EV was released into the market for first time and it shows that for recent years there is a high tendency to use Li-ion batteries in EV applications. Simply Because, as explained in [17], lithium is the metal with the highest negative potential and lowest atomic weight, batteries using lithium have the greatest potential for attaining the technological breakthrough that will provide EVs with the greatest performance characteristics in terms of acceleration and range. Each manufacturer creates its own Li-ion battery packs and they configure the cells of the pack in series, parallel or as usually seen, their own series-parallel configuration.

This table also let us know how Li-ion batteries play an important roll to be considered as domain of research to be widely studied not only in optimal atmospheric conditions, but also in extreme weather conditions to guarantee the best performance of EVs at all times.

As it was said before and as it will be seen in the subsequent chapters, this work will be focused in studying the behavior of Li-ion batteries for EVs when the vehicle is exposed to an ambient temperature below zero degrees Celsius and in the next section will be itemized the problematic to be studied.

1.2 Problematic

The literature tells us that the characteristics of performance in Li-ion batteries are sensitive to the cell operating temperature. The recoverable power and capacity can be reduced significantly when batteries are operated or stored at low temperatures [18]. These low temperatures also lead to variate the ohmic resistance that reduce the deliverable power and the extractable energy is significantly reduced. For example, in [19] was discussed that poor

[3] In average between 13 and 24 $kWh \cdot 100km^{-1}$, depending on the month.

performance of Li-ion batteries at low temperatures is linked to poor charge transfer at the electrode/electrolyte interface. Hence, it is imperative that Li-ion batteries used in BEVs and HEVs applications be held at temperatures below 50 °C but rapidly heated or self-heated through cycling between acceptable limits prior to operating at cold temperatures. In cold temperature environments, batteries must be heated rapidly to improve both cycle life and energy extraction.

Research in thermal issues for Li-ion battery need further exploration. New, simple and efficient techniques of energy estimation should be considered to limit capacity fade due to cold storage. Temperature control to improve performance and better discharge time estimation to have a reference in how to increase the amount of energy that can be extracted.

The location of HEVs and BEVs in transport systems for geographic areas where winter season is extremely long and cold (Quebec climate for example, see Table 1.4), requires the development of reliable and efficient estimation methods for energy and discharge time to reduce the risk of irreversible damage of the battery.

Indeed, exposure of the battery to temperatures below zero degrees for a considerable period of time without operation will cause that the internal temperature of the battery gets down slowly or quickly depending on the characteristics of thermal insulation layers implanted on it. Previews work have proved that convective heating requires the least heating time, while mutual pulse heating can consume the least battery capacity. Mutual pulse heating has the additional advantage of uniform internal heating and is free of convective heat transfer system [20]. In addition, long before the lowest temperature is reached (-40 °C typically), the battery performance degrade rapidly. Thus, autonomy and dynamic performances of vehicles

Table 1.4: 1981 to 2010 Canadian temperatures, Trois-Rivieres, Quebec [4]

	Jan	**Feb**	**Mar**	**Apr**	**May**	**Jun**	**Jul**	**Aug**	**Sep**	**Oct**	**Nov**	**Dec**
Daily Average (°C)	-12.1	-9.7	-3.6	4.8	12.3	17.6	20	18.9	14.2	7.4	0.5	-7.4
Extreme Minimum (°C)	-41.1	-35.6	-35	-17.2	-6.1	-1.5	3.5	1.1	-7.2	-10.6	-25.6	-35.5

are greatly diminished [18, 19, 21, 22].

Before thinking in how to prevent the formation of ice when the battery is exposed to freezing conditions, first it is important to understand well the battery and learn with how much energy we can really work. In real applications, car manufacturers like Honda or Toyota take preventive measures by implementing mechanisms to assist in starting through auxiliary heating system to minimize degradation of the battery [23, 24]. But the problem here is that they do not know exactly how much energy is left in the battery or at least how much has been consumed, they are usually based in simple look up tables.

The need of time to prepare the battery to start properly brings an additional complexity in the energy management module of the battery pack. Indeed, this module should be able to know how much energy can give the battery to allow some of this energy to be use for the cold start of the EV.

Therefore, in this research project as first necessity is the development of an effective, simple and approximative electrothermal model that prepares the battery to supply power properly after the EV has been turned off for a period of time in low temperature conditions [25–27].

Since the thermal management of the battery will require to know how much energy it has left, it would be then a second necessity to develop a simple algorithm that estimates the consumed energy.

A third and last necessity concerns the on-line estimation of the discharge time of the battery by selecting a robust and simple method that can be fitted in any computer of an EV, all this without consuming a large amount of energy from the battery pack.

1.3 Objectives

This work proposes a comprehensive strategy for thermal management and energy management of a Li-ion battery when the EVs are exposed to cold weather conditions. This

strategy could generate an optimal and efficient temperature control of the battery, seeking the best electrical performance. All this without forgetting the amount of energy and the physical and temporal limitations of battery pack involved.

The ultimate goal is then to obtain a high energy efficiency by allowing the system and user to have a better acknowledgment of the energy consumption from the battery pack and the available discharge time of the battery when the EV is exposed to low temperature conditions, which at the end will be reflected in the improvement of battery's life time.

The following secondary objectives are defined according to the problematic previously identified before:

- The development of a strategy and algorithm for temperature control of the battery: This strategy contemplates an efficient and optimal method to joint the thermal and electrical equations that rule the battery model, the impact of outdoor temperature on the thermal evolution of the pack must be taken into account and also the operating constraints imposed by the battery energy management system. Furthermore, different heat exchange phenomena that occur in the pack will be considered to increase the performance of the energy estimation algorithm;

- The analysis and development of a simple method to identify the internal resistance, the specific heat and the heat capacity of the battery by measuring the open circuit voltage through time. For instance, this will let to know how to manage the energy of the battery required to perform the cold start of the EVs;

- However, it is necessary to have a comprehensive strategy and algorithm to estimate the residual energy in the pack by using a trained method or even a direct method that allows processing the data in real time;

- The development of an algorithm that allows the on-line estimation of the end of discharge time of the battery pack. This takes special importance when the discharge current amplitude varies through time.

1.4 Methodology

The University of Quebec at Trois-Rivières (Université du Québec à Trois-Rivières - UQTR) is proud to have one of Canada's leading institutions in hydrogen research called the Hydrogen Research Institute (Institut de Recherche sur l'Hydrogène - IRH) established in 1994 [28]. Its mission is to advance science and technology for the establishment of a sustainable energy system for HEVs and BEVs and particularly in the field of energy storage, its safety and use. This facility also gives the perfect environment to research in the field of batteries, due to the specialized equipment for performing the battery discharge and recharge and a cooling chamber acquired for cold weather environment simulation. All the studies for this work will be performed in the IRH including research and experimental validations.

This work has six different phases to be consider:

1.4.1 Test Bench Set Up

The test bench will consist of a dynamic electronic load that will permit to discharge the battery with any profile needed; a power electronic source that allows to recharge the battery with any profile needed; a cooling chamber or specialized industrial refrigerator that will allow to set its temperature as low as -40 °C; a data acquisition system to receive the signals of the temperature sensors, voltage and current; and finally a workstation computer that will process and record all the data acquired. All this equipment will be necessary to experiment on a battery pack formed by ten cells connected in series.

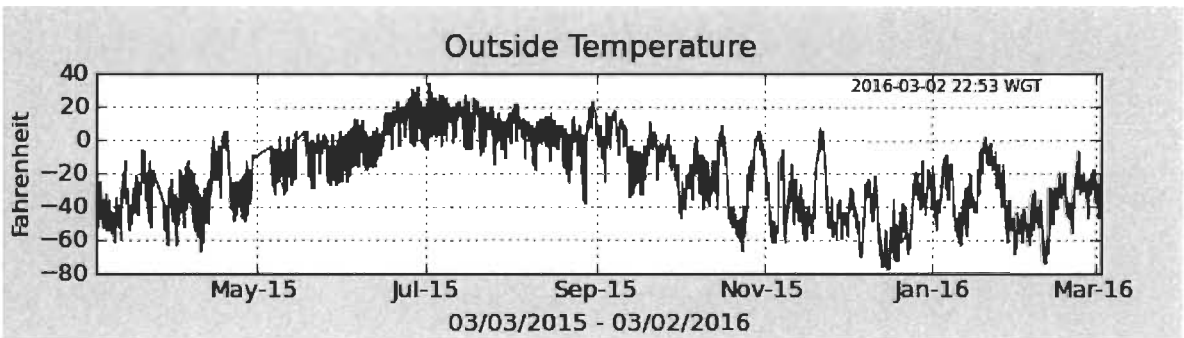

Figure 1.4: Outside temperature at Summit Station in one year [7]

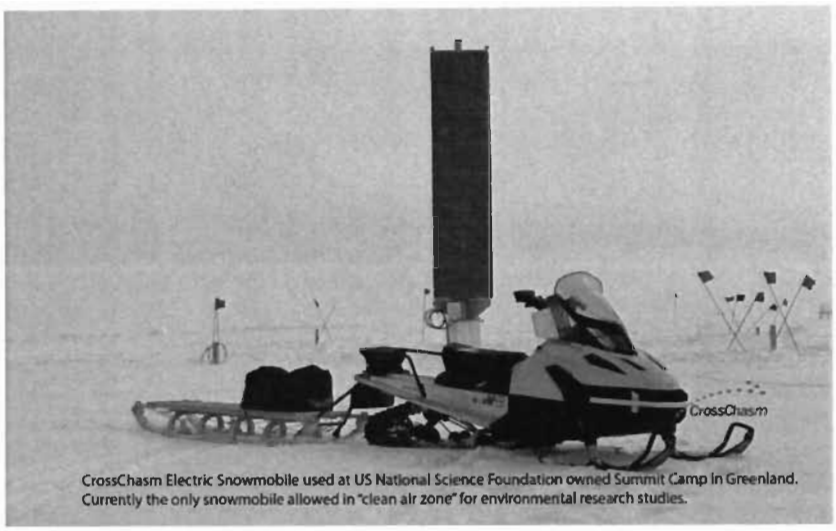

Figure 1.5: CrossChasm electric snowmobile [8]

The battery cells used in this work are manufactured by the German company "GAIA Advanced Battery Systems" and they are classified in America as MIL-SPEC (military grade). The battery pack is composed by ten GAIA battery cells connected in series. The battery pack is constructed by CrossChasm for its Electric Snowmobile used at US National Science Foundation research base named Summit Station in Greenland. In Figure 1.4 is seen the outside temperature at the station with an average value of -22.5 °F or -30.3 °C.

The CrossChasm EV is currently the only snowmobile allowed in "clean air zone" for environmental research studies, see Figure 1.5. CrossChasm is a company with headquarters in Waterloo, ON and also based in Montreal, QC. The focus of this company is to help vehicle manufactures build best-in-class hybrid, electric and plug-in vehicles and guide large-scale end users of those vehicles, such as fleet managers and fleet owners in accurately assessing the full life cycle costs of next generation vehicle adoption [29].

More detailed explanation of the test bench will be given in Chapter 2.

1.4.2 Battery Characterization

In this stage the battery will be characterized recording different discharge tests. The tests will be done with five different temperatures and three different currents of discharge. The

characterization will start with low current[4] and from ideal temperature[5] to low temperature conditions. Also, the recharge cycle will be measured once at ideal temperature and taken into account to characterize the battery.

1.4.3 Electrothermal Model

The study of the electrothermal model will include the constraints of the project. In this stage, all mathematical representation with electrical and thermodynamic principles will be expressed in order to define the equations and their variables. For instance, those equations include variables such as thermal mass of the battery, specific heat, heat capacity, voltage, current and so on.

1.4.4 Residual Energy

This phase will have as main objective to identify the residual energy in the battery using two efficient estimation methods, for instance a trained method like the artificial neuronal networks (ANN) and a direct method, the results of this methods will be highly necessary for the next phase of the methodology. The ANN will have as a main inputs the voltage and temperature and as output will be given some curves of energy obtained from the direct method, this curve estimations are based on measurements taken from the characterization of the battery.

1.4.5 Discharge Time Estimation

Using the electrothermal model previously defined and the estimation of residual energy in the battery, it will be created an algorithm to estimate the discharge time. This will allow to know how much time the driver has before the battery is completely discharged. This algorithm must be able to run in real time taking into account the data inputs from the EV

[4] A current close to the nominal value given by te battery manufacturer
[5] Ideal range of temperature for the battery, approx. 20 to 25 °C

(such as voltage, current, temperature, residual energy estimation) and without requiring a lot of processing resources. Thus, in this phase must be taken into account some restrictions:

- The amount of energy available determined by the residual energy estimation method must be respected;
- The time that the EV is going to be stopped and shut down will be previously set by the user and must be respected;
- The thermal system control must adapt continually to the ambient temperature at every instant of time.

1.4.6 Experimental Validation

Every single phase of the methodology proposed will be tested experimentally at the IRH to corroborate previous calculations and to validate if the algorithms and the models proposed are accurate and if the time prediction is satisfactory.

1.5 Memory Overview

This work is organized as follows: Chapter 2 will help the reader to understand more the context of this work and the battery characterization will be introduced and explained, including the general test bench design, the discharge algorithm and the recharge profile; Chapter 3 will give a brief update in the state of art for the concerning topics of this work and the selected battery model will be presented, including the electrothermal equations for the model, also will be presented the residual energy estimation of the battery and the estimation of the discharge time with its respective experimental validation; and finally in Chapter 4, the general conclusions and the perspectives for this work will be presented.

Chapter 2

Li-ion Battery Characterization

If we start by defining a battery we find that it is basically a device that converts the chemical energy contained in its active materials directly into electric energy by means of an electrochemical oxidation-reduction reaction. In the case of a rechargeable system, the battery is recharged by a reversal of the process. This type of reaction involves the transfer of electrons from one material to another through an electric circuit [30].

The electrolyte of a battery can be a liquid, gel or solid material. Batteries such as lead-acid (Pb-acid), nickel-cadmium (NiCd) have used a liquid electrolyte. This electrolyte may either be acidic or alkaline, depending on the type of battery. In many of the advanced batteries developed for EV applications, the electrolyte is a gel, paste, or resin. These battery types are usually sealed Pb-acid, NiMH, and Li-ion batteries [17].

A Li-ion battery is a primary or secondary battery, depending on its application, with an organic solvent electrolyte and positive and negative electrodes which utilize an intercalation compound in which lithium is stored [31]. As mentioned before in Chapter 1, the Li-ion batteries have great features as batteries for EVs, for instance: high-energy density can be attained with one charge, this provides a long range or mileage; the high-energy density makes it possible to attain stable power with deep discharge characteristics, this allows acceleration and ascending power capability of the EV; long cycle life with maintenance free and high safety mechanisms built into the battery; wide acceptance as a recyclable battery from the environmental standpoint; also can charge and discharge faster than Pb-acid and NiMH

batteries [17].

As we can see, these great features make Li-ion batteries a perfect choice for EVs applications. However, in Section 1.2 it was questioned that when ambient temperature drops drastically, can it be possible to withdraw the same amount of energy from the battery or is the battery going to be completely discharge in the same expected time? This thermal issues need further exploration and new techniques should be explored to avoid cold storage to limit capacity fade of the battery. In order to solve this issues, it is necessary to start by understanding and characterizing the battery.

In this second chapter is presented the characterization of the battery: It is explained the design of the test bench; the discharge algorithm is introduced and explained; since the battery requires to be not only discharged but also charged, then the charge profile is introduced; the discharge tests at different temperatures and currents are presented and explained; and conclusions are discussed at the end of chapter.

2.1 Test Bench Description

All simulations, calculations and estimations presented in this work are based on recorded test bench data. A detailed description of this test bench is provided in this section to picture the data acquisition process properly.

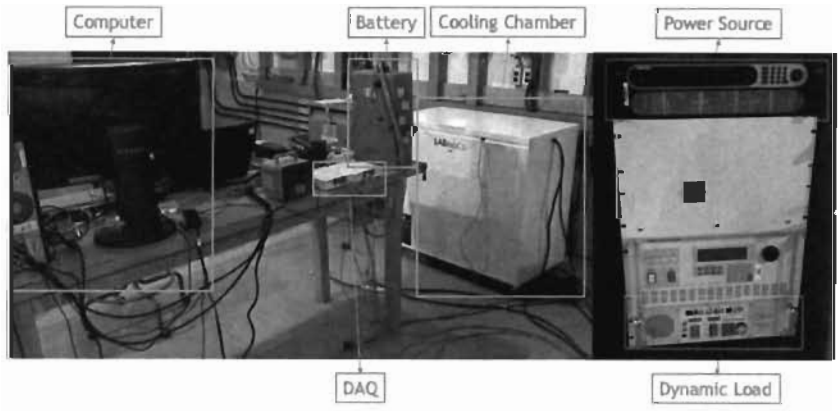

Figure 2.1: General workbench photo

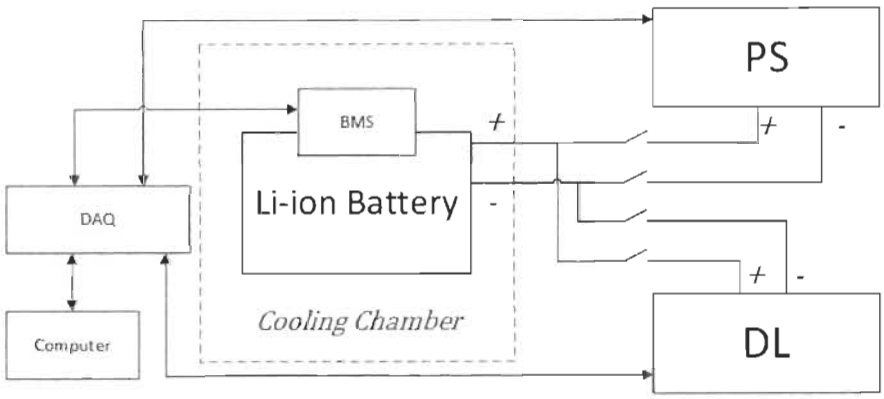

Figure 2.2: General workbench schema

As shown in Figure 2.1 and Figure 2.2, the test bench will consist of six main elements: one Li-ion battery pack with a simple Battery Management System (BMS); one data acquisition (DAQ) system to receive the signals of the temperature sensors, voltage and current; the DAQ system will be connected to a workstation (Computer) that will process and record all the data acquired; one power electronic source (PS) that gives up to 100 V - 100 A in order to recharge the battery; one dynamic electronic load (DL) that will permit to request a total power of up to 12 kW if necessary; and a cooling chamber or specialized industrial freezer that will allow to set its temperature as low as -40 °C.

For this specific case, the Li-ion battery pack is formed by ten cells connected in series and the BMS is dedicated only to security measures such as extreme over heating or extreme high currents that can not be supported by the cells. Each battery cell has a cathode of lithium nickel cobalt oxide ($LiNi_{x.x}Co_{x.x}O_2$) and an anode of graphite. As shown in Figure 2.3, each cell has a temperature sensor on the positive electrode and three cells have three temperature sensors installed on the walls. These sensors will allow to see the thermal behavior of the cells and the battery pack in general, this will be further explained in Section 2.4.1.

In Figure 2.2 are shown the power outputs of DL and PS connected in parallel to the battery electrodes through security power switches. The DL current and the PS on/off output signals are controlled from the computer through the DAQ system. In addition, the DAQ system receives the measurements from all the equipment, such as the DL voltage and current,

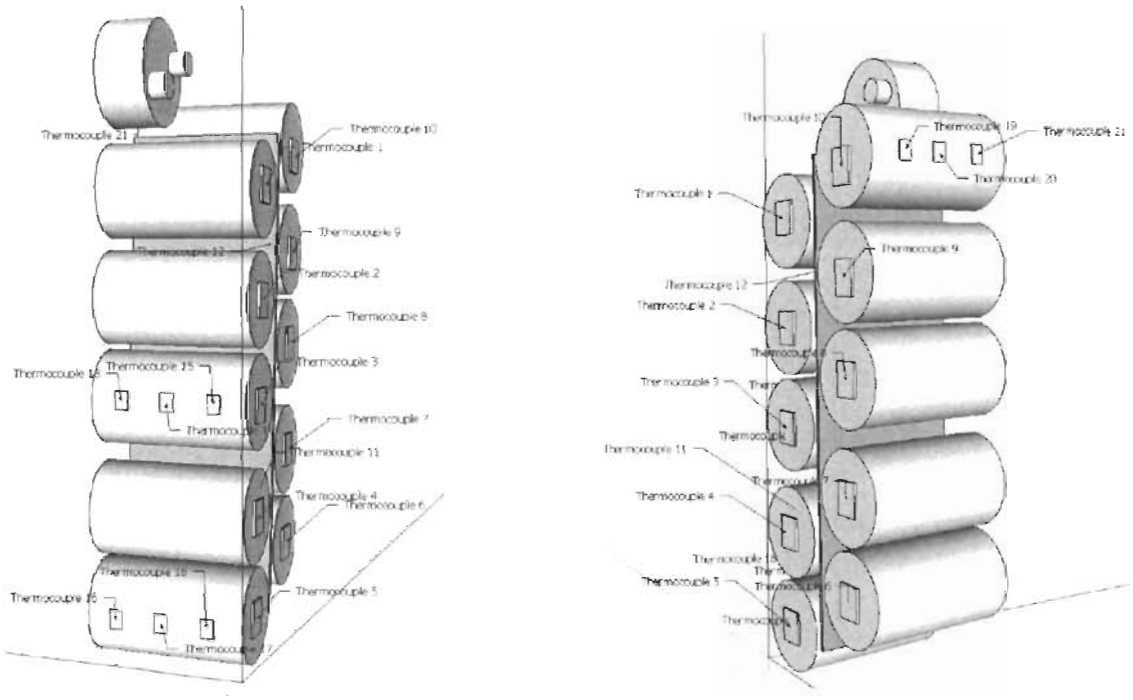

(a) Right Lateral View (b) Left Lateral View

Figure 2.3: Temperature sensors distribution for the battery

the battery voltage, current and temperature (through the BMS), and the PS voltage and current output. The software LabVIEW 11 is installed in the workstation computer to control and process all the information acquired by the DAQ system. The cooling chamber is set to a defined temperature manually between 0 °C and -40 °C depending on the test required.

More technical detail of the battery cells and equipment can be found on the specifications listed in Appendix C.

2.2 Discharge Algorithm

The discharge process is conducted with the algorithm shown in Table 2.1, and an outline of the main step is synthesized hereafter. It is important to follow this procedure in order to not damage the battery due to over passing the limits of design established by the manufacturer, especially because the goal of the characterization is not to degrade the battery, but to know how it behaves in between its ranges of operation.

Table 2.1: Discharge algorithm

Algorithm 1. Discharge test.

Set

- Restriction values $V_{B_{min}}$ and T_{max}
- Sample time of 1000 ms

Specify

- Type of discharge for i_B: Driving current profile or constant current profile

Inputs

- $V_B(t), i_B(t), T(t)$ voltage, current and temperature of the battery, respectively

1: **Initialization of elapsed time t to zero**
2: Start discharge
3: Apply selected current profile
4: **Measure and record** $i_B(t)$, $V_B(t)$ **and** $T(t)$
5: Compare and verify, if $V_B(t) < V_{B_{min}}$ then go to step 7, if not then go back to step 4
6: Compare and verify, if $T(t) > T_{max}$ then go to step 7, if not then go back to step 4
7: End of discharge

First are set the restriction values of the minimum voltage and the maximum temperature supported by the battery and also the sampling time is set. The restriction values are given by the battery cell manufacturer, see Appendix C. Then, it is demanded to the battery a current profile that can be either constant or a specified driving profile from an EV. This current profile will be imposed by the DL. At every sample time the voltage, current and temperature are measured and recorded. Then it is compared the battery voltage against the minimum restriction value and the battery temperature against the maximum restriction value. If any of those values are under or over, respectively, then the DL will stop requesting current and the discharge will be completely finished.

In this algorithm $T(t)$ is the temperature measured through time, $i_B(t)$ is the current, $V_B(t)$ is the voltage of the battery, $V_{B_{min}}$ is the minimum voltage recommended by the manufacturer and T_{max} is the maximum temperature recommended by the manufacturer. The sample rate of the algorithm is equal to one second, this value was chosen in order to have the maximum available data without overloading memory and machine resources of the workstation.

2.3 Charge Profile

As mentioned before in Section 2.1, the PS can be programed or controlled remotely to impose any desired profile to charge the battery. In this case the profile of charge recommended by the manufacturer is the well known charging regime constant current - constant voltage or also known as CC/CV charging regime, the explanation of the charging algorithm for Li-ion batteries is well explained in [32].

After the battery was completely discharged we proceed to charge it. Since the scope of this work is not focused in the effect of the charge at low temperatures, then the charge only starts when the battery is under optimal ambient temperature conditions and its internal temperature is within the optimal recommended temperature range, this to ensure the lowest degradation possible for the battery.

In Figure 2.4, a recorded charge cycle made to the battery with the test bench shows the three main phases of the charge protocol. In the first phase the PS gives a constant current to the battery $i_{cc} = 1C$, where C is the nominal capacity of the battery in Ah (C = 45 Ah), and the voltage starts to raise. The second phase starts when the maximum recommended voltage of the battery is reached $V_{B_{max}} = 41.7$ V. The PS keeps this voltage constant and lets the current to decrease with a slope required by the battery. Finally, the third phase starts when the current of the battery has reached $i_{cc_{min}} = C/100$. When the battery is in the third phase we can say that the battery is fully charged and the charging process stops.

This same procedure was used every time that was required to charge the battery.

2.4 Battery Discharge Tests

There were used three different currents to test and characterize the battery. The three values of this currents were established considering the normal current operation range required by the snowmobile and the recurrence of the mean currents used by it. Since 50 A is the typical average current used by the snowmobile, there were selected the following currents:

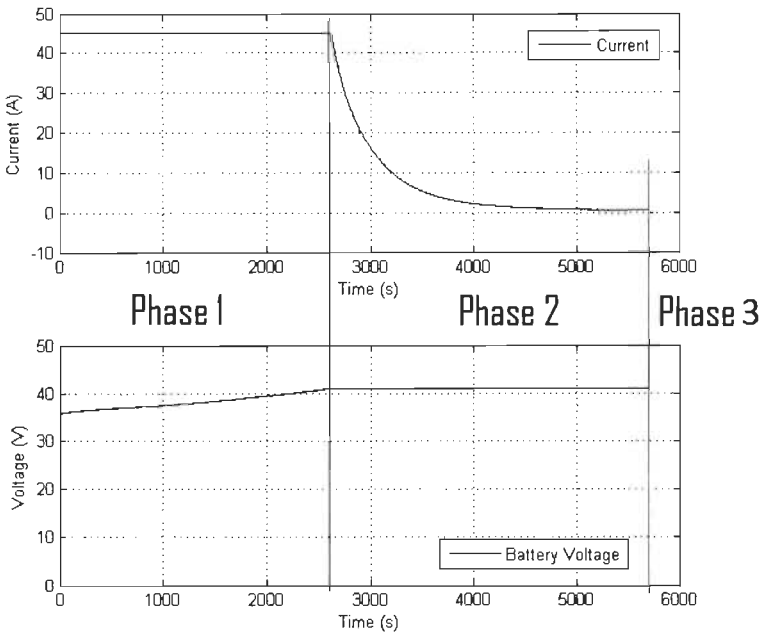

Figure 2.4: Charge profile for Li-ion battery

1.1C = 50 A, 2.7C = 125 A, 4.4C = 200 A. It is necessary to remark that the battery should not have any difficulties to deliver this currents because the maximum discharge current established by the manufacturer is 10C = 450 A and the recommended discharge current for regular use is 2C = 90 A[1].

During the characterization was introduced the distribution of temperature and voltage of the cells. It was also studied the effect of the ambient temperature on the behavior of the battery. The battery was considered completely discharged when it reached the minimum voltage of $V_{B_{min}} = 27$ V or $V_{B_{mincell}} = 2.7$ V/cell, this applies for all the tests performed during this work.

With the aim of comparing the results, it was required a discharge protocol. This protocol ensures that the discharge cycle is always executed under the same conditions and it was conformed by 5 stages:

1. Starting with the battery completely charged, the cooling chamber temperature is set to the low ambient temperature required for the test;

[1]Under optimal conditions at ambient temperature of 20 °C.

2. Meanwhile, the battery is kept in the chamber until its temperature reaches thermal equilibrium, i.e. the temperature test, if the temperature test is 24 °C then the cooling chamber is not required;

3. This step is the core of the discharging protocol. Here is performed the discharge of the battery. The aim of this test is to fully investigate the discharge behavior of the cell, however battery's degradation is crucial as regards [33] and because of this, the recommended limits of the battery will be monitored at all times.

4. Once the discharge cycle is done, the cooling chamber is set to room temperature. The battery is left inside warming slowly until it has the same temperature of the room;

5. The charge process is performed with the protocol presented in Section 2.3. Since the temperature of the battery rises during the charge, then it is necessary to let the battery to cool down until it reaches the same room temperature before the next discharge test.

It is also important to remark that all the data and figures presented in this entire work are comparable between each other. In the following subsections are explained in detail the tests of the third step of the protocol made to characterize the battery.

2.4.1 Voltage and Temperature Distribution

As mentioned in Section 2.1 there are three temperature sensors on the walls of three cells and one sensor in each positive node of the cells that will allow to see the thermal behavior of the cells and the battery pack in general. The sensors on the walls of the cells were located at the top, middle and bottom. The cells chosen to have sensors on the walls were the number one, six and eight. This three cells were chosen due to their location inside the battery pack, since the number one is located at the top, number six is located at the bottom and number eight is located at the middle, see Figure 2.3.

In literature [34] has been discussed that other authors have proven the non-uniformity of the temperature of the core (T_{core}) along the cell core, but a more sophisticated model, such

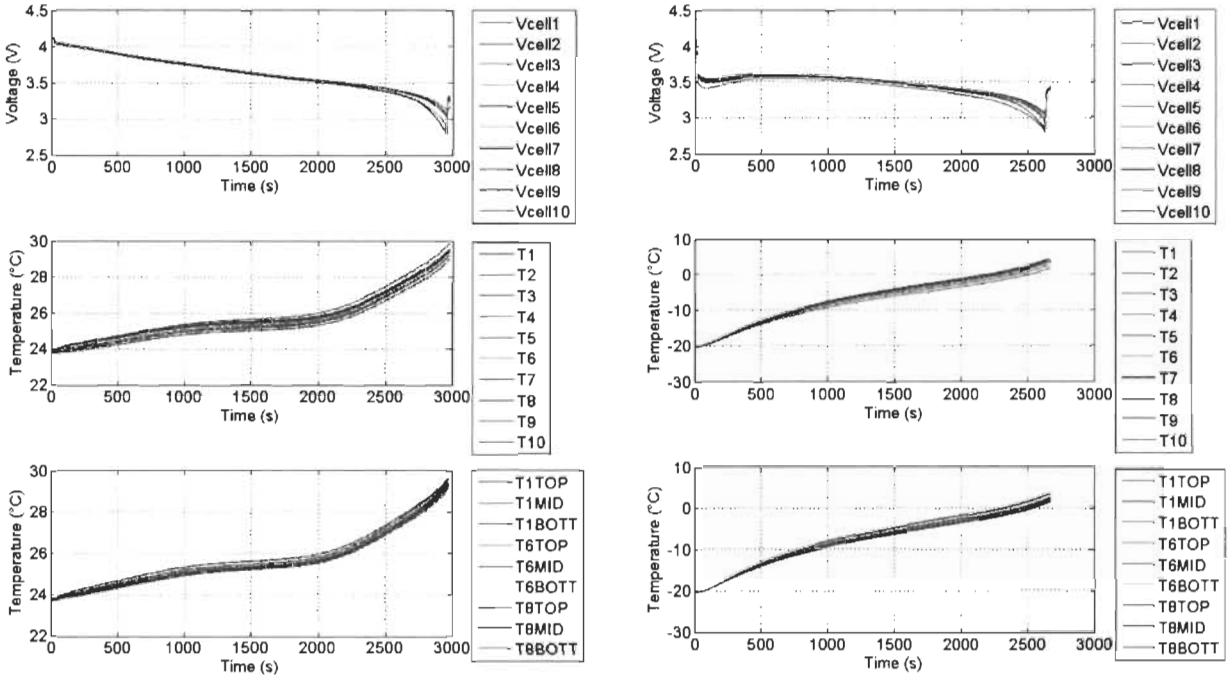

(a) Ambient Temperature 24 °C

(b) Ambient Temperature -20 °C

Figure 2.5: Temperature and voltage distribution of the battery pack

as an electrochemical one, is used to model thermal rejection. However, they also explained that due to the moving liquid electrolyte inside the core, T_{core} can be guessed to be uniform and the uniformity of T_{core} happened to be sufficient for simple thermal simulation.

If there is some uniformity of T_{core}, then the temperature measured between the positive electrode and the negative electrode can be practically the same, this assumption was tested in the lab. In Figure 2.5, are shown two figures with the measurements of the voltages of each cell and the temperature of the cells when the battery is discharged at constant current of 50 A. Figure 2.5a is the result when ambient temperature is 24 °C showing a maximum temperature of 29.83 °C and a minimum of 29.01 °C at the end of discharge, this gives us a temperature delta of 0.815 °C between the highest and the lowest cell temperature. Figure 2.5b is the result when ambient temperature is -20 °C showing a maximum temperature of 4.27 °C and a minimum of 1.55 °C at the end of discharge, this gives us a temperature delta of 2.72 °C. It is clear that the temperature unbalance is much higher when the ambient temperature is lower. However, if each of these temperature deltas are compared against the temperature delta of

each complete discharge test we obtain a 13.48 % and a 11.07 % of total relative temperature unbalance respectively.

Voltage and temperature uniformity of the cells did not have a significant variation in relation to the complete discharge test. Then we use the main temperature of the cells and total voltage of the battery pack for all the figures presented during this work.

This measurements were made all along the tests performed for this work and the two figures presented in Figure 2.5 are shown as examples. As additional note, the scope of this work is not focused on the unbalances presented between the cells and so, they are not or will not be fully studied.

2.4.2 Optimal Ambient Temperature

As recommended by the manufacturer, the best range of ambient temperature for optimal operation of the battery is between 20 °C and 28 °C. The IRH's test center has a controlled ambient temperature between 23 °C and 24.5 °C. This gives the chance to see how the battery behaves under this conditions, which sets an excellent starting point for the characterization.

Figure 2.6 shows three different battery discharge tests with an ambient temperature of 24 °C. As mentioned before, this tests were made requesting a constant current until the battery was completely discharged.

In Figure 2.6a is shown a discharge test with the current of 50 A, in Figure 2.6b with the current of 125 A and in Figure 2.6c with the current of 200 A. In each one of the three figures are presented the current, voltage and temperature of the battery pack. The voltage is measured between the positive node of the cell number one and the negative node of the cell number ten. The temperature shown is measured in the positive node of the cell number one.

The discharge tests presented in Figure 2.6 show three characteristics of high importance to be remarked in this work. The first one is the amount of time required to completely discharge the battery using a specific constant current, this will be used as reference for esti-

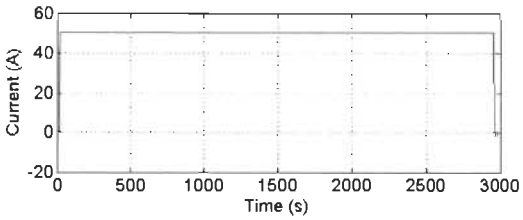

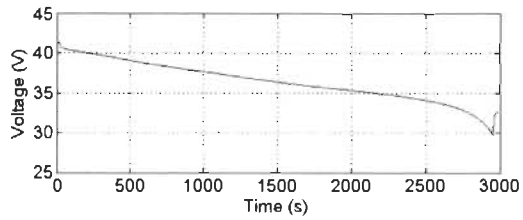

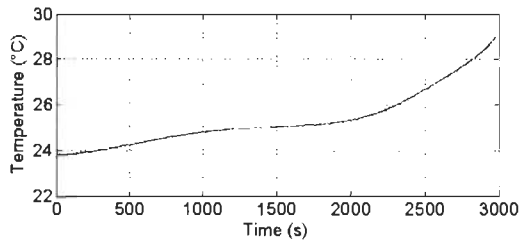

(a) Constant current: 50 A

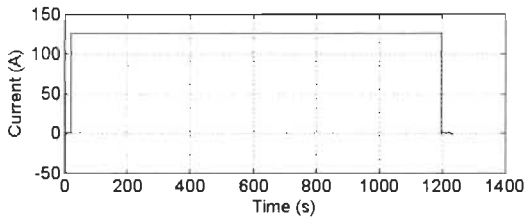

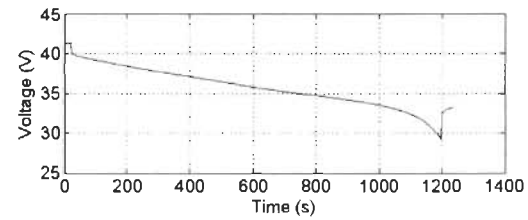

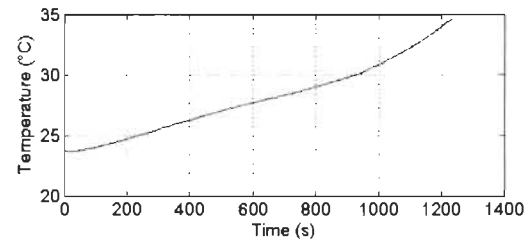

(b) Constant current: 125 A

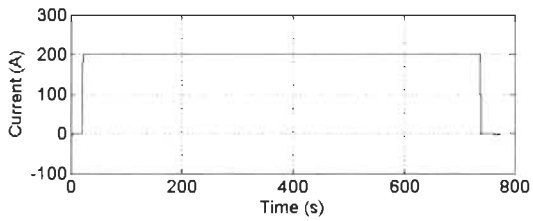

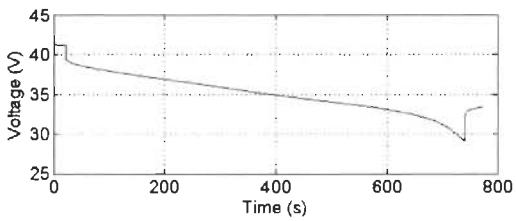

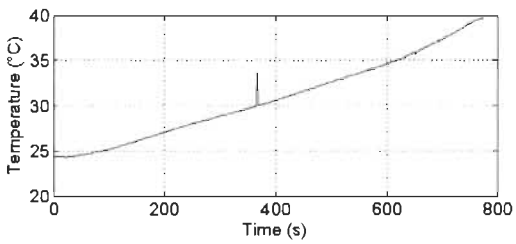

(c) Constant current: 200 A

Figure 2.6: Characterization with ambient temperature of 24 °C

mations performed in Chapter 3; The second is the voltage drop at the beginning of discharge, this allows to compare the effect not only of the current but also of the temperature over the behavior of the battery voltage; The third one is the delta temperature between the beginning and the end of discharge, this let us see the direct effect of the current over the thermal behavior of the battery for later to be compared in Section 2.4.3 with the low temperature tests and understand the impact of the ambient temperature on the battery pack. The three characteristics of interest are shown in Figure 2.7 comparing the discharges with three different currents.

Figure 2.7a clearly presents the big difference of the discharge time due to current. For instance, with a current of 50 A the total time of discharge was 2942 s or 49.03 min, while with a current of 125 A was 1179 s or 19.65 min and with 200 A was 722 s or 12.03 min. In Figure 2.7b is presented the increase of voltage drop due to current. When is imposed a current of 50 A the voltage drop was 0.57 V, while with a current of 125 A was 1.13 V and with 200 A was 1.89 V. This voltages drop are not very considerable, because if the battery is fully charged then it can withstand a maximum voltage drop of 14.7 V before the BMS opens the circuit. In Figure 2.7c is seen how temperature increases due to current too. With a current of 50 A the ΔT was 5 °C, while with a current of 125 A was 10.3 °C and with 200 A was 14.4 °C. This tell us that, when the battery is exposed to optimal ambient temperature, there is an average increase of 4.7 °C every 75 A, which gives a relation of 0.0627 °C·A^{-1}.

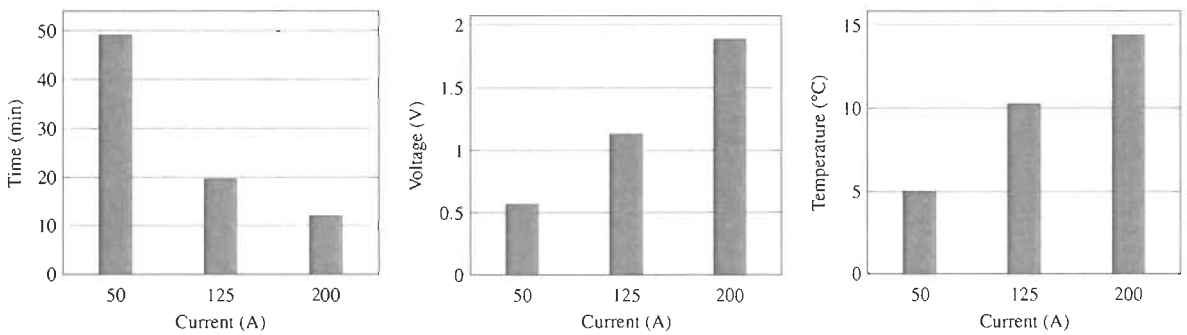

(a) Discharge Time (b) Voltage Drop (c) Δ Temperature

Figure 2.7: Discharge comparison at 24 °C

The temperature of the battery rises up because of a heat generation happening from the electrochemical reaction inside the cell which shows what occurs truthfully in a realistic HEV driving cycle as regarded in [35].

2.4.3 Low Ambient Temperatures

The previous section allowed us to see how the battery behaves under optimal ambient temperature and showed the impact of withdrawing current from the battery. The objective in this section is to see if the battery can withstand the harsh conditions of the low temperatures, even when requesting high currents. The results will be compared with the results obtained in the precedent section.

Now, to see the effect of low ambient temperatures on the battery pack is required to use the cooling chamber shown in Figure 2.1. This chamber is set in four different representative low ambient temperatures, 0 °C, -10 °C, -20 °C and -30 °C. This temperatures are selected considering the usual temperatures at the Summit Station, as shown in Chapter 1, Figure 1.4.

The discharge tests were made using the same conditions of Section 2.4.2, with the exception of the optimal ambient temperature. Three discharges were made for every ambient temperature selected. These discharges were made using the same constant currents of 50 A, 125 A and 200 A. In Appendix A is presented the discharge test for the three currents. Figure A.1, Figure A.2, Figure A.3 show the discharges made to the battery using the three constant currents under the four ambient temperatures that were proposed. In each one of the three figures are presented the current, voltage and temperature of the battery pack for each ambient temperature. Again, the voltage was measured between the positive node of the cell number one and the negative node of the cell number ten. The temperature shown is measured in the positive node of the cell number one.

The results obtained in the figures of Appendix A and the ones obtained in Section 2.4.2 are resumed in Figure 2.8. In Figure 2.8a are presented the voltages and temperatures for the four low ambient temperatures and the optimal ambient temperature using a discharge

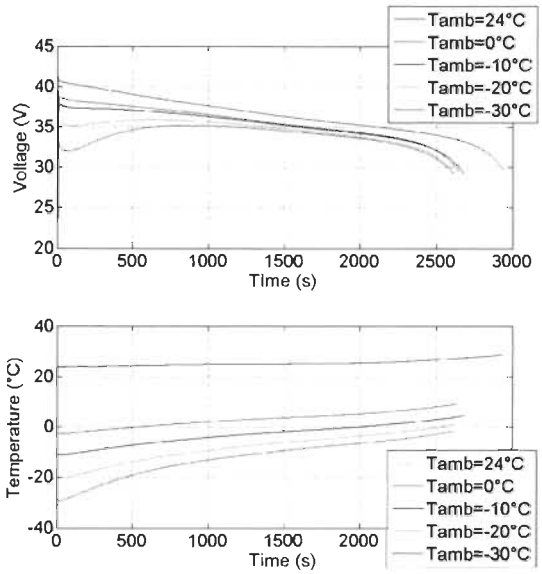

(a) Constant current: 50 A

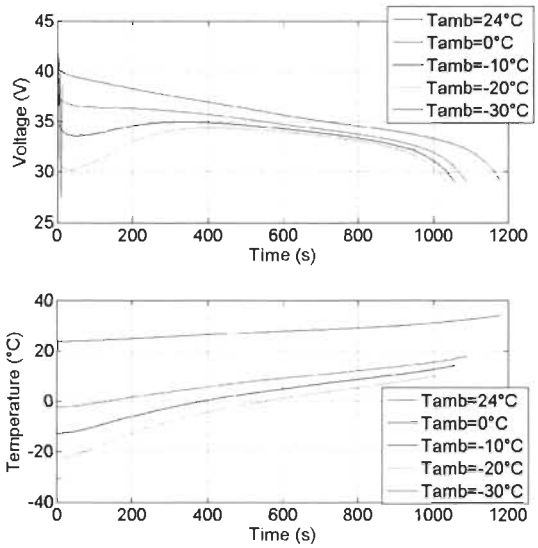

(b) Constant current: 125 A

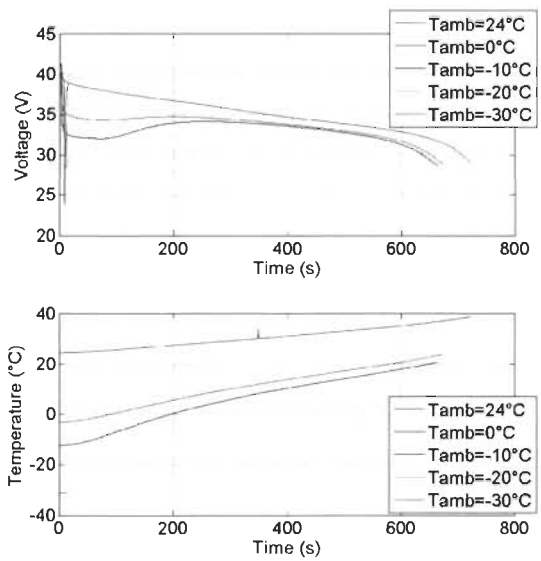

(c) Constant current: 200 A

Figure 2.8: Characterization results for all currents and temperatures

current of 50 A. In Figure 2.8b and Figure 2.8c are presented the same results but with a discharge current of 125 A and 200 A, respectively. Each color of the curves represents a specific ambient temperature: blue is for 24 °C, red is for 0 °C, black is for -10 °C, cyan is for -20 °C and magenta is for -30 °C.

As mentioned in Section 2.4.2, when a current is requested from the battery it is observed

a voltage drop phenomena. This phenomena gets bigger when ambient temperature (T_{amb}) is colder and gets even worst if the current increases. In Figure 2.8b it is observed, with an ambient temperature of -30 °C, that the voltage drop was too big making the discharge to be stopped in order to preserve the health of the battery. In Figure 2.8c it is observed the same behavior but this time for ambient temperatures of -20 °C and -30 °C. This voltage drop is caused by the behavior of the internal resistance of the battery [20, 36], this will be explained more in Section 3.1. Also, with low temperatures the operating voltages and energy delivered are reduced because a cold environment lengthens the diffusivity of Li+ inside the cell [34, 37].

Figure 2.9 shows the same three characteristics that were presented in Section 2.4.2, but with the difference that this time are also included the results for low ambient temperatures presented in Figure 2.8.

Figure 2.9a presents the discharge time due to current for the five T_{amb} of interest. It is clear to see a big difference of values in the discharge time due to the current, but the temperature did not have a big impact in this matter. The percentages shown in column Δt of Table 2.2 present the reduction suffered for the discharge time due to the decrease of temperature in reference to the optimal $T_{amb} = 24$ °C. The average reduction between the tests that were not stopped due to high voltage drop was -9.63 %. Then it can be said, this is the average discharge time reduction due to temperature if the voltage drop does not exceed the limits established for the battery.

Figure 2.9b presents the voltage drop due to current for the five T_{amb} of interest. It can be seen the increment of the voltage drop due to current but also due to the T_{amb}. The values shown in column Difference between V_{drop} (V) of Table 2.2 shows how much the voltage drop increased due to the decrease of temperature in reference to the optimal $T_{amb} = 24$ °C. As expected, the biggest V_{drop} difference is present when the current is high and the T_{amb} becomes extremely low.

Figure 2.9c also shows how temperature increases due to current for the five T_{amb} of

interest. This figure becomes very attractive because it allows to understand the battery's temperature behavior which becomes useful to tackle the cold start problem. For instance, a high discharging current value can be applied to heat the cells, but as a downside effect it accelerates the battery's deterioration and shortens the life of the cells [38]. The values shown in column Difference between ΔT (°C) of Table 2.2 shows how much the ΔT increased due to the low temperature in reference to the optimal $T_{amb} = 24$ °C.

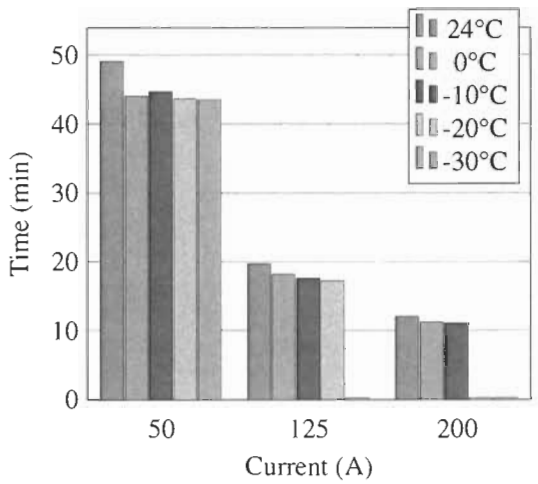

(a) Discharge Time

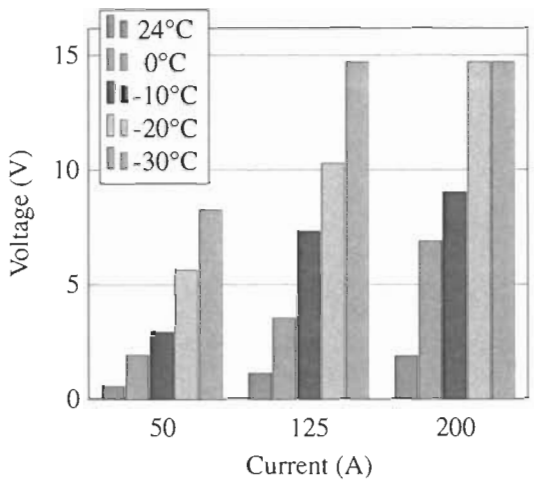

(b) Voltage Drop

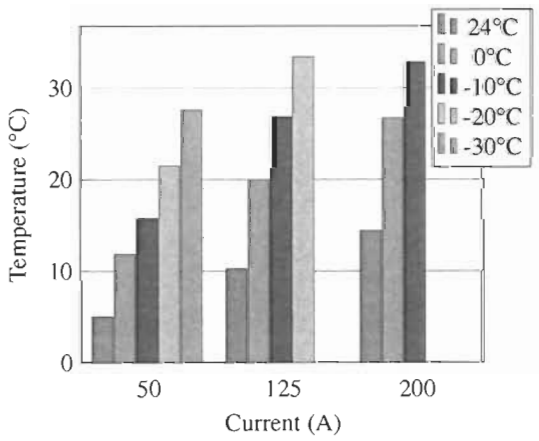

(c) Δ Temperature

Figure 2.9: Discharge comparison for all currents and temperatures

Table 2.2: Results variation due to T_{amb}

Comparison (°C)	Δt (%)			Difference between V_{drop} (V)			Difference between ΔT (°C)		
	at 50A	at 125A	at 200A	at 50A	at 125A	at 200A	at 50A	at 125A	at 200A
24 Vs 0	-10.25	-7.63	-6.78	1.37	2.40	5.00	6.85	9.74	12.31
24 Vs -10	-8.97	-10.44	-8.18	2.34	6.18	7.13	10.73	16.56	18.4
24 Vs -20	-10.97	-12.21	-97.74	5.08	9.17	10.23	16.45	23.15	-14.33
24 Vs -30	-11.28	-98.70	-97.88	7.70	11.22	14.21	22.57	-10.21	-14.35

2.5 Energy Calculation

Finally, the amount of energy extracted from the battery during characterization tests is calculated with (2.1).

$$W = \int V_B(t) \cdot i_B(t) dt \tag{2.1}$$

where W is the energy delivered in Joules.

In Table 2.3 are presented the calculated amounts of energy for each test performed during the characterization process in kWh. This values will be later compared in Section 3.2.1 with results of energy estimation obtained using the methods proposed.

Table 2.3: Characterization discharge energy

	24 °C	0 °C	-10 °C	-20 °C	-30 °C
50 A	1.498	1.315	1.320	1.265	1.234
125 A	1.462	1.310	1.238	1.184	0.003
200 A	1.400	1.251	1.205	0.006	0.004

† The energy of the battery given by the manufacturer is 1.620 kWh. All values in this table are given in kWh

2.6 Conclusion

In this Chapter was presented the basics of batteries, was discussed the type of batteries and how they are built inside. Then, the battery characterization was introduced and explained, including in it the test bench design and its components, the discharge algorithm was explained and the battery charge profile was introduced and explained.

During the characterization process was discussed the discharge tests realized at the IRH. It was explained the discharge protocol and was compared the behavior of the battery under different low ambient temperatures and the optimal ambient temperature. The characterization tries to show the behavior of the battery system during operation in different low temperature conditions. Thus, a simulated ambient temperature has been implemented using a cooling chamber to proceed with the different temperature conditions. The experimental tests were performed requesting three constant currents to compare between the effect of ambient temperature and the effect of the current increase on the battery.

The battery charge was always performed under optimal ambient temperature conditions to avoid battery degradation.

Due to the scope of this work, battery cell's unbalances were presented but not fully studied. However, the results obtained for voltage and temperature uniformity of the cells showed that it did not have a big variation in relation to the complete discharge test. Then it was possible to use the main temperature of the cells and total voltage of the battery pack for all the figures presented during this work.

After showing the results obtained, it was seen the big change in the discharge time due to the current, but the temperature did not have a big impact in this matter. On the other hand, for the voltage drop was not the same case. This voltage drop caused by the behavior of the internal resistance of the battery had a big magnitude increase due to low temperatures. With low temperatures the operating voltages are reduced because a cold environment lengthens the diffusivity of Li+ inside the cell.

The comparison of ΔT gets a highlight because it allows to understand the battery's tem-

perature behavior which becomes useful to tackle the cold start problem. For instance, a high discharging current value can be applied to heat the cells. But as a downside effect this current accelerates the battery's deterioration and shortens the life of the cells.

The Chapter 3 will use the characterization presented here to help in the selection of the battery model, including the electrothermal equations for the model and also will be used for the residual energy estimation of the battery and the estimation of the end of discharge time.

Chapter 3

Li-ion Battery: Model, Energy and Time

In this third chapter is given a short introduction to get into context and understand the assumptions made in order to proceed with the battery model. It is presented the selected battery model used in this work, including the integration of the electrothermal equations and its constraints and variables, such as the convective heat, heat capacity and internal resistance; it is introduced and explained the two methods used in this work to estimate the residual energy of the battery and it is presented the driving profiles of current recorded from the snowmobile; it is presented and explained the discharge time estimation of the battery and the results are compared using experimental validation; finally conclusions are discussed at the end of chapter.

3.1 Battery's Electrothermal Model

Several models of batteries had been used before [39–48], but most of the time the state-of-charge (SOC) is presented in order to calculate all the parameters of the battery model, even when the temperature is not taken into account.

Battery modeling is a highly important task for battery technology development and it is necessary in all EVs applications. For instance, EVs range prediction is only possible through the use of battery modeling and estimation techniques to determine current state and predict its residual energy [49].

As explained in literature [34, 39], it can be found three main types of battery models. First, there are electrochemical models, they have better accuracy but are generally much more complex, take a lot of computational resources [50–52] and require specific battery chemical inputs. Second, there are the empirical models, that are basically mathematical models [53], they do not give direct relationships between phenomena [54] and sometimes they are not very accurate for the prediction of the SOC when there are variable currents [50]. Third, there are equivalent circuit models, they are built with several degrees of complexity, depending on the desired accuracy [55, 56]. The parameters of these models can be measurable quantities such as temperature, current and sometimes they just use historic values [51, 57].

When it is required to know the physical parameters of a battery model there are two ways to do it: one, it can be found in literature; or two, with an experimental exploration. For the sake of getting more accurate values of this specific battery and not just some generic values, then the second option has been chosen for this work and in subsequent sections will be presented the selected battery model with the steps followed to obtain all the parameters needed to operate with that model.

3.1.1 Context

This document focuses on Li-ion batteries for EVs under cold ambient temperature conditions, specially when the vehicles are driven for a non specific amount of time and later the vehicles are parked for a period of time[1] and it is not possible to connect them to the electrical network for that period of time to charge them, e.g. the snowmobile in the Summit Station in Greenland.

It is important to remark that some points must be taken into consideration before continuing with the selection of the battery model:

- As first point, for the scope of this work there is no interest about the relaxation effect

[1] Normally more than 1 hour.

produced in the battery, this will allow to have a simple but efficient model of the battery that will not require much resources from the system in order to produce the desired estimations, it will be better introduced and explained in Section 3.1.2;

- Second, Lithium Nickel based cells provide up to 30 % higher energy density than Cobalt based and they also have the highest exothermic reaction which could give rise to cooling problems in high power applications, but in this application due to low power consumption[2], there will not be enough energy expenditure to consider a high radiation effect of the battery, even if the cold start problem is tackled by self-heating the battery;
- Third, in this specific case the battery cells are isolated with the shell structure of the battery itself and the power consumption is low;
- And last but not least, since the walls of the battery shell are in contact only with the surrounding environment, then the convective heat through the air will be taken into account.

Obtaining an estimation of the internal resistance and the specific heat allows to have an approximated model of the battery, this can be used to estimate the residual energy in it and later on will lead to develop a way of estimating the discharge time of the battery.

3.1.2 Selected Battery Model

The electro-thermal model taken as reference was well explained in [39], however, in this case are not used the capacitor and the resistance connected in parallel because, as mentioned in Chapter 3.1.1, the scope of this work has no interest on the relaxation effect [42, 58].

As its name is written, the electro-thermal model is divided in two main parts: first is the electrical model where is represented the battery as an electric circuit; and second, the thermal model where are expressed the thermal variables involved in the behavior of the battery. Here it is established a relation between the electrical and the thermal behavior of the battery.

[2]Usually, for very high power batteries, is considered low power consumption when is less than 10 kW.

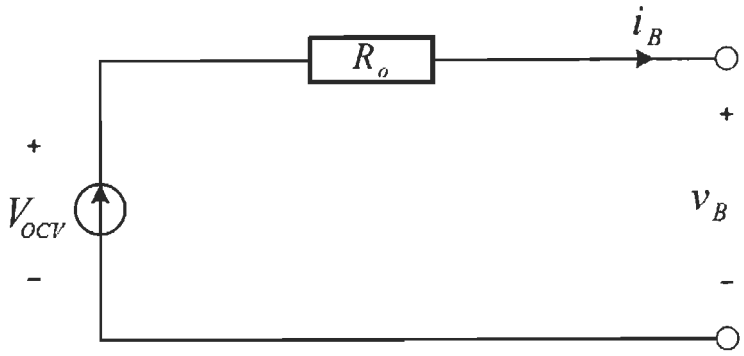

Figure 3.1: Approximated battery model

Electrical Model

For this work was selected a simple approximated electrical model [48], shown in Figure 3.1. The aim of this model is not to provide a very accurate description of the battery, but to reduce computing processes and add simplicity to a bigger integrated power system, e.g. in HEVs, BEVs or any type of EV, in this case an electric snowmobile. This model is expressed mathematically in (3.1).

$$V_{OCV} = R_o i_B + V_B \tag{3.1}$$

Here V_{OCV} represents voltage of open circuit voltage, V_B is the voltage measured between the electrodes of the battery, i_B is the current and R_o equivalent resistance of the battery.

As can bee seen, this model has only two parameters to be estimated (V_{OCV} and R_o), but these parameters are not fixed. Due to some variations, it is necessary to define a thermal model that allows to relate the temperature variations to the electrical model.

In Section 3.1.4 and in Section 3.1.5 will be explained how the two electrical parameters of this model were obtained.

Thermal Model

Heat is defined as a form of energy transferred to or from a system other than by work or the transfer of matter. This energy is always transferred from a hotter to a colder system. A supply of heat may correspond to an increase of thermodynamic temperature or to other

effects, such as phase transition or chemical processes.

The chemical process that occurs inside a battery due to the flow of current, makes the battery to dissipate energy in the form of heat. This can be studied to define a thermal model that allows to relate the change of internal thermal energy and the heat transfer with the electrical constraints of the battery. The first law of thermodynamics will work as starting point to define the model.

According to the first law of thermodynamics for a closed system [59], the thermal energy balance in general is given by (3.2)

$$\frac{\delta U}{\delta t} = Q - W_k \tag{3.2}$$

Where $\delta U/\delta t$ is the rate of change of internal thermal energy with time, Q is the heat transfer rate, W_k is the work transfer rate. But, since our system has no work process, then (3.2) is now expressed as (3.3).

$$\frac{\delta U}{\delta t} = Q \tag{3.3}$$

Since the substance undergoing this process is incompressible, i.e. the volume is constant for any pressure variation, then (3.4) presents that the specific heat capacities[3] at constant volume and constant pressure are equal [59].

$$mC_v\frac{\delta T}{\delta t} = \frac{\delta U}{\delta t} = Q = \frac{\delta H}{\delta t} = mC_p\frac{\delta T}{\delta t} \tag{3.4}$$

Where H is the enthalpy, $\delta T/\delta t$ is change in temperature through time and C_v and C_p are the specific heat capacities at constant volume and constant pressure, respectively. The battery has a mass of $m = 15$ kg.

Now, the heat transfer rate can be expressed as the difference between the heat generated

[3]The specific heat is a quantity of heat necessary to raise or reduce the temperature of unit mass of substance by 1K [60].

and the heat loss, then we have (3.5).

$$Q = Q_{gen} - Q_{loss} \tag{3.5}$$

Due to the simplicity of our model, the heat generated will be equivalent to the Ohmic losses, i.e. the heat generated due to current flowing through the internal resistance of the battery (3.6).

$$Q_{gen} = R_o i_B^2 \tag{3.6}$$

In the other hand, the heat loss will be simply the heat transferred from the battery to its surroundings due to the differences of temperature. This heat can be transferred by two means: one, through heat conduction and two, through heat convection. But, because of the third and fourth points remarked in Section 3.1.1, we have that the heat conduction will be the same as the convective heat, hence we define (3.7).

$$Q_{loss} = Q_{cond} = Q_{conv} \tag{3.7}$$

Then the convective heat through the air is expressed in (3.8).

$$Q_{conv} = hs(T - T_{amb}) \tag{3.8}$$

Where hs represents the convective heat transfer coefficient multiplied by the superficial area $s = 0.3952\ m^2$. Now, the heat transfer rate from (3.5) can be expressed as in (3.9).

$$Q = R_o i_B^2 - hs(T - T_{amb}) \tag{3.9}$$

Once defined the heat transfer rate and the internal energy rate, then we replace (3.4) in (3.9) to obtain (3.10).

$$mC_p \frac{\delta T}{\delta t} = R_o i_B^2 - hs(T - T_{amb}) \tag{3.10}$$

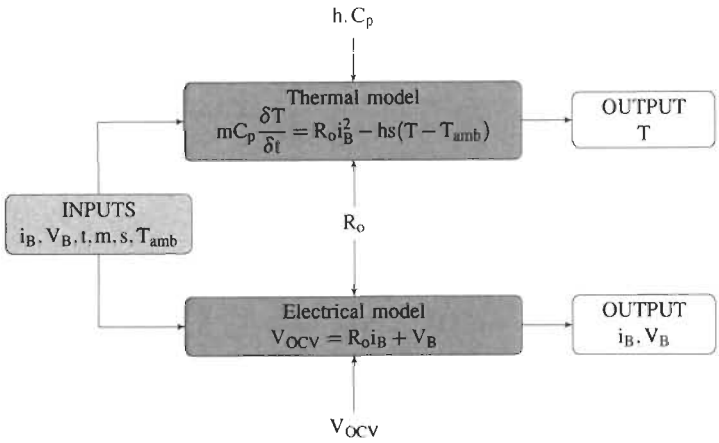

Figure 3.2: Electrothermal model flow chart

For all previous equations, T is the temperature measured on the electrodes of the battery. This temperature is due to the environment but also due to the current requests made by the load. T_{amb} represents only the ambient temperature at the moment of the test. The time in seconds is represented by t.

As result, equation (3.10) defines the thermal model that gives an approximation to thermal behavior of the battery and also gives a relation between the electrical and the thermal model.

Now, we understand that for this electrothermal model to work properly, it is necessary to obtain some variables like the V_{OCV}, C_p, R_o and h. In following sections will be explained how were obtained the values of these variables for the two models, i.e. the variables for equations (3.1) and (3.10). Figure 3.2 let us see how the electrothermal model is formed.

3.1.3 Convective Heat Transfer Coefficient Calculation

There is two different ways to calculate the h. The first method is by using the exposure to cold curve, Figure 3.3. The battery was exposed to the cold inside the cooling chamber in open circuit mode, i.e. no load or power source attached to it, at -30 °C to see the voltage behavior of the battery and the temperature curve in order to calculate the h. The Figure 3.3 shows that the voltage of the battery tends to drop with the same trend curve of the

temperature, but not with the same ratio.

After getting the temperature of the exposure to cold curve, the first step is to solve the equation (3.10) for T(t), then we have (3.11a).

$$T(t) = C_1 e^{-\left(\frac{hs}{mC_p}\right)t} + T_{amb} \tag{3.11a}$$

This can be also expressed as (3.11b).

$$T(t) = C_1 e^{-(t/\tau)} + T_{amb} \tag{3.11b}$$

where C_1 is a constant that can be simply obtained by evaluating (3.12). τ is obtained from the curve of temperature in Figure 3.3 by tracing a tangent to the curve from T(0) to the crossing point between T_{amb} and the projection of $T(\tau)$, i.e. the slope of this line will be τ.

$$C_1 = \lim_{t\to\infty} T(t) - \lim_{t\to 0} T(t) \tag{3.12}$$

Since $1/\tau = hs/mC_p$, then h can be easily determined. However, in our case we do not know

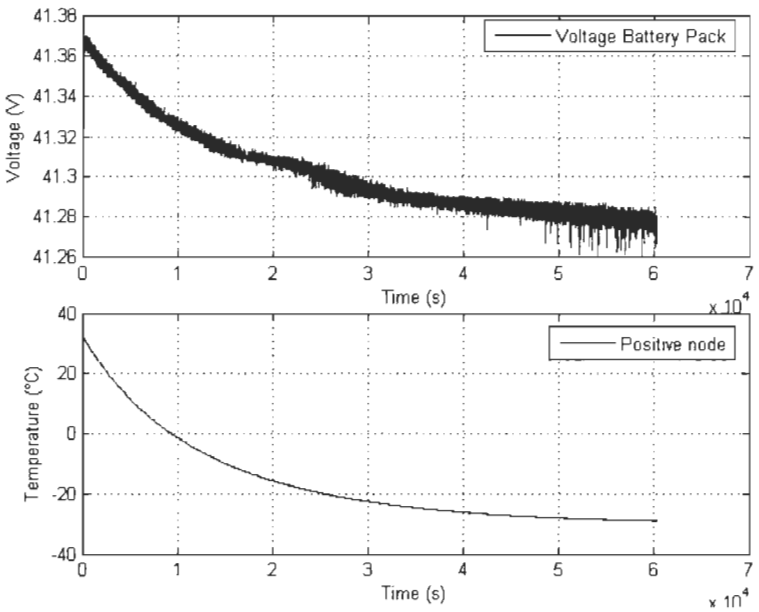

Figure 3.3: Curve of battery's exposure to cold

C_p and so, h can not be calculated by this method. This is when the second method comes in place.

For the second method we start by calculating the Grashof number (3.13), which is a dimensionless group. It represents the ratio of the buoyancy force to the viscous force acting on the fluid [61].

$$Gr = \frac{g\beta(T - T_{amb})\alpha^3}{\upsilon^2} \tag{3.13}$$

where g is the gravitational acceleration in $m \cdot s^{-2}$, β is the coefficient of volume expansion in K^{-1}, α is the characteristic length of the geometry in m, υ is the kinematics viscosity of the fluid in $m^2 \cdot s^{-1}$.

Then, it is required to have the Prandtl number (Pr) to calculate the Rayleigh number (Ra). The ratio of momentum diffusivity to thermal diffusivity of a fluid is known as the Prandtl number [62]. The Pr was obtained using a simulation tool from the University of Waterloo [63], this number is dimensionless and it is dependent only on the fluid and the fluid state, which in this case the fluid is air.

The Rayleigh number is defined as the product of the Grashof and Prandtl numbers, then we have (3.14).

$$Ra = GrPr \tag{3.14}$$

Once Ra has been calculated, we can proceed to obtain the Nusselt number (Nu). In natural convection the Nusselt number is given by (3.15).

$$Nu = C_N Ra^n \tag{3.15}$$

where C_N and n depend on the geometry of the surface and the flow. The Table 3.1 shows a resume of some possible cases that shows the values of the variables required to calculate Nu [61].

After the Nu number has been calculated we can proceed to calculate h. The convective

Table 3.1: Some of Nusselt number cases

Type	Characteristic	Cases		
Isothermal Vertical Plate	$\alpha = L$ and for ideal gases $\beta = 1/T_{amb}$	$Nu =$	$0.59Ra^{1/4}$	$10^4 < Ra < 10^9$
			$0.1Ra^{1/3}$	$10^9 < Ra < 10^{13}$
Isothermal Horizontal Plate	For upper surface of a hot plate and $\alpha = A/p$	$Nu =$	$0.54Ra^{1/4}$	$10^4 < Ra < 10^7$
			$0.15Ra^{1/3}$	$10^7 < Ra < 10^{11}$
	For lower surface of a hot plate and $\alpha = A/p$	$Nu =$	$0.27Ra^{1/4}$	$10^5 < Ra < 10^{11}$

† The length is L, the surface area for that plate is A and perimeter is p.

heat transfer coefficient is then described as (3.16), in $W \cdot m^{-2}K^{-1}$.

$$h = \frac{kNu}{\alpha} \tag{3.16}$$

where k is the thermal conductivity of air in $W \cdot m^{-1}K^{-1}$.

For each T_{amb} there is a constant h that can be calculated using the Rayleigh number and Nusselt number [59].

Now, if we calculate hs for the five temperatures proposed in the characterization, we have (3.17)

$$hs = (hh \cdot sh) + (2 \cdot hv \cdot sv1) + (2 \cdot hv \cdot sv2) \tag{3.17}$$

where hh is the convective heat transfer coefficient for the upper horizontal plate in $W \cdot m^{-2}K^{-1}$; hv is the convective heat transfer coefficient for the vertical plates in $W \cdot m^{-2}K^{-1}$; sh is the superficial area for the horizontal plate in m^2; sv1 and sv2 are the superficial areas for the two vertical plates also in m^2, if the battery had the same depth and width then sv1=sv2. The result values are shown in Table 3.2.

This calculation can be realized several times at different set points of temperature in order to calculate the convective heat transfer at any ambient temperature.

Table 3.2: hs for electrothermal model

T_{amb} °C	hs $W \cdot K^{-1}$
24	1.4063
0	1.6171
-10	1.7362
-20	1.7592
-30	1.7441

3.1.4 Open Circuit Voltage

Several methods had been proposed to obtain the open circuit voltage (V_{OCV}) [64–70]. Some methods focus on the V_{OCV} in equilibrium by simply using a pulse current [64], for this method usually, the suggested rest time is between 1 h and 3 h for each point measured. However, in literature [65] has been established that using an interpolation between the points, can be reduced the rest time to few minutes. Even in literature, an adaptive V_{OCV} relaxation model was presented to shorten the traditional rest time of several hours for obtaining the V_{OCV} in the equilibrium state [67, 69].

In order to measure the open circuit voltage in our case, it was necessary to impose an pulse current or on-off current. The V_{OCV} was measured every time that the current was interrupted for a period of time, repeating this procedure until the battery was completely

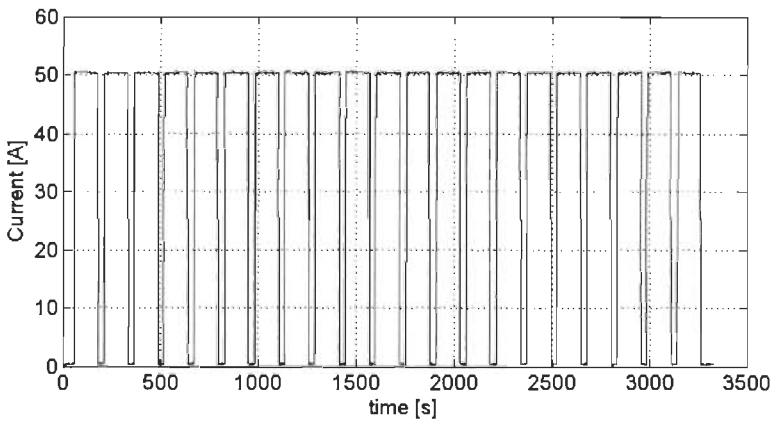

Figure 3.4: Current over time

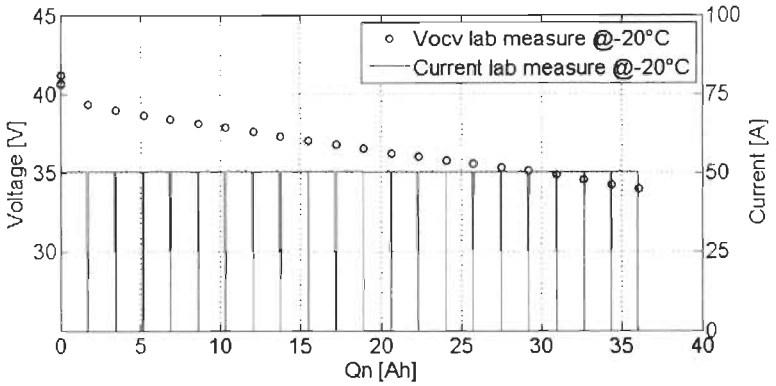

Figure 3.5: Measured current and V_{OCV} at $T_{amb} = -20°C$

discharged. Then, the points were interpolated to obtain a trend curve. As an example, it was taken the $T_{amb} = -20$ °C test.

The current i_B shown in Figure 3.4 is the on-off current imposed by the DL to the battery. This current was 50 A constant when the DL was in on mode and 0 A when the DL was in off mode. Then the voltage is measured and every time the current is zero it is obtained each one of the blue circles shown in Figure 3.5, those blue circles are giving the tendency of the V_{OCV} during the discharge of the battery. The x-axis of Figure 3.5 represents the capacity Q_n in Ah.

3.1.5 Internal Resistance and Heat Capacity

In literature has been used the Recursive Least Squares (RLS) adaptive method for identifying the battery's internal resistance and V_{OCV}, i.e. is an on-line estimation method of the model parameters developed by using an adaptive control approach [71]. However, since our model is based directly on electro thermal equations and we already know the V_{OCV} from previous section, then R_o can be easily estimated by just solving our electrical model equation, i.e. after measuring the voltages V_{OCV} and V_B is possible to calculate R_o with (3.1).

In the other hand, once the R_o has been calculated we can proceed to estimate C_p for the thermal behavior of the battery, just by using the equation (3.10), since all the other

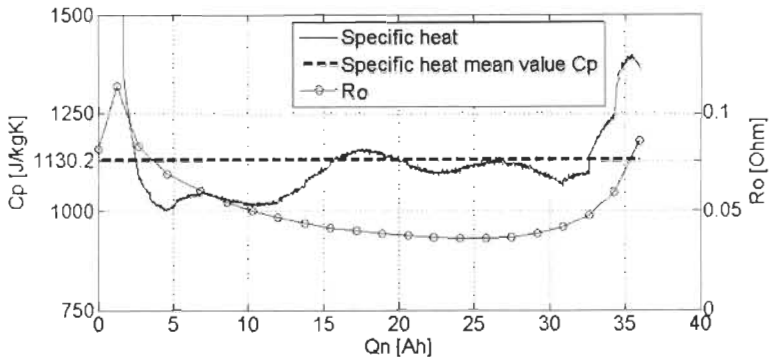

Figure 3.6: Estimated values of Ro and specific heat

parameters are known by now.

When R_o is calculated it presents some drops due to the pulses of i_B and since those are not realistic because the R_o can not be zero, then can be said that the real R_o will be given by the maximum points of the measure, this tendency is shown in the green curve with circles in Figure 3.6, where the circles represent the maximum points of measure and the line between the points is just a linear interpolation between them.

It is possible to calculate C_p, blue curve in Figure 3.6, by replacing R_o in (3.10) and using the temperature that was measured during the test, shown in the blue curve in Figure 3.7.

As can be seen in Figure 3.6, for the specific heat C_p our finding indicates that it is changing due to computational estimations and off course, because the model is just an approximative model, so it does not have a high level of accuracy. Since the specific heat is mostly constant within the range of temperature of interest we compute the mean value of the specific heat as the most representative value of the C_p and because it was the single parameter that has been identified from (3.10), then we can reasonably say that it is close to a real value commonly found in literature [30, 34]. In this order it is possible to obtain the mean value of $C_p = 1130.2\ \mathrm{J \cdot kg^{-1} K^{-1}}$, blue dashed line in Figure 3.6.

The only way to assume that R_o is the real value can be justified by calculating the temperature of the battery using (3.10), this gives as result the green curve presented in Figure 3.7. It can be seen as result an acceptable matching between estimated and measured temperature, this is traduced in an error inferior to 1.58 %.

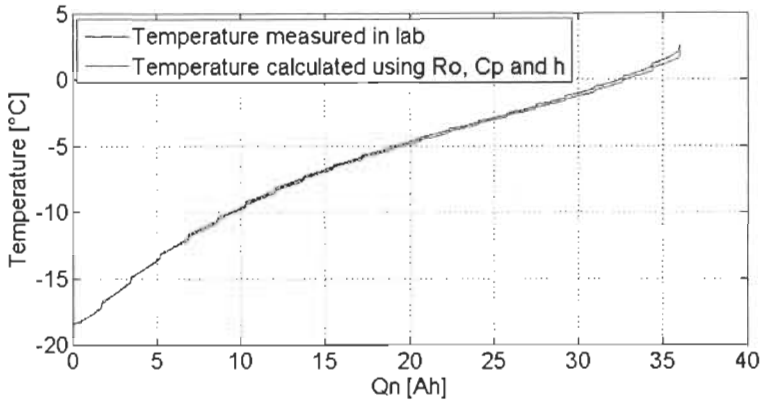

Figure 3.7: Battery temperature

Finally, it is necessary to say that the only two variables that can change due to the ambient temperature will be the R_o and h and they will have to be estimated every time T_{amb} changes. Now, the C_p, m, s are the only values from (3.10) that will be constant and they will not change due to the ambient temperature.

3.2 Residual Energy

The coulomb counting is frequently used to estimate the SOC and the SOC is expressed as in (3.18)

$$SOC = SOC_0 - \int \frac{i_B}{C_{ini}} dt \tag{3.18}$$

where C_{ini} is the initial capacity measured of the battery in Ah and SOC_0 is the initial state-of-charge of the battery. However as literature explains, the SOC estimation always is a considerable problem in all models [72, 73]. It is always necessary to have either a more complex electrochemical model [34] or simply it can be taken into account the thermal losses of the battery to have an approximative estimation of the residual energy of the battery.

The following subsections will explain how can be estimated this residual energy with a simple method; then, using a more powerful method will allow to estimate the residual energy for any ambient temperature; and at last but not least, will be shown some driving profiles of the snowmobile and the residual energy will be estimated accordingly.

3.2.1 Simple Residual Energy Estimation

Since in previous section were defined and estimated the parameters of the electrothermal model formed by (3.1) and (3.10) for the five ambient temperatures proposed in Chapter 2, then we can use those values to determine the residual energy (RE) of the battery.

It is frequent to find in literature how authors use the internal resistance of the battery to estimate the RE. For instance [74] estimates the RE using the dynamic measured on-line terminal voltage, internal resistance and current. Their estimation technique combines the indirect and direct methods.

In our case we used a direct method by simply using the energy estimation of Chapter 2

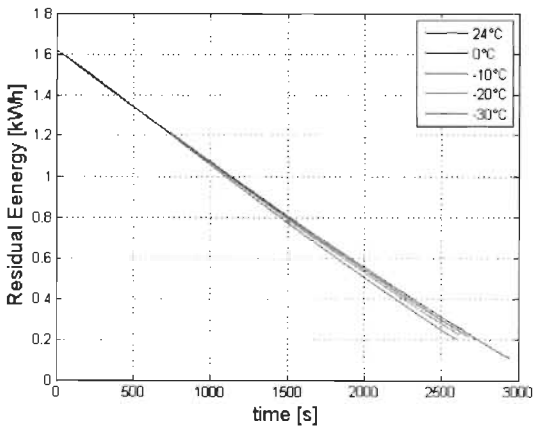

(a) With 50 A discharge current

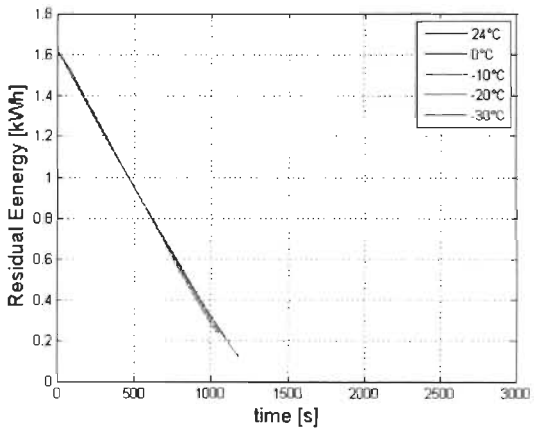

(b) With 125 A discharge current

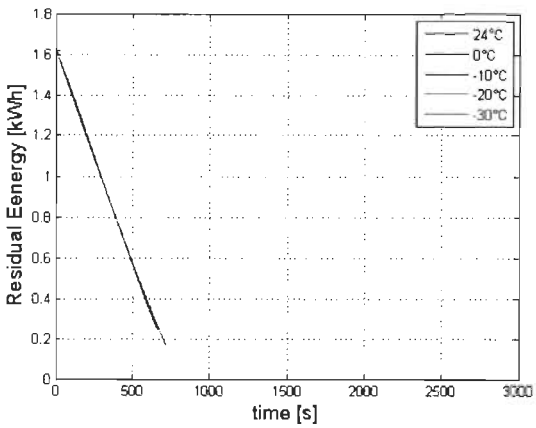

(c) With 200 A discharge current

Figure 3.8: Residual energy curves

Table 3.3: Discharge energy comparison

	24 °C		0 °C		-10 °C		-20 °C		-30 °C	
	W	$W+W_{th}$	W	$W+W_{th}$	W	$W+W_{th}$	W	$W+W_{th}$	W	$W+W_{th}$
50 A	1.498	1.513	1.315	1.372	1.320	1.405	1.265	1.397	1.234	1.424
125 A	1.462	1.499	1.310	1.404	1.238	1.382	1.184	1.379	0.003	0.003
200 A	1.400	1.453	1.251	1.375	1.205	1.372	0.006	0.006	0.004	0.004

† The energy of the battery given by the manufacturer is 1.620 kWh. All values in this table are given in kWh

and adding the thermal losses from (3.10). Then we have (3.19)

$$\mathrm{RE} = W_o - (W + W_{th}) \tag{3.19}$$

where $W_o = 1.62$ kWh is the maximum energy capacity that can be obtained from the battery given by the manufacturer and $W_{th} = \mathrm{R_o i_B^2}$ is the energy expended due to thermal losses. Then, (3.19) can be expressed as (3.20) if we replace all known parameters obtained so far.

$$\mathrm{RE} = W_o - \int (\mathrm{V_B(t)} \cdot \mathrm{i_B(t)} + \mathrm{R_o(t)} \cdot \mathrm{i_B^2(t)}) dt \tag{3.20}$$

here RE will be in kWh.

Now, as an example it was calculated the RE of the five ambient temperatures presented in Chapter 2 for the 50 A, 125 A and 200 A constant current discharge, obtaining as result what is shown in Figure 3.8.

As it was said in Chapter 2, a comparison will be made between the energy estimation made in that chapter and the energy estimation made in this section were W_{th} is included.

In Table 3.3 is shown this results comparison. There was an average increment of 0.108 kWh in the energy measured due to adding W_{th}.

If it is desired to estimate the RE for any ambient temperature with a given main current, then it is necessary to use a more robust and complex method that can be based on the direct method previously presented. This will be explained in the following Section 3.2.2.

3.2.2 Residual Energy With Trained Algorithm

As it was said before in Section 3.1.5, there is only two variables that can change due to the ambient temperature the R_o and h and they will have to be estimated every time T_{amb} changes. However, since they were already estimated for the five temperatures of the characterization and the RE was already estimated for this five temperatures using the direct method, then they can be used as training curves for a trained method like Artificial Neural Networks (ANN) [9, 75–79] to estimate the RE in any ambient temperature.

In literature, several authors had used the ANN to estimate the energy, residual energy, the state of health (SOH) or the SOC of batteries [9, 75, 76, 80–82], but the temperature is not usually taken as a main input for the ANN. However, we are giving more importance to temperature since our model is based in a electrothermal model and, as said before, the ANN can be trained using the RE that was estimated with the direct method.

Based on [9, 77, 80, 81] our ANN will be a feed-forward back-propagation, Levenberg-Marquardt Algorithm (LMA) [76, 83–85] based model. The problem for the LMA, as for many fitting algorithms, is that it may find only a local minimum, which is not necessarily the global minimum [84]. This is in an open-loop model called nonlinear input-output (NIO) model that uses the measured V_B and T as inputs. The block diagram for the model with k neurons in the hidden layer, n input neurons and one output neuron are shown in Figure 3.9.

Feed-forward back-propagation network (FBN) configuration is considered as a good

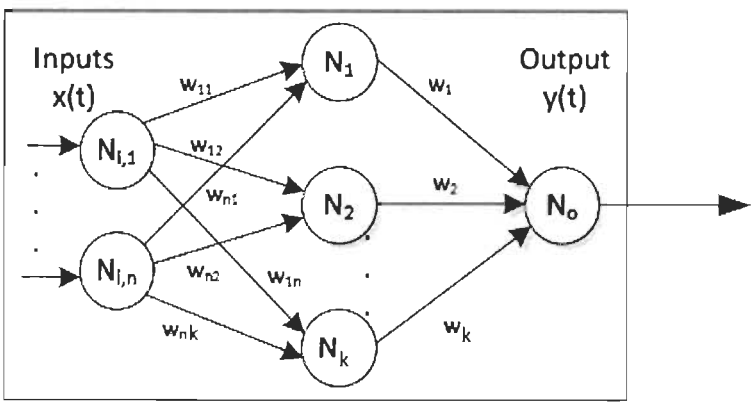

Figure 3.9: A block diagram of the ANN model [9]

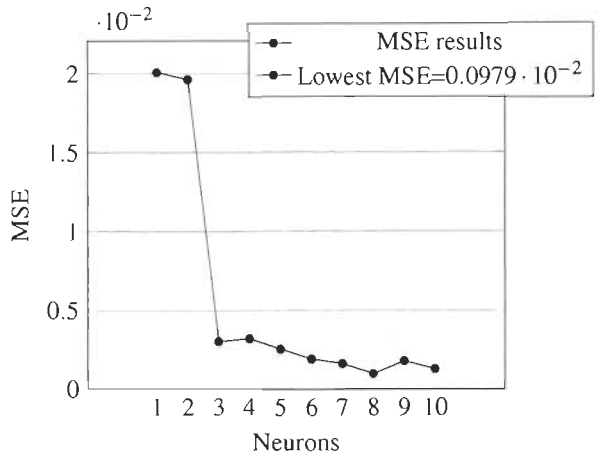

Figure 3.10: ANN - MSE for neurons in the hidden layer

nonlinear function approximate [78, 79, 86, 87] and according to [86], the optimal configuration of FBN for parameters identification has two layers: a hidden layer and an output layer.

It has been proven in [86] that feed-forward ANN configurations in predictor mode and trained with a back-propagation algorithm are suitable for process identification. In our study, we use this configuration and set the number of layers to two. This initial configuration is over sized with ten neurons on the hidden layer and one neuron on the output layer, the number of neurons in the hidden layer will be changed in order to obtain the best training result. Then the mean square error (MSE) [77] will be calculated for each training with every amount of neurons in the hidden layer in order to know which one is the best training result. As it is shown in Figure 3.10, if the results of the MSE for every amount of neurons in the hidden layer are too low or too high, then the MSE is high and this is why there is no purpose in using less than 3 neurons or more than 11 neurons. It also seen that the best result is for k=8 neurons.

The activation functions are the hyperbolic tangent and linear transfer functions, respectively, for the hidden and output layers. To complete this configuration we used two inputs and one output for the ANN:

- One input for the matrix that contains the five vectors of voltage measured in five

different ambient temperatures

$V_B(t) = [V_{B_{23}}(t),\ V_{B_0}(t),\ V_{B_{-10}}(t),\ V_{B_{-20}}(t),\ V_{B_{-30}}(t)]$

- One input for the matrix that contains the five vectors of temperature of the battery measured also in five different ambient temperatures

  $T(t) = [T_{23}(t),\ T_0(t),\ T_{-10}(t),\ T_{-20}(t),\ T_{-30}(t)]$

- One output for the matrix that contains the five vectors of residual energy in the battery registered in five different ambient temperatures

  $RE(t) = [RE_{23}(t),\ RE_0(t),\ RE_{-10}(t),\ RE_{-20}(t),\ RE_{-30}(t)]$

Then we have, in continuous-time domain:

$$x_1(t) = V_B(t) \tag{3.21}$$

$$x_2(t) = T(t) \tag{3.22}$$

$$y(t) = RE(t) \tag{3.23}$$

were $V_B(t)$ is given by direct measure and represented as (3.1), $T(t)$ is given by direct measure and represented as (3.10) and $RE(t)$ depends of $(V_B(t), i_B(t), R_o(t))$ and is given by (3.20). In discrete-time domain:

$$x_{1,j} = V_{B_j} \tag{3.24}$$

$$x_{2,j} = T_j \tag{3.25}$$

$$y_j = RE_j = W_{o_j} - (W_{j-1} + (V_{B_j} \cdot i_{B_j})\Delta t + W_{th_{j-1}} + (R_{o_j} \cdot i_{B_j}^2)\Delta t) \tag{3.26}$$

where j is the time index, t is time. As can be seen, for the input neurons we have n=2.

Now that are known the inputs, the output and the amount of neurons in the hidden layer we can proceed with the training of the ANN. As mentioned before, the training was performed with the Levenberg-Marquardt Algorithm (LMA) using the five curves of RE ob-

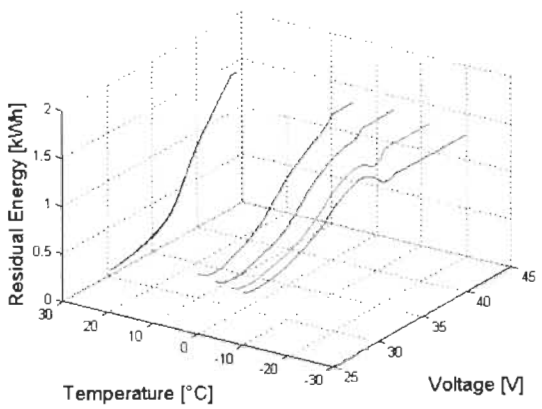

(a) For 50 A

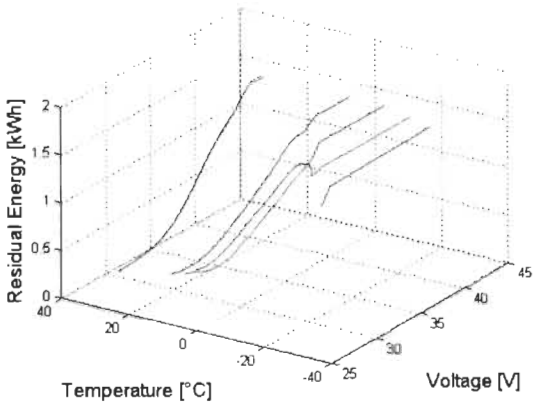

(b) For 125 A

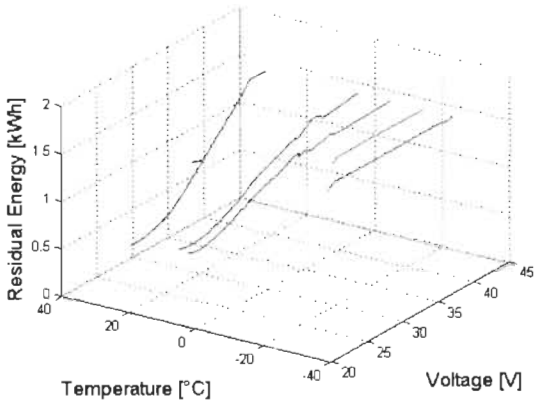

(c) For 200 A

Figure 3.11: ANN training curves

tained in Section 3.2.1 for the three currents discharge. This training curves are shown in Figure 3.11, here they were plotted in a 3D space formed by V_B in the x-axis, T in the y-axis and RE in the z-axis. It can be appreciated the decreasing behavior of the residual energy when the voltage drops and the temperature increases.

If we take as example the 50 A discharge, the we have that the training progress and the performance of the ANN for 8 neurons in the hidden layer took only took 80 iterations for the algorithm to converge and a total training time of 11 seconds, which is a very good result for the requirement of the application. The best validation performance is located at the iteration number 74 and with a MSE value shown in Figure 3.10 for 8 neurons.

The data given to the inputs and the output for training is normalized in order to obtain better and more accurate results.

After obtaining good training results for the five curves, it is time to see if the ANN can calculate the residual energy for every single point of voltage and temperature proposed randomly. In order to see this result it is necessary to plot a mesh of the residual energy for any value of voltage and any value of temperature.

It can be seen that the results are satisfactory for the estimation of the residual energy in Figure 3.12, because the behavior of the mesh curves are close to the behavior of the single curves presented in Figure 3.11. This can also be verified by looking at the regressors, they tend to 1, i.e. it is a good fit, see Figure 3.13.

If we compare this ANN method to the previous method, we see that the ANN method do not allow us to obtain a RE in real time (it is necessary to be off-line). However the big advantage is that the ANN allows to have the temperature as input directly while in the direct

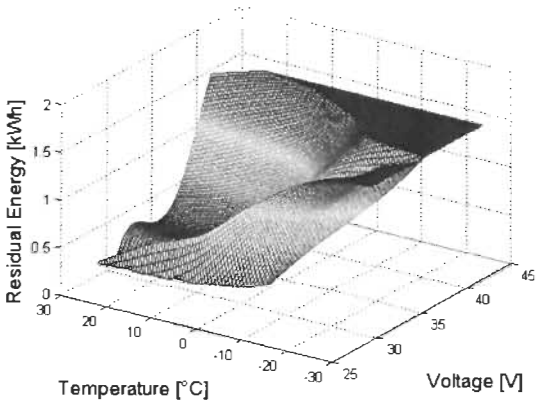

(a) For 50 A

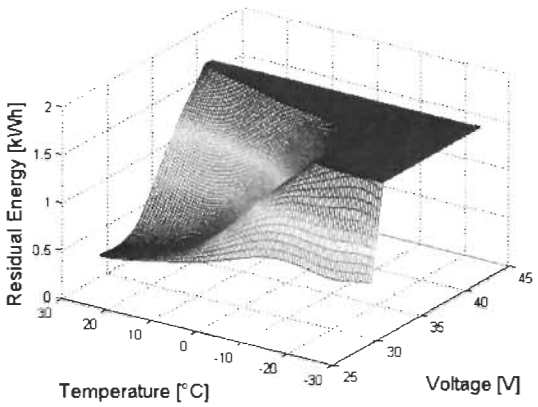

(b) For 125 A

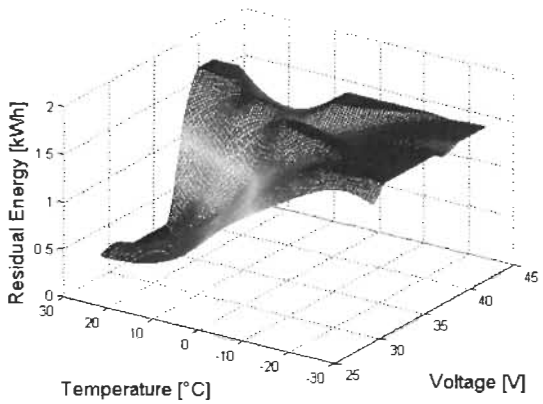

(c) For 200 A

Figure 3.12: ANN mesh result

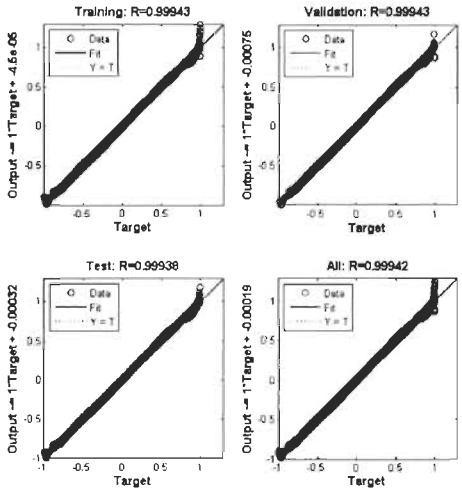

(a) For 50 A

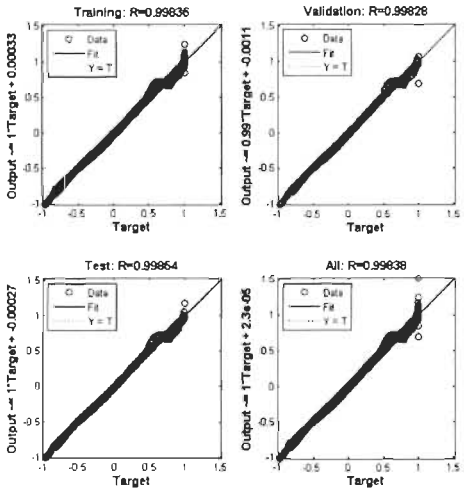

(b) For 125 A

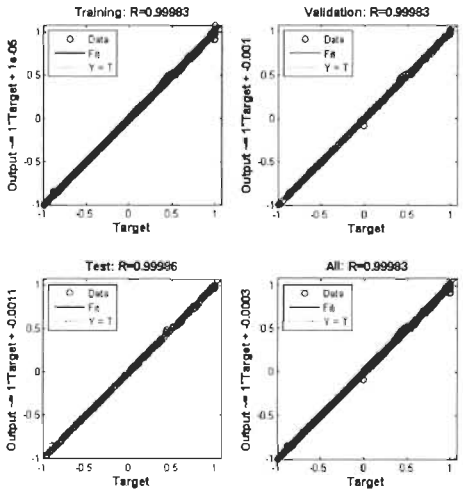

(c) For 200 A

Figure 3.13: ANN regression results

method the temperature is not directly measured to do the RE estimation.

3.3 End of Discharge Time

Predicting the end of discharge (EOD) time for Li-ion batteries is one of the most important problems in the field of battery health management. Several authors had worked in this issue before [88–91].

In literature [88], they propose a linear regression model to describe the relationship between the end of discharge time and discharge cycle, their model verification shows that the discharge cycle has significant effect on the end of discharge time. While others [89], study the Lithium-ion battery EOD time prediction problem under the particle filtering (PF) algorithm framework. The work voltage degradation process with six states is formulated by the nonlinear state-space model, and the states such as unknown model parameters and work voltage are estimated by PF algorithm. In particular, they discuss how to choose appropriate parameters in PF algorithm to improve its performance in predicting EOD time. Another approach [91] uses a statistical characterization of battery with profiles to estimate the SOC, and predict the discharge time of Li-ion batteries.

Now for our case, it was set as a contribution of this work to develop a new efficient approach to estimate the EOD time. In order to do so, it was simply used the variance of the current and the residual energy obtained from the method exposed in the previous section. In this order, to estimate the EOD time it was defined the following methodology:

3.3.1 Driving Profile

The snowmobile was driven for a period of 158 seconds or 2.63 minutes and during this time was obtained a recording of the current sensor, see Figure 3.14. This snowmobile current profile (SCP) has a mean current of 50 A.

With the help of this SCP, there were created three other profiles to simulate the full discharge of the battery. In Figure 3.15 are shown the three profiles that were given to the DL to perform the discharge, the figure also shows the voltage of the battery measured during each discharge and the residual energy estimated using the method explained in the previous section. The three experimental tests were made under an ambient temperature of $T_{amb} = -20$ °C. The three profiles were designed in a way that the mean current was always 50 A, this to compare the effect of the current amplitude on the energy consumption.

For the first profile, it begins with a constant current of 50 A and after 1000 seconds it

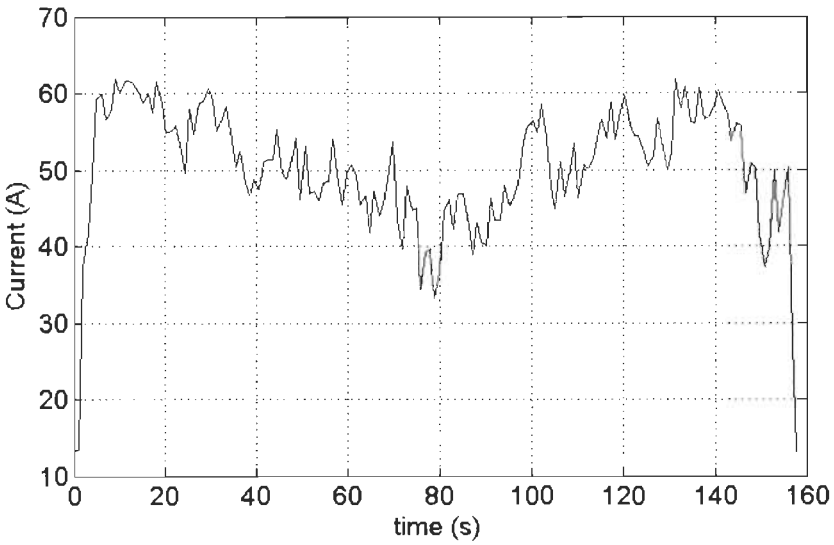

Figure 3.14: Current profile of the snowmobile

was repeated the SCP several times until the battery is completely discharged, for us this will be called the low amplitude current (LAC), see Figure 3.15a. For the second profile, it begins with a constant current of 50 A and after 1000 seconds it was repeated the SCP several times, but now with an amplitude of 1.5 times the original amplitude of the SCP until the battery is completely discharged, for us this will be called the medium amplitude current (MAC), see Figure 3.15b. For the third profile, it was made the same thing of the second profile, but now with an amplitude of 2 times the original amplitude of the SCP until the battery is completely discharged, for us this will be called the high amplitude current (HAC), see Figure 3.15c.

As we can see, it will not matter if the current amplitude is higher or lower, what matters is to maintain the same mean current in order to have practically the same residual energy of the battery at the end of discharge.

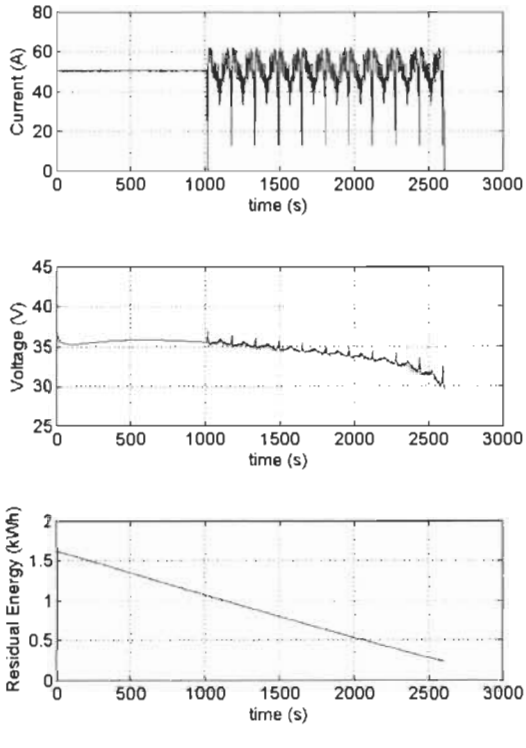

(a) Low amplitude current discharge

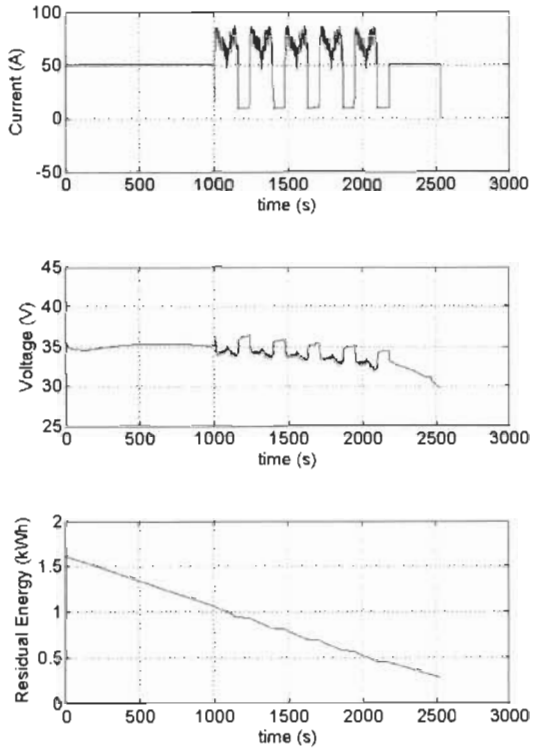

(b) Medium amplitude current discharge

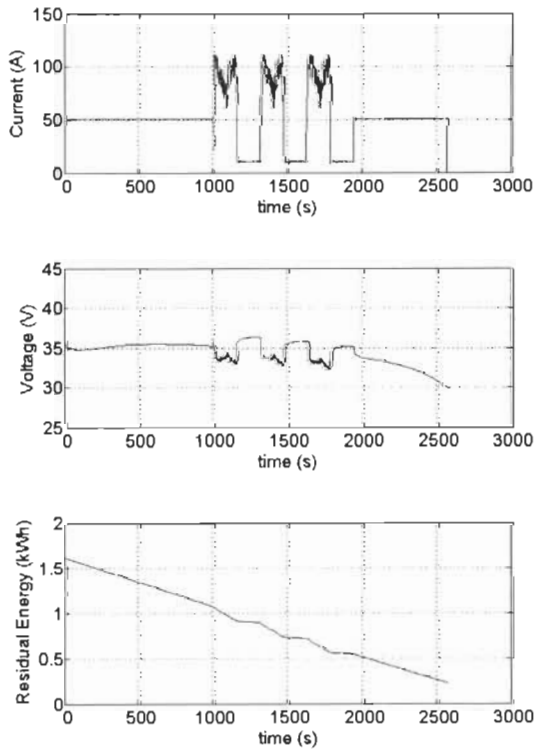

(c) High amplitude current discharge

Figure 3.15: Driving profiles with $i_{B_{mean}} = 50$ A and $T_{amb} = -20$ °C

3.3.2 Current Variance and Residual Energy

About a new approach to estimate the EOD time, it was thought that having a relation between the variance of the current and the residual energy at the end of the discharge will allow to estimate the EOD time in a faster and much simpler way.

From the three profiles presented in the preceding section, it is possible to calculate the variance of the current. This variance (Var) was given by (3.27)

$$\mathrm{Var} = \frac{1}{N-1}\sum_{j=1}^{N} |i_{B_j} - \mu|^2 \tag{3.27}$$

where N is the number of observation samples in the past and μ is the mean of the current i_B given by (3.28)

$$\mu = \frac{1}{N}\sum_{j=1}^{N} i_{B_j} \tag{3.28}$$

Off course, if i_B is constant, then the variance will be zero.

If the estimated RE at the end of the discharge is plotted versus the variance of the current for the complete discharge (Final Residual Energy - FRE), then we obtain the blue mark points of Figure 3.16. There we have the three variance of the driving profiles and the Var = 0 of the constant current profile presented in Chapter 2 for the 50 A current.

The purple curve that crosses through the blue marks is a curve fitting of third degree.

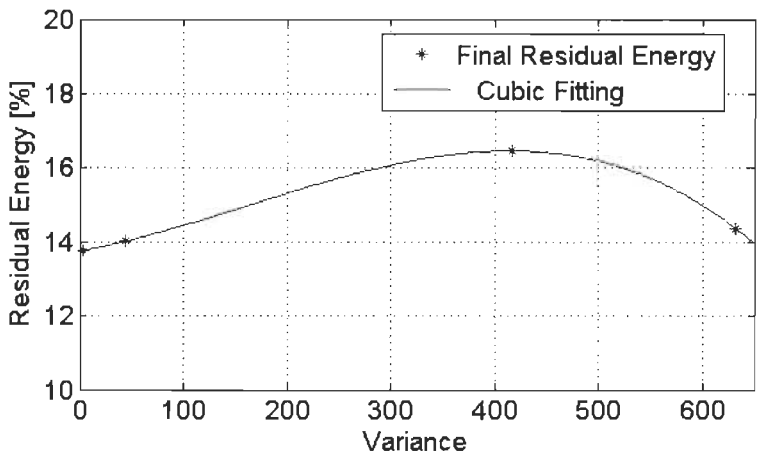

Figure 3.16: Variance Vs Residual Energy

The cubic fitting curve of the final residual energy in percentage of the total energy given by the manufacturer versus the variance is described by (3.29)

$$FRE = a \cdot Var^3 + b \cdot Var^2 + c \cdot Var + d \tag{3.29}$$

where $a = -4.5076 \cdot 10^{-8}$, $b = 2.1611 \cdot 10^{-5}$, $c = 5.3435 \cdot 10^{-3}$, $d = 13.744$ are constants.

Now, it has been defined an equation to have the FRE as dependent variable of the variance, this will allow to have an approximation of the FRE at any time during the discharge and therefore it will be possible to estimate the EOD time.

3.3.3 EOD Time Results

As said in the precedent section, in order to obtain the EOD time, it was calculated every sample time (every 1000 ms) the variance and then it is estimated the FRE during the discharge of the battery. For this work, every sample time that the Var and FRE are calculated, it is called iteration and will be represented with the subindex m. Then, we have for every sampled time a Var_m and a FRE_m.

The best way to explain the estimation of the EOD time is with the algorithm itself. This algorithm is shown in Table 3.4. First are set the initial values and restrictions of the discharge; then, is specified the type of discharge to be made, but off course in this case we know it will be performed the driving profile; after that, we start getting the readings from the input values and the discharge can start; once the discharge starts, the algorithm begins to count the iterations, estimates the Var_m and FRE_m; then, it is taken the measured data of the inputs from 1 to j and added to the vectors of current, voltage and temperature several times until the estimated RE_m is lower than the expected FRE_m, when this happens the EOD time is estimated for that iteration; then, the EOD time is saved and the algorithm continues with next iteration until the battery is completely discharged. The estimated EOD time of the last iteration should be the same as or at least close to the EOD time measured.

Table 3.4: EOD time algorithm

Algorithm 2. EOD time estimation.

Set

- Restriction values $V_{B_{min}}$ and T_{max}
- RE_0 initial residual energy in %, this will be the reference for all iterations
- Iteration m=0

Specify

- Type of discharge for i_B: Driving current profile or constant current profile

Inputs

- $V_{B_{j,m}}, i_{B_{j,m}}, T_{j,m}$ voltage, current and temperature of the battery, respectively

1: **Initialization of elapsed time t to zero**
2: Start discharge
3: m=m+1
4: Calculate $Var_m(i_{B_{1:j,m}})$
5: Estimate $FRE_m(Var_m)$
6: Repeat and add set of data to vectors $V_{B_{j,m}}, i_{B_{j,m}}, T_{j,m}$
7: Estimate RE_m
8: Compare if $V_{B_{min}} <= V_B$ if yes continue to step 9, if not then save EOD time and continue to step 10
9: Compare if $RE_m >= FRE_m$, if yes go back to step 6, if not then save EOD time and go back to step 3
10: End of discharge

Figure 3.17 shows the calculated Var_m and the estimated FRE_m for the three driving profiles, where Figure 3.17a is for the low amplitude current profile, Figure 3.17b is for the medium amplitude current profile and Figure 3.17c is for the high amplitude current profile.

Figure 3.18 shows the measured and the estimated EOD times with the relative error between the measured and the estimation for the three driving profiles, where Figure 3.18a is for the low amplitude current profile with a maximum relative error of 2.05 % and a final relative error of 0.43 %, Figure 3.18b is for the medium amplitude current profile with a maximum relative error of 3.35 % and a final relative error of 1.00 % and Figure 3.18c is for the high amplitude current profile with a maximum relative error of 8.41 % and a final relative error of 0.96 %.

This means that since the relative error is low, then it can be said that the EOD time estimation algorithm is accurate enough to use it in real applications.

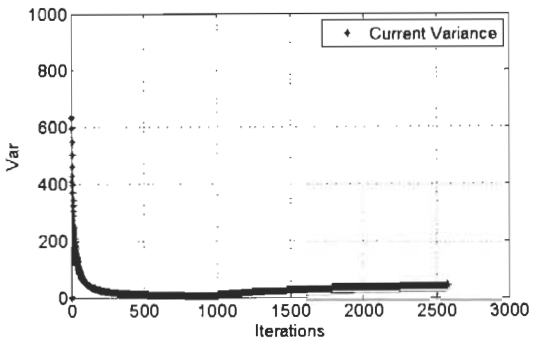

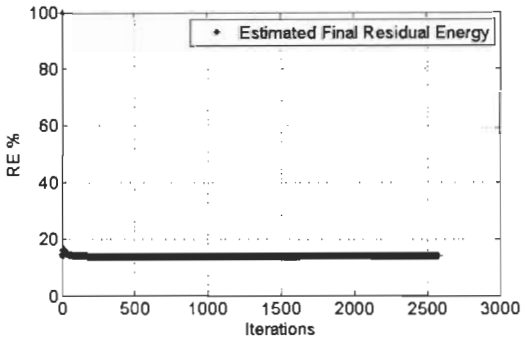

(a) Low amplitude current discharge

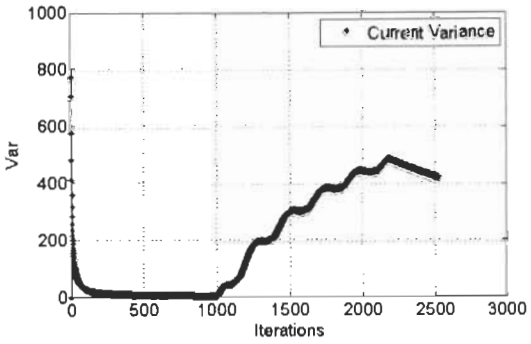

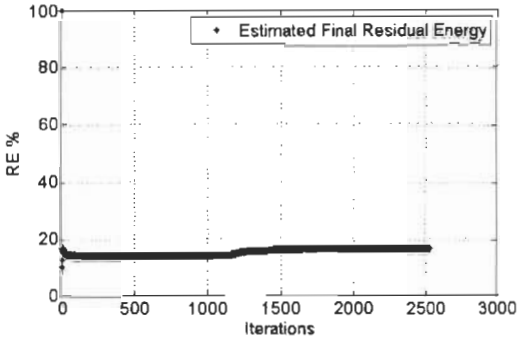

(b) Medium amplitude current discharge

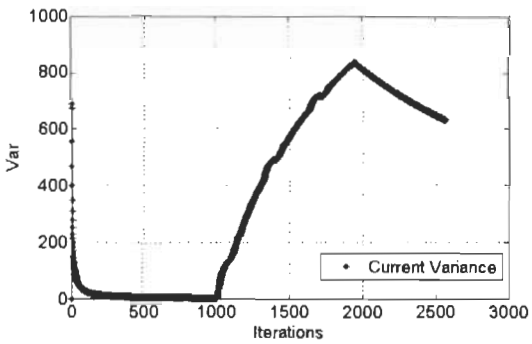

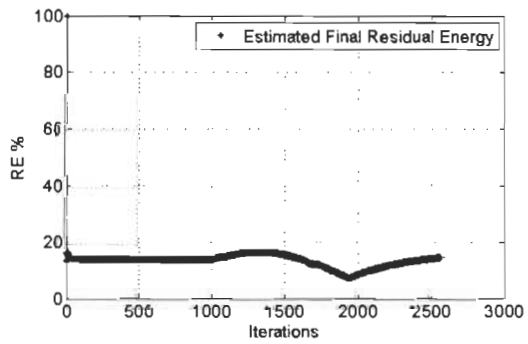

(c) High amplitude current discharge

Figure 3.17: Variance and FRE with $T_{amb} = -20$ °C

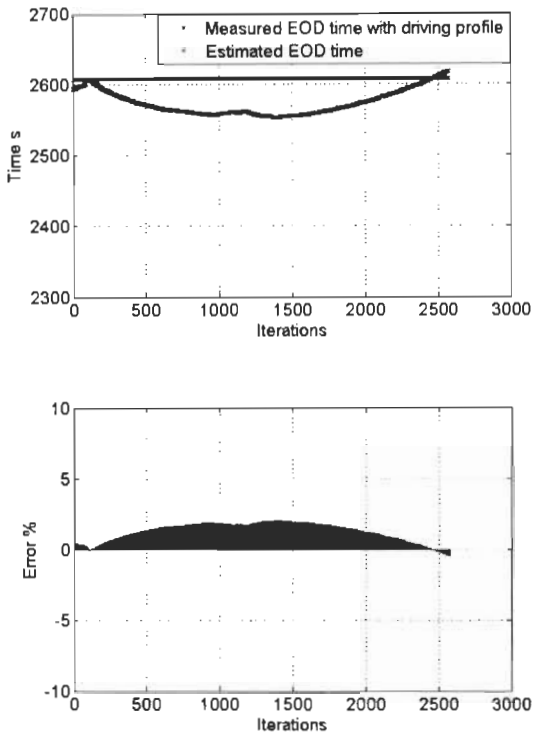

(a) Low amplitude current discharge

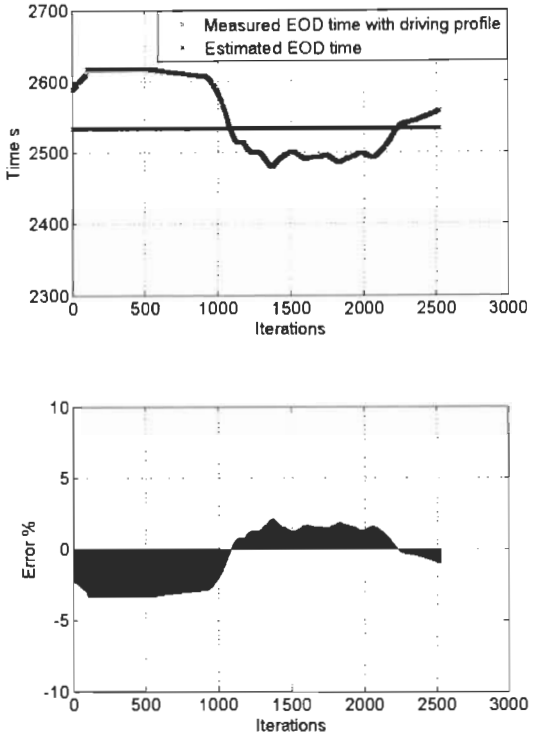

(b) Medium amplitude current discharge

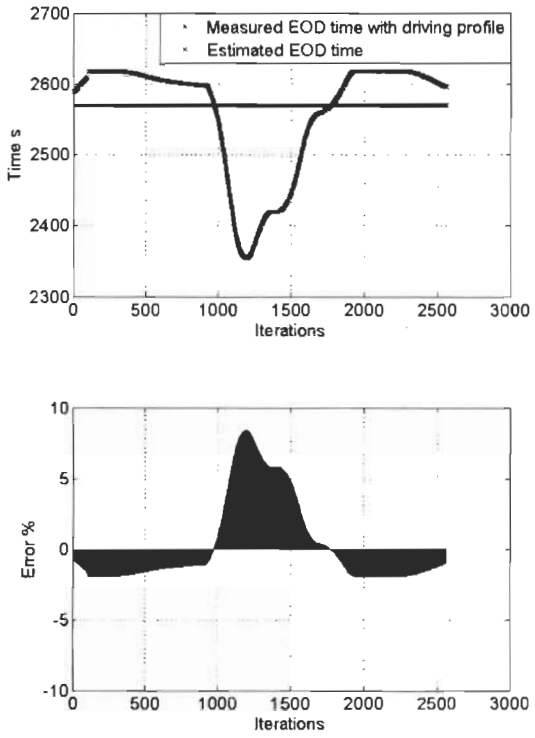

(c) High amplitude current discharge

Figure 3.18: EOD time estimation with $T_{amb} = -20$ °C

3.4 Conclusion

This chapter presented an electrothermal model with a simple experimental method to identify its internal resistance and the specific heat of the battery. This was made by measuring the open circuit voltage through time and estimating the other parameters using thermodynamic equations.

The chemical dynamics and the relaxation effect of the battery have been neglected in this proposed model, then accordingly no conclusions on that field have been made. The specific heat of the battery was estimated accordingly to literature results giving a reasonable mean value of the specific heat as the most representative value. The results were validated by comparing them with experimental results obtained in controlled tests in the lab.

A simple and efficient method was presented to estimate the residual energy of the battery. This by adding the thermal losses to the energy estimation. This allowed a more precise approximation of the residual energy than the simple coulomb counting,

The artificial neuronal network was implemented based on the voltage temperature and residual energy previously estimated for certain ambient temperatures. It was successfully trained in each stage of the methodology suggested. It shows a good convergence with a very acceptable mean squared error result and good regressors approximation to 1. As expected, the ANN does work to generalize and calculate the residual energy in the battery for each data input of tension and temperature. If the ANN is trained with more experimental curves, it will show better results in the MSE and will show a smoother and precise curve of the residual energy mesh.

The EOD time estimation was presented and implemented. This by relating the variance of the current and the final residual energy. The results for this method were successful, giving a low relative error between the measurement and the estimation of the EOD time.

In Chapter 4 will be found the general conclusions and future perspectives of this work.

Chapter 4

General Conclusions and Perspectives

This chapter summarizes the main achievements and offer the perspectives of the contributions. The possible deepening of research given by this work are many, it will be mention the most promising avenues for future work.

Through this work was increased the energy efficiency by allowing the system and the user to have a better acknowledgment of the energy consumption of the battery pack and the available discharge time for the battery when the EV is exposed to low temperature conditions, which at the end was reflected in the improvement of battery's life time.

In Chapter 2 were explained the basics of batteries. That explanation got us into the characterization of the battery, in which the test bench design and its components were explained. Then, the battery charge profile was introduced and explained. After that, as main core of this chapter the discharge algorithm was explained and all the discharge tests were performed under the low temperatures proposed.

With the results presented it was seen the big change in the discharge time due to the current, but the temperature did not have a big impact in this matter. On the other hand, for the voltage drop was not the same case. This voltage drop caused by the behavior of the internal resistance of the battery had a big magnitude increase due to low temperatures. With low temperatures the operating voltages are reduced because a cold environment lengthens the diffusivity of Li+ inside the cell. This makes that the possible energy to be subtracted

from the battery be inferior to energy subtracted under optimal ambient temperatures.

Chapter 3 allowed us to show the main core of the methodology proposed for this work. It was developed a strategy and algorithm that contemplated an efficient and optimal method to joint the thermal and electrical equations that rule the battery model, the impact of outdoor temperature on the thermal evolution of the pack was taken into account and also the operating constraints imposed by the battery energy management system were implemented. Furthermore, different heat exchange phenomena that occur in the pack was considered to increase the performance of the energy estimation algorithm.

It was analyzed and developed a simple method to identify the internal resistance, the specific heat and the heat capacity of the battery by measuring the open circuit voltage through time.

It was estimated the residual energy in the pack by using a trained method and a direct method allowing to process the data in real time. This by adding the thermal losses to the energy estimation. This allowed a more precise approximation of the residual energy than the simple coulomb counting. The artificial neuronal network was implemented based on the voltage temperature and residual energy previously estimated for certain ambient temperatures. It was successfully trained in each stage of the methodology suggested. The ANN does work to generalize and calculate the residual energy in the battery for each data input of voltage and temperature.

It was implemented an algorithm to allow the on-line estimation of the EOD time of the battery pack by simply relating the variance of the current and the final residual energy. The results for this method were successful, giving a low relative error between the measurement and the estimation of the EOD time.

The perspectives for future work are several, however, here are presented some of the possible research paths that can be taken by using the results of this memory:

1. Getting the resulting electrothermal model with the internal resistance and specific heat capacity by implementing the measure of the open circuit voltage can be of great use to predict the internal temperature behavior of the battery due to changes given by variable currents, which at the end it will be traduced in having a better control of the thermal losses;

2. For future work it could be interesting to implement a model to manage the energy of the battery to perform the cold start of the EVs, for instance, using the residual energy that is estimated during the discharge, the model could define the best and most efficient energy splitting for the systems of the EV and even a battery heat pad;

3. The implementation of a heat pad that allows to have a better control of the thermal losses of the battery but seeking at the same time not loose all the residual energy of the battery on the pad;

4. From the EOD time estimation, it would be interesting to compare all the EOD times during several amount of cycles at different ambient temperatures through the complete life of the battery. This will give a better idea of the degradation of the battery due to temperature and life cycling, which can be used to implement prognosis of the state of health of the battery.

5. Implementing the use of the residual energy estimation and the EOD time can provide a more efficient and precise system of information for the user of the EV.

Bibliography

[1] Environment Canada, "National Inventory Report 1990-2012: Greenhouse Gas Sources and Sinks in Canada - Executive Summary," Canadian Government, Tech. Rep., 2014. [Online]. Available: http://ec.gc.ca/ges-ghg/3808457C-9E9E-4AE3-8463-05EE9515D8FE/NIR2014-ExecSum-Web-Final.pdf

[2] X. Chen, W. Shen, T. T. Vo, Z. Cao, and A. Kapoor, "An overview of lithium-ion batteries for electric vehicles," in *2012 10th International Power & Energy Conference (IPEC)*. IEEE, nov 2012, pp. 230–235. [Online]. Available: http://ieeexplore.ieee.org/lpdocs/epic03/wrapper.htm?arnumber=6523269

[3] M. Allen, "Cold Weather Fuel Efficiency : Electric Versus Gasoline Showdown," p. 1, 2014. [Online]. Available: http://www.fleetcarma.com/cold-weather-fuel-efficiency/

[4] "Canadian Climate Normals 1981-2010 Station Data," sep 2013. [Online]. Available: http://climate.weather.gc.ca/climate_normals/results_1981_2010_e.html?stnID=5201&lang=e&dCode=1&province=QUE&provBut=Go&month1=0&month2=12

[5] J. de Santiago, H. Bernhoff, B. Ekergård, S. Eriksson, S. Ferhatovic, R. Waters, and M. Leijon, "Electrical Motor Drivelines in Commercial All-Electric Vehicles: A Review," *IEEE Transactions on Vehicular Technology*, vol. 61, no. 2, pp. 475–484, feb 2012. [Online]. Available: http://ieeexplore.ieee.org/xpls/abs_all.jsp?arnumber=6093982

[6] E. W C Lo, "Review on the configurations of hybrid electric vehicles," in *2009 3rd International Conference on Power Electronics Systems and Applications*, 2009, pp. 1–4. [Online]. Available: http://repository.lib.polyu.edu.hk/jspui/handle/10397/1548

[7] Summit Station, "Facility Temperatures at Summit Station," 2016. [Online]. Available: http://www.summitcamp.org/status/environmental/?period=year

[8] CrossChasm, "CrossChasm Electric Snowmobile," 2013. [Online]. Available: http://www.crosschasm.com/crosschasms-stealth-snowmobile-loki/dsc_0100_small_wtext/

[9] A. a. Hussein, "Capacity fade estimation in electric vehicles Li-ion batteries using artificial neural networks," in *2013 IEEE Energy Conversion Congress and Exposition*, no. 2. IEEE, sep 2013, pp. 677–681. [Online]. Available: http://ieeexplore.ieee.org/lpdocs/epic03/wrapper.htm?arnumber=6646767

[10] G. Duleep, H. van Essen, B. Kampman, and M. Grunig, "Impacts of Electric Vehicles - Deliverable 2 Assessment of electric vehicle and battery technology," Delft, p. 68, 2011. [Online]. Available: http://ec.europa.eu/clima/policies/transport/vehicles/studies_en.htm

[11] National Research Council, *Advancing the Science of Climate Change*. National Academies Press, 2010. [Online]. Available: http://dge.stanford.edu/labs/caldeiralab/Caldeira_research/pdf/ACC_Science_2010.pdf

[12] R. Pool, "The sweetest solution [biofuel vehicles]," *Power Engineer*, vol. 20, no. April-May, pp. 12–17, 2006. [Online]. Available: http://ieeexplore.ieee.org/stamp/stamp.jsp?tp=&arnumber=1637908&isnumber=34334

[13] W. Matters, "The MIT Energy Initiative's Symposium on Electrification of the Transportation System," *Electrification of the Transportation System*, p. 156, 2010. [Online]. Available: http://www.eenews.net/assets/2011/01/14/document_gw_03.pdf#page=15

[14] N. Vachon, "Electric vehicle charging," p. 2, 2013. [Online]. Available: http://news.hydroquebec.com/media/filer_private/2013/11/28/fiche_dinformation_recharge_vfinaleang.pdf

[15] NathalieVachon, "Highlights Field testing of 30 all-electric vehicles," p. 2, 2013. [Online]. Available: http://news.hydroquebec.com/media/filer_private/2013/11/28/fiche_dinformation_programme_dessai_boucherville_vfinaleang.pdf

[16] Vachon-Nathalie, "Quebec's first quick-charge station for electric vehicles is now in service," p. 2, 2013. [Online]. Available: http://news.hydroquebec.com/en/press-releases/474/quebecs-first-quick-charge-station-for-electric-vehicles-is-now-in-service/#.UwyeEuNdVAY

[17] S. Dhameja, *Electric Vehicle Batteries*, 1st ed. Elsevier, 2002, no. Book. [Online]. Available: http://store.elsevier.com/product.jsp?isbn=9780750699167&pagename=search

[18] T. M. Bandhauer, S. Garimella, and T. F. Fuller, "A Critical Review of Thermal Issues in Lithium-Ion Batteries," *Journal of The Electrochemical Society*, vol. 158, no. 3, p. R1, 2011. [Online]. Available: http://jes.ecsdl.org/content/158/3/R1.short

[19] S. Zhang, K. Xu, and T. Jow, "The low temperature performance of Li-ion batteries," *Journal of Power Sources*, vol. 115, no. 1, pp. 137–140, mar 2003. [Online]. Available: http://linkinghub.elsevier.com/retrieve/pii/S0378775302006183

[20] Y. Ji and C. Y. Wang, "Heating strategies for Li-ion batteries operated from subzero temperatures," *Electrochimica Acta*, vol. 107, no. 2013, pp. 664–674, sep 2013. [Online]. Available: http://www.sciencedirect.com/science/article/pii/S0013468613005707

[21] H. Song, J. Jeong, and B.-h. Lee, "Experimental study on the effects of pre-heating a battery in a low-temperature environment," in *2012 IEEE Vehicle Power and Propulsion Conference*. IEEE, oct 2012, pp. 1198–1201. [Online]. Available: http://ieeexplore.ieee.org/xpls/abs_all.jsp?arnumber=6422509

[22] C. Alaoui and Z. Salameh, "A Novel Thermal Management for Electric and Hybrid Vehicles," *IEEE Transactions on Vehicular Technology*, vol. 54, no. 2, pp. 468–476, mar 2005. [Online]. Available: http://ieeexplore.ieee.org/xpls/abs_all.jsp?arnumber=1412068

[23] M. Zolot, A. a. Pesaran, and M. Mihalic, "Thermal Evaluation of Toyota Prius Battery Pack," in *SAE International*, jun 2002. [Online]. Available: http://papers.sae.org/2002-01-1962/

[24] M. Zolot, K. Kelly, M. Keyser, and M. Mihalic, "Thermal Evaluation of the Honda Insight Battery Pack," in *36th Intersociety Energy Conversion Engineering Conference (IECEC'01)*, no. June. Savannah: National Renewable Energy Laboratory, 2001, p. 9. [Online]. Available: http://www.osti.gov/scitech/biblio/783430

[25] M. Cosley and M. Garcia, "Battery thermal management system," in *2004 10th International Workshop on Computational Electronics (IEEE Cat. No.04EX915)*. IEEE, 2004, pp. 38–45. [Online]. Available: http://ieeexplore.ieee.org/lpdocs/epic03/wrapper.htm?arnumber=1401442

[26] P. Nelson, D. Dees, K. Amine, and G. Henriksen, "Modeling thermal management of lithium-ion PNGV batteries," *Journal of Power Sources*, vol. 110, no. 2, pp. 349–356, aug 2002. [Online]. Available: http://www.sciencedirect.com/science/article/pii/S0378775302001970

[27] J. Yi, U. S. Kim, C. B. Shin, T. Han, and S. Park, "Modeling the temperature dependence of the discharge behavior of a lithium-ion battery in low environmental temperature," *Journal of Power Sources*, vol. 244, pp. 143–148, dec 2013. [Online]. Available: http://www.sciencedirect.com/science/article/pii/S0378775313003844

[28] Université du Québec à Trois-Rivères, "Institut de Recherche sur l'Hydrogène," 1994. [Online]. Available: www.uqtr.ca/IRH

[29] CrossChasm, "CrossChasm Overview," 2014. [Online]. Available: http://www.crosschasm.com/corporate/

[30] D. Linden and T. Reddy, *Handbook of Batteries*, 3rd ed. New York, NY, U.S.A: McGraw-Hill, 2002. [Online]. Available: http://www.mhprofessional.com/product.php?isbn=0071414754

[31] International Electrotechnical Commission, "Lithium ion battery," 2004. [Online]. Available: http://www.electropedia.org/iev/iev.nsf/display?openform&ievref=482-05-07

[32] H. J. Bergveld, W. S. Kruijt, and P. H. L. Notten, *Battery Management Systems*. Dordrecht: Springer Netherlands, 2002. [Online]. Available: http://link.springer.com/10.1007/978-94-017-0843-2

[33] S. Kelouwani, K. Agbossou, Y. Dubé, and L. Boulon, "Fuel cell Plug-in Hybrid Electric Vehicle anticipatory and real-time blended-mode energy management for battery life preservation," *Journal of Power Sources*, vol. 221, pp. 406–418, jan 2013. [Online]. Available: http://dx.doi.org/10.1016/j.jpowsour.2012.08.016

[34] J. Jaguemont, L. Boulon, and Y. Dube, "Characterization and Modeling of a Hybrid-Electric-Vehicle Lithium-Ion Battery Pack at Low Temperatures," *IEEE Transactions on Vehicular Technology*, vol. 65, no. 1, pp. 1–14, jan 2016. [Online]. Available: http://ieeexplore.ieee.org/lpdocs/epic03/wrapper.htm?arnumber=7006731

[35] J. Jaguemont, L. Boulon, Y. Dube, and D. Poudrier, "Low Temperature Discharge Cycle Tests for a Lithium Ion Cell," in *2014 IEEE Vehicle Power and Propulsion Conference (VPPC)*, UQTR. Trois Rivieres: IEEE, oct 2014, pp. 1–6. [Online]. Available: http://ieeexplore.ieee.org/lpdocs/epic03/wrapper.htm?arnumber=7007097

[36] S. Zhang, K. Xu, and T. Jow, "Charge and discharge characteristics of a commercial LiCoO2-based 18650 Li-ion battery," *Journal of Power Sources*, vol. 160, no. 2, pp. 1403–1409, oct 2006. [Online]. Available: http://linkinghub.elsevier.com/retrieve/pii/S0378775306004447

[37] J. Wang, P. Liu, J. Hicks-Garner, E. Sherman, S. Soukiazian, M. Verbrugge, H. Tataria, J. Musser, and P. Finamore, "Cycle-life model for graphite-LiFePO4 cells," *Journal of Power Sources*, vol. 196, no. 8, pp. 3942–3948, apr 2011. [Online]. Available: http://dx.doi.org/10.1016/j.jpowsour.2010.11.134

[38] J. Jaguemont, L. Boulon, P. Venet, Y. Dube, and A. Sari, "Lithium Ion Battery Aging Experiments at Sub-Zero Temperatures and Model Development for Capacity Fade Estimation," *IEEE Transactions on Vehicular Technology*, vol. 9545, no. c, pp. 1–1, 2015. [Online]. Available: http://ieeexplore.ieee.org/lpdocs/epic03/wrapper.htm?arnumber=7226857

[39] N. Watrin, H. Ostermann, B. Blunier, and A. Miraoui, "Multiphysical Lithium-Based Battery Model for Use in State-of-Charge Determination," *IEEE Transactions on Vehicular Technology*, vol. 61, no. 8, pp. 3420–3429, oct 2012. [Online]. Available: http://ieeexplore.ieee.org/lpdocs/epic03/wrapper.htm?arnumber=6220281

[40] A. Rahmoun and H. Biechl, "Modelling of Li-ion batteries using equivalent circuit diagrams," *PRZEGLAD ELEKTROTECHNICZNY*, vol. 2, no. 7, pp. 152–156, 2012. [Online]. Available: http://red.pe.org.pl/articles/2012/7b/40.pdf

[41] Y. Tan, J. Mao, and K. Tseng, "Modelling of battery temperature effect on electrical characteristics of Li-ion battery in hybrid electric vehicle," in *2011 IEEE Ninth International Conference on Power Electronics and Drive Systems*, no. December. IEEE, dec 2011, pp. 637–642. [Online]. Available: http://ieeexplore.ieee.org/lpdocs/epic03/wrapper.htm?arnumber=6147318

[42] H. Rahimi-Eichi, F. Baronti, and M.-Y. Chow, "Modeling and online parameter identification of Li-Polymer battery cells for SOC estimation," *2012 IEEE International Symposium on Industrial Electronics*, pp. 1336–1341, may 2012. [Online]. Available: http://ieeexplore.ieee.org/lpdocs/epic03/wrapper.htm?arnumber=6237284

[43] N. A. Windarko, J. Choi, and G.-B. Chung, "SOC estimation of LiPB batteries using Extended Kalman Filter based on high accuracy electrical model," in *8th International Conference on Power Electronics - ECCE Asia*. IEEE, may 2011, pp. 2015–2022. [Online]. Available: http://ieeexplore.ieee.org/lpdocs/epic03/wrapper.htm?arnumber=5944483

[44] T. Huria, M. Ceraolo, J. Gazzarri, and R. Jackey, "High fidelity electrical model with thermal dependence for characterization and simulation of high power lithium battery cells," in *2012 IEEE International Electric Vehicle Conference*. IEEE, mar 2012, pp. 1–8. [Online]. Available: http://ieeexplore.ieee.org/lpdocs/epic03/wrapper.htm?arnumber=6183271

[45] H. He, R. Xiong, and J. Fan, "Evaluation of Lithium-Ion Battery Equivalent Circuit Models for State of Charge Estimation by an Experimental Approach," *Energies*, vol. 4, no. 12, pp. 582–598, mar 2011. [Online]. Available: http://www.mdpi.com/1996-1073/4/4/582/

[46] R. Benger, H. Wenzl, H. Beck, M. Jiang, D. Ohms, and G. Schaedlich, "Electrochemical and thermal modeling of lithium-ion cells for use in HEV or EV application," *World Electric Vehicle Journal*, vol. 3, pp. 0342–0351, 2009. [Online]. Available: http://www.evs24.org/wevajournal/volumes/volume.php

[47] M. Corno and S. M. Savaresi, "A diffusive electro-equivalent Li-ion battery model," in *2013 IEEE International Symposium on Circuits and Systems (ISCAS2013)*. IEEE, may 2013, pp. 2976–2979. [Online]. Available: http://ieeexplore.ieee.org/lpdocs/epic03/wrapper.htm?arnumber=6572504

[48] L. Boulon, D. Hissel, and M.-C. Péra, "Multi Physics Model of a Nickel Based Battery Suitable for Hybrid Electric Vehicle Simulation," *Journal of Asian Electric Vehicles*, vol. 6, no. 2, pp. 1175–1179, 2008. [Online]. Available: http://joi.jlc.jst.go.jp/JST.JSTAGE/jaev/6.1175?from=CrossRef

[49] A. Fotouhi, D. J. Auger, K. Propp, S. Longo, and M. Wild, "A review on electric vehicle battery modelling: From Lithium-ion toward Lithium–Sulphur," *Renewable and Sustainable Energy Reviews*, vol. 56, pp. 1008–1021, apr 2016. [Online]. Available: http://linkinghub.elsevier.com/retrieve/pii/S1364032115013921

[50] J. Larminie and J. Lowry, *Electric Vehicle Technology Explained*. Chichester, UK: John Wiley and Sons Ltd, aug 2012. [Online]. Available: http://doi.wiley.com/10.1002/9781118361146

[51] N. Chaturvedi, R. Klein, J. Christensen, J. Ahmed, and A. Kojic, "Algorithms for Advanced Battery-Management Systems," *IEEE Control Systems Magazine*, vol. 30, no. 3, pp. 49–68, jun 2010. [Online]. Available: http://ieeexplore.ieee.org/lpdocs/epic03/wrapper.htm?arnumber=5466167

[52] M. Chen and G. Rincon-Mora, "Accurate Electrical Battery Model Capable of Predicting Runtime and I–V Performance," *IEEE Transactions on Energy Conversion*, vol. 21, no. 2, pp. 504–511, jun 2006. [Online]. Available: http://ieeexplore.ieee.org/lpdocs/epic03/wrapper.htm?arnumber=1634598

[53] A. Capel, "Mathematical model for the representation of the electrical behaviour of a lithium cell," in *2001 IEEE 32nd Annual Power Electronics Specialists Conference (IEEE Cat. No.01CH37230)*, vol. 4, no. 502. IEEE, 2002, pp. 1976–1981. [Online]. Available: http://ieeexplore.ieee.org/lpdocs/epic03/wrapper.htm?arnumber=954411

[54] R. C. Kroeze and P. T. Krein, "Electrical battery model for use in dynamic electric vehicle simulations," in *2008 IEEE Power Electronics Specialists Conference*. IEEE, jun 2008, pp. 1336–1342. [Online]. Available: http://ieeexplore.ieee.org/lpdocs/epic03/wrapper.htm?arnumber=4592119

[55] S. X. Chen, K. J. Tseng, and S. S. Choi, "Modeling of Lithium-Ion Battery for Energy Storage System Simulation," in *2009 Asia-Pacific Power and Energy Engineering Conference*. IEEE, mar 2009, pp. 1–4. [Online]. Available: http://ieeexplore.ieee.org/lpdocs/epic03/wrapper.htm?arnumber=4918501

[56] J. Van Mierlo, "Models of energy sources for EV and HEV: fuel cells, batteries, ultracapacitors, flywheels and engine-generators," *Journal of Power Sources*, vol. 128, no. 1, pp. 76–89, mar 2004. [Online]. Available: http://linkinghub.elsevier.com/retrieve/pii/S0378775303009753

[57] M. Urbain, S. Rael, and B. Davat, "Energetical Modeling of Lithium-Ion Batteries," in *2007 IEEE Industry Applications Annual Meeting*, no. Umr 7037. IEEE, sep 2007, pp. 714–721. [Online]. Available: http://ieeexplore.ieee.org/lpdocs/epic03/wrapper.htm?arnumber=4347862

[58] H. Rahimi-Eichi, F. Baronti, and M.-Y. Y. Chow, "Online adaptive parameter identification and state-of-charge coestimation for lithium-polymer battery cells," *IEEE Transactions on Industrial Electronics*, vol. 61, no. 4, pp. 2053–2061, apr 2014. [Online]. Available: http://ieeexplore.ieee.org/lpdocs/epic03/wrapper.htm?arnumber=6517243

[59] J. Lienhard IV and J. Lienhard V, *A Heat Transfer Textbook*, 4th ed. Cambridge, Massachusetts, U.S.A: Phlogiston Press, 2015, no. 2.03. [Online]. Available: http://web.mit.edu/lienhard/www/ahtt.html

[60] International Electrotechnical Commission, "Specific Heat," 2004. [Online]. Available: http://www.electropedia.org/iev/iev.nsf/display?openform&ievref=841-21-11

[61] M. Bahrami, N. C. Consider, and S. Water, "Natural Convection," in *ENSC 388 Engineerimg Thermodynamics and Heat Transfer*. Surrey, BC, Canada: Simon Fraser University, 2011, vol. 388, ch. 10, pp. 1–7. [Online]. Available: http://www.sfu.ca/$\sim$mbahrami/ensc388.html

[62] OECD Nuclear Energy Agency and Nuclear Science Committee, *Handbook on Lead-bismuth Eutectic Alloy and Lead Properties, Materials Compatibility, Thermal-hydraulics and Technologies*. OECD Nuclear Energy Agency, 2007, no. 6195. [Online]. Available: https://www.oecd-nea.org/science/reports/2007/pdf/lbe-handbook-complete.pdf

[63] Microelectronics Heat Transfer Laboratory - University of Waterloo, "Simulation Tools - Thermal Fluid Properties Calculator," 1984. [Online]. Available: http://www.mhtl.uwaterloo.ca/

[64] F. Baronti, R. Saletti, and W. Zamboni, "Open Circuit Voltage of Lithium-ion batteries for energy storage in DC microgrids," in *2015 IEEE First International Conference on DC Microgrids (ICDCM)*. IEEE, jun 2015, pp. 343–348. [Online]. Available: http://ieeexplore.ieee.org/lpdocs/epic03/wrapper.htm?arnumber=7152066

[65] M. Petzl and M. A. Danzer, "Advancements in OCV Measurement and Analysis for Lithium-Ion Batteries," *IEEE Transactions on Energy Conversion*, vol. 28, no. 3, pp. 675–681, sep 2013. [Online]. Available: http://ieeexplore.ieee.org/lpdocs/epic03/wrapper.htm?arnumber=6517504

[66] D. Herrera Vega, S. Kelouwani, and L. Boulon, "Efficient Internal Resistance and Specific Heat Identification of Li-Ion Battery at Low Temperature Conditions," in *2015 IEEE Vehicle Power and Propulsion Conference (VPPC)*. IEEE, oct 2015, pp. 1–6. [Online]. Available: http://ieeexplore.ieee.org/lpdocs/epic03/wrapper.htm?arnumber=7352939

[67] L. Pei, C. Zhu, and R. Lu, "Relaxation model of the open-circuit voltage for state-of-charge estimation in lithium-ion batteries," *IET Electrical Systems in Transportation*, vol. 3, no. 4, pp. 112–117, dec 2013. [Online]. Available: http://digital-library.theiet.org/content/journals/10.1049/iet-est.2013.0020

[68] C. Unterrieder, R. Priewasser, M. Agostinelli, S. Marsili, and M. Huemer, "Comparative study and improvement of battery open-circuit voltage estimation methods," in *2012 IEEE 55th International Midwest Symposium on Circuits and Systems (MWSCAS)*. IEEE, aug 2012, pp. 1076–1079. [Online]. Available: http://ieeexplore.ieee.org/lpdocs/epic03/wrapper.htm?arnumber=6292210

[69] L. Pei, T. Wang, R. Lu, and C. Zhu, "Development of a voltage relaxation model for rapid open-circuit voltage prediction in lithium-ion batteries," *Journal of Power Sources*, vol. 253, pp. 412–418, may 2014. [Online]. Available: http://linkinghub.elsevier.com/retrieve/pii/S0378775313020624

[70] B. Pattipati, B. Balasingam, G. Avvari, K. Pattipati, and Y. Bar-Shalom, "Open circuit voltage characterization of lithium-ion batteries," *Journal of Power Sources*, vol. 269, pp. 317–333, dec 2014. [Online]. Available: http://linkinghub.elsevier.com/retrieve/pii/S037877531401026X

[71] Y.-H. Chiang, W.-Y. Sean, and J.-C. Ke, "Online estimation of internal resistance and open-circuit voltage of lithium-ion batteries in electric vehicles," *Journal of Power Sources*, vol. 196, no. 8, pp. 3921–3932, apr 2011. [Online]. Available: http://linkinghub.elsevier.com/retrieve/pii/S0378775311000772

[72] M. Verbrugge and E. Tate, "Adaptive state of charge algorithm for nickel metal hydride batteries including hysteresis phenomena," *Journal of Power Sources*, vol. 126, no. 1-2, pp. 236–249, feb 2004. [Online]. Available: http://linkinghub.elsevier.com/retrieve/pii/S037877530301005X

[73] S. Cho, H. Jeong, C. Han, S. Jin, J. H. Lim, and J. Oh, "State-of-charge estimation for lithium-ion batteries under various operating conditions using an equivalent circuit model," *Computers and Chemical Engineering*, vol. 41, pp. 1–9, jun 2012. [Online]. Available: http://dx.doi.org/10.1016/j.compchemeng.2012.02.003

[74] S. Chen, H. Gooi, N. Xia, and M. Wang, "Modelling of lithium-ion battery for online energy management systems," *IET Electrical Systems in Transportation*, vol. 2, no. 4, p. 202, 2012. [Online]. Available: http://digital-library.theiet.org/content/journals/10.1049/iet-est.2012.0008

[75] J. Lv, H. Yuan, and Y. Lv, "Battery State-of-charge Estimation Based on Fuzzy Neural Network and Improved Particle Swarm Optimization Algorithm," in *2012 Second International Conference on Instrumentation, Measurement, Computer, Communication and Control*, no. 61273165. IEEE, dec 2012, pp. 22–27. [Online]. Available: http://ieeexplore.ieee.org/lpdocs/epic03/wrapper.htm?arnumber=6428845

[76] M. T. Hagan and M. B. Menhaj, "Training feedforward networks with the Marquardt algorithm." *IEEE transactions on neural networks / a publication of the IEEE Neural Networks Council*, vol. 5, no. 6, pp. 989–93, jan 1994. [Online]. Available: http://www.ncbi.nlm.nih.gov/pubmed/18267874

[77] G. Dreyfus, M. Samuelides, J.-M. Martinez, M. Gordon, F. Badran, S. Thiria, and L. Hérault, "Les réseaux de neurones : pourquoi et pour quoi faire ?" in *Les réseaux de neurones*, Eyrolles, Ed., 2004.

[78] K. Hornik, M. Stinchcombe, and H. White, "Multilayer feedforward networks are universal approximators," *Journal of Neural Networks*, vol. 2, no. 5, pp. 359–366, jan 1989. [Online]. Available: http://linkinghub.elsevier.com/retrieve/pii/0893608089900208

[79] S. Kelouwani and K. Agbossou, "Nonlinear Model Identification of Wind Turbine With a Neural Network," *IEEE Transactions on Energy Conversion*, vol. 19, no. 3, pp. 607–612, sep 2004. [Online]. Available: http://ieeexplore.ieee.org/lpdocs/epic03/wrapper.htm?arnumber=1325301

[80] Y. Wang, C. Zhang, and Z. Chen, "A method for state-of-charge estimation of LiFePO4 batteries at dynamic currents and temperatures using particle filter," *Journal of Power Sources*, vol. 279, pp. 306–311, apr 2015. [Online]. Available: http://linkinghub.elsevier.com/retrieve/pii/S0378775315000063

[81] G. Dong, X. Zhang, C. Zhang, and Z. Chen, "A method for state of energy estimation of lithium-ion batteries based on neural network model," *Energy*, vol. 90, pp. 879–888, oct 2015. [Online]. Available: http://linkinghub.elsevier.com/retrieve/pii/S0360544215010154

[82] M. Ceraolo and G. Pede, "Techniques for estimating the residual range of an electric vehicle," *IEEE Transactions on Vehicular Technology*, vol. 50, no. 1, pp. 109–115, 2001. [Online]. Available: http://ieeexplore.ieee.org/lpdocs/epic03/wrapper.htm?arnumber=917893

[83] D. W. Marquardt, "An Algorithm for Least-Squares Estimation of Nonlinear Parameters," *Journal of the Society for Industrial and Applied Mathematics*, vol. 11, no. 2, pp. 431–441, jun 1963. [Online]. Available: http://epubs.siam.org/doi/abs/10.1137/0111030

[84] H. Gavin, "The Levenberg-Marquardt method for nonlinear least squares curve-fitting problems," Department of Civil and Environmental Engineering of Duke University, Duke, Tech. Rep., 2013.

[85] K. Madsen, H. Nielsen, and O. Tinglef, "Methods for non-linear least squares problems," Informatics and Mathematical Modeling, Technical University of Denmark, Tech. Rep., apr 2004. [Online]. Available: http://www2.imm.dtu.dk/pubdb/views/edoc_download.php/3215/pdf/imm3215.pdf

[86] C. Alippi and V. Piuri, "Experimental neural networks for prediction and identification," *IEEE Transactions on Instrumentation and Measurement*, vol. 45, no. 2, pp. 670–676, apr 1996. [Online]. Available: http://ieeexplore.ieee.org/lpdocs/epic03/wrapper.htm?arnumber=492807

[87] S. Billings, "An overview of nonlinear systems identification," 1985. [Online]. Available: http://eprints.whiterose.ac.uk/76930/

[88] Z. Zhou, Z. Shi, G. Ai, Y. Lu, and Y. En, "End of discharge time prediction for Li-ion battery," in *2013 International Conference on Quality, Reliability, Risk, Maintenance, and Safety Engineering (QR2MSE)*. IEEE, jul 2013, pp. 1938–1941. [Online]. Available: http://ieeexplore.ieee.org/lpdocs/epic03/wrapper.htm?arnumber=6625958

[89] Z. Zhou, Y. Huang, Y. Lu, Z. Shi, X. Li, J. Wu, and H. Li, "Lithium-ion battery end-of-discharge time prediction using particle filtering algorithm," in *2014 Prognostics and System Health Management Conference (PHM-2014 Hunan)*. IEEE, aug 2014, pp. 658–663. [Online]. Available: http://ieeexplore.ieee.org/lpdocs/epic03/wrapper.htm?arnumber=6988255

[90] P. Pascoe and A. Anbuky, "VRLA Battery Discharge Reserve Time Estimation," *IEEE Transactions on Power Electronics*, vol. 19, no. 6, pp. 1515–1522, nov 2004. [Online]. Available: http://ieeexplore.ieee.org/lpdocs/epic03/wrapper.htm?arnumber=1353342

[91] D. A. Pola, H. F. Navarrete, M. E. Orchard, R. S. Rabie, M. A. Cerda, B. E. Olivares, J. F. Silva, P. A. Espinoza, and A. Perez, "Particle-Filtering-Based Discharge Time Prognosis for Lithium-Ion Batteries With a Statistical Characterization of Use Profiles," *IEEE Transactions on Reliability*, vol. 64, no. 2, pp. 710–720, jun 2015. [Online]. Available: http://ieeexplore.ieee.org/lpdocs/epic03/wrapper.htm?arnumber=7004078

Appendix A

Tests Results for Low Temperature Battery Discharge

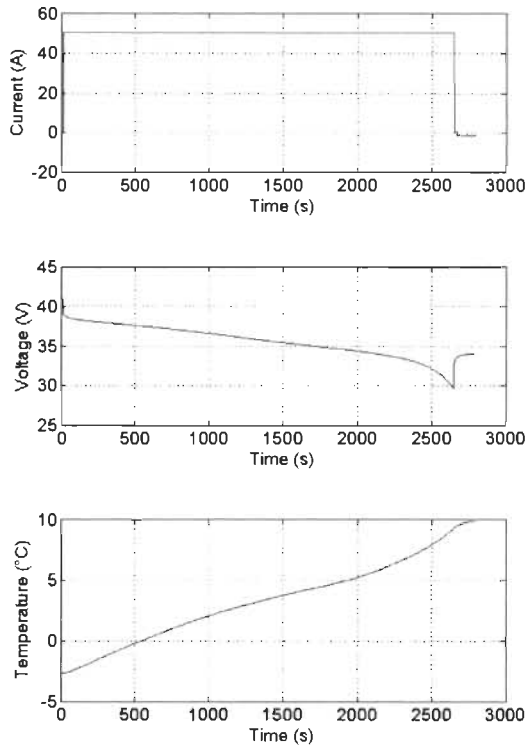

(a) Ambient Temperature: 0 °C

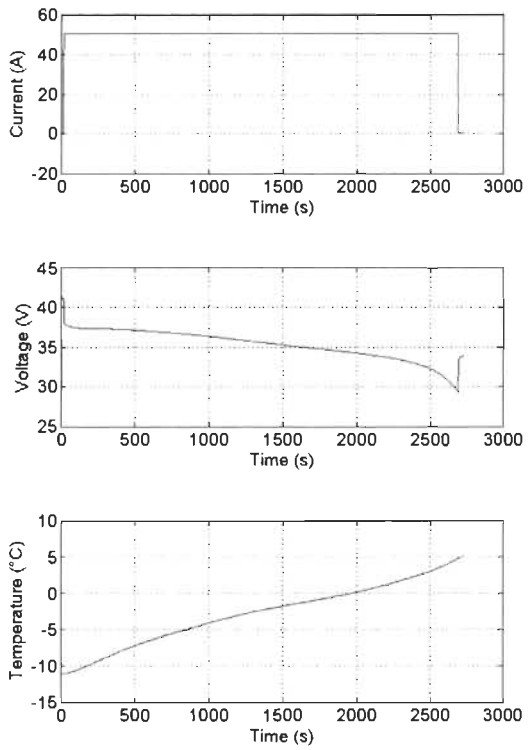

(b) Ambient Temperature: -10 °C

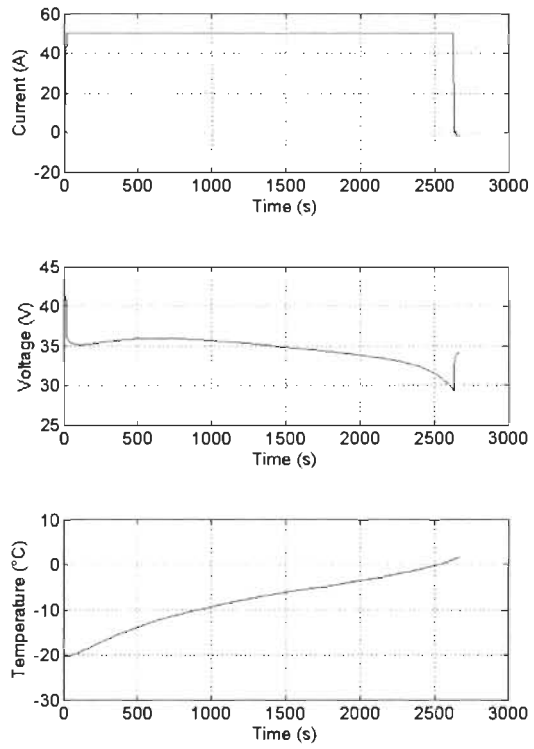

(c) Ambient Temperature: -20 °C

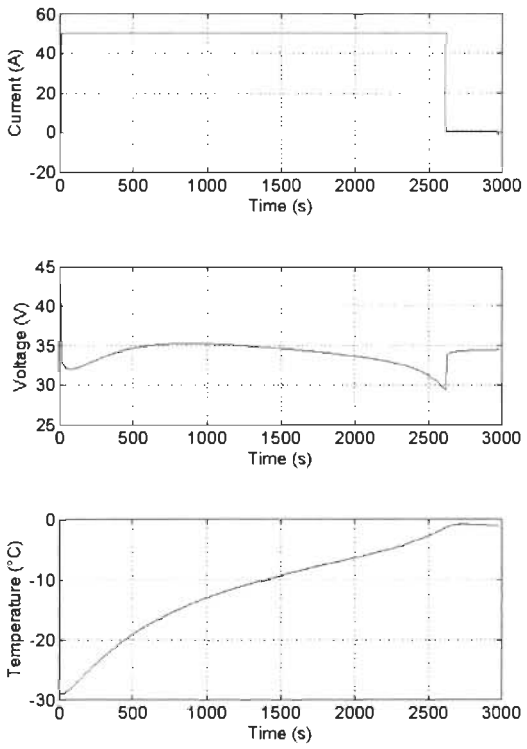

(d) Ambient Temperature: -30 °C

Figure A.1: Characterization with 50 A constant current

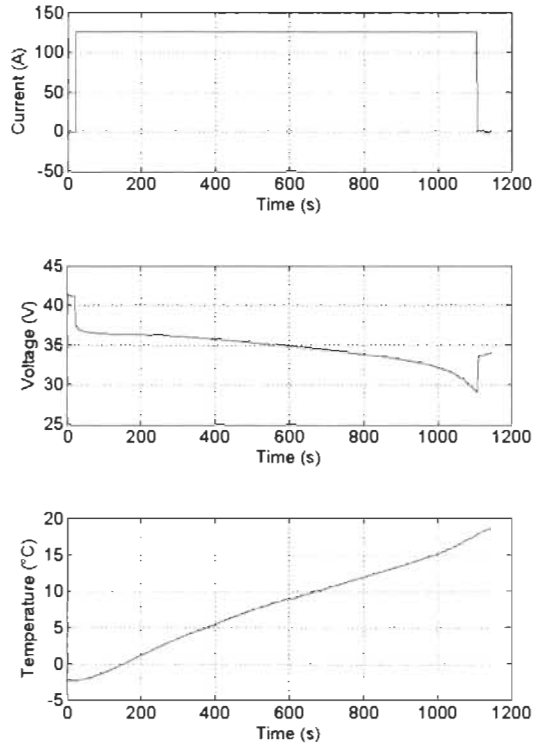

(a) Ambient Temperature: 0 °C

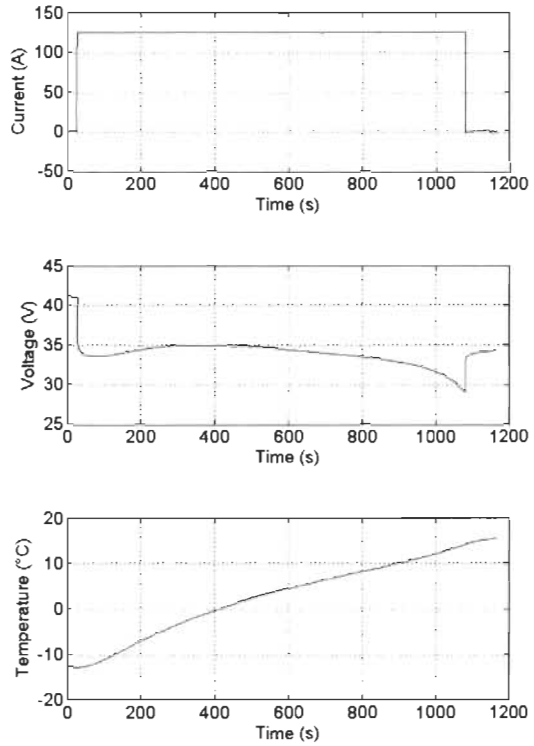

(b) Ambient Temperature: -10 °C

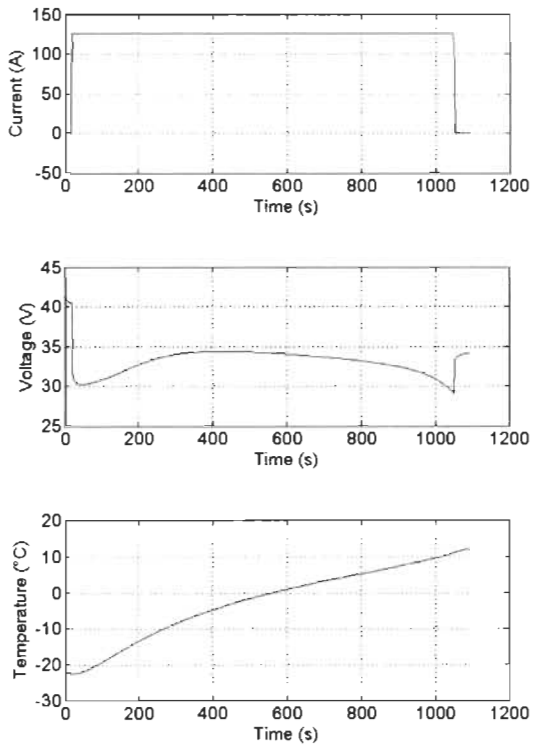

(c) Ambient Temperature: -20 °C

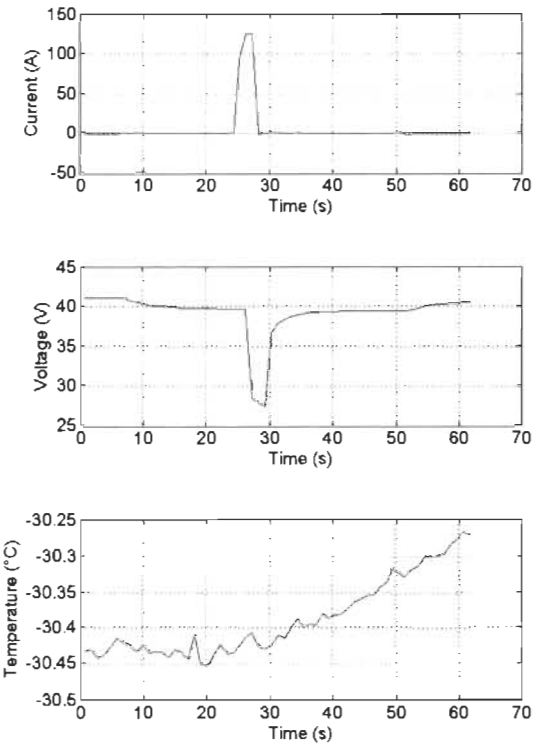

(d) Ambient Temperature: -30 °C

Figure A.2: Characterization with 125 A constant current

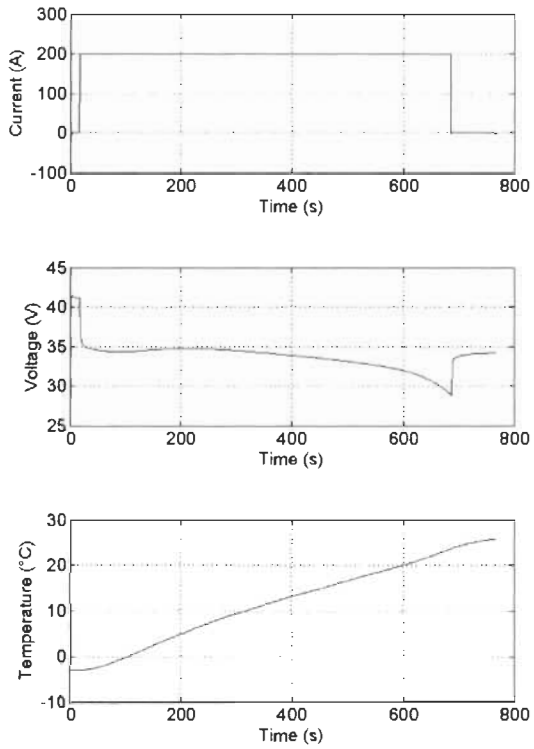

(a) Ambient Temperature: 0 °C

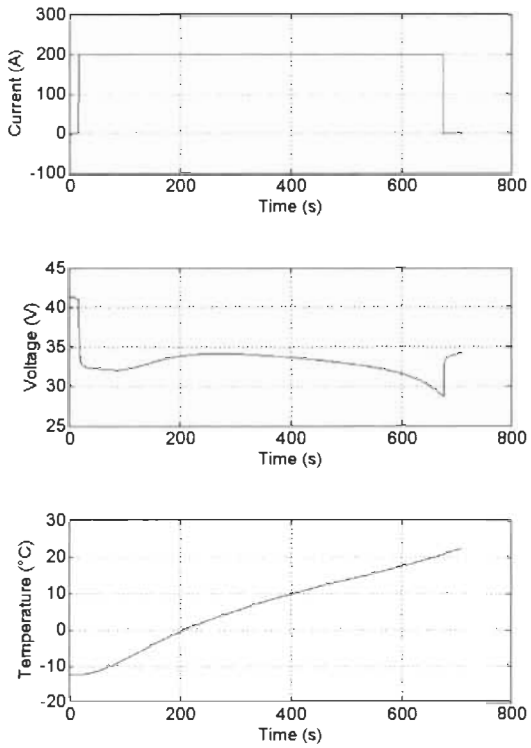

(b) Ambient Temperature: -10 °C

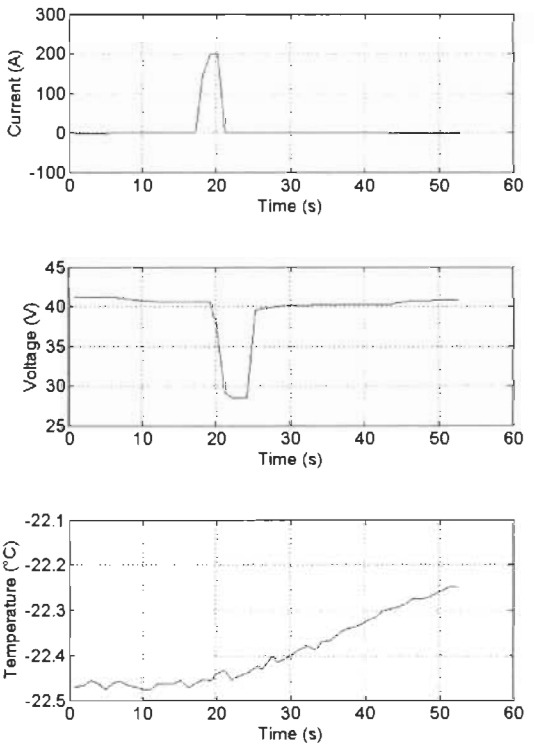

(c) Ambient Temperature: -20 °C

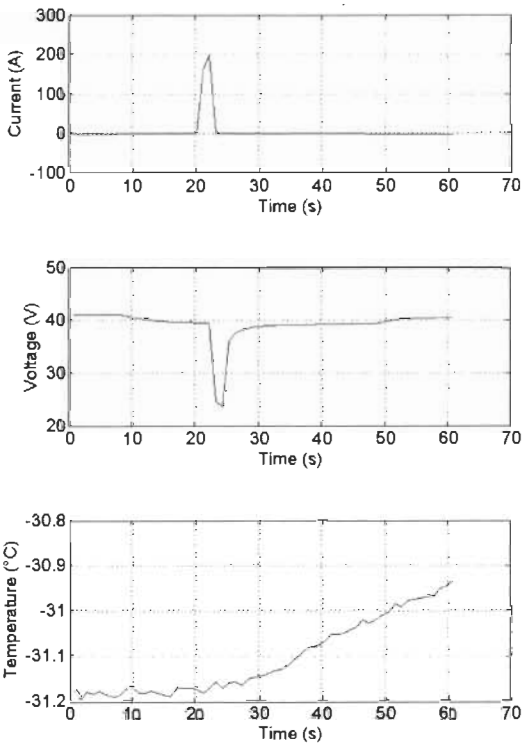

(d) Ambient Temperature: -30 °C

Figure A.3: Characterization with 200 A constant current

Appendix B

Complementary Tables

Table B.1: Data of the most representative EVs models on the market [5]

Model	Battery Type	Energy Storage (kWh)	Nominal Range (km)	Market Release	Power (kW)	Motor Type
Tesla Model S	Li	42	258	2012	215	IM
Tesla Model S	Li	65	370	2012	215	IM
Tesla Model S	Li	85	483	2012	215	IM
Lightning GT	Li	40	240	2012	150	PM
Hyundai BlueOn	Li	16.4	140	2012	61	PM
Honda Fit EV	Li		113	2012		IM
Toyota RAV4 EV	Li	30	160	2012		IM
Saab 9-3 ePower	Li	35.5	200	2011	135	
CODA Sedan	Li	34	193	2011	100	
Ford Focus Electric	Li	23	160	2011	100	IM
Skoda Octavia Green E Line	Li	26.5	140	2011	85	
Volvo C30 DRIVe Electric	Li	24	150	2011	82	
Renault Fluence Z.E.	Li	22	161	2011	70	SB
Renault ZOE	Li	22	160	2011	60	SB
Tata Indica Vista EV	Li	26.5	241	2011	55	PM
Ford Tourneo Connect EV	Li	21	160	2011	50	IM
Kangoo Express Z.E.	Li	22	170	2011	44	SB
Fiat Doblò	Li	18	140	2011	43	IM
Peugeot iOn	Li	16	130	2011	35	PM
Renault Twizy	Li	7	100	2011	15	
REVA NXR	Pb	9.6	160	2011	13	IM
BYD F3M	Li	15	100	2010	125	PM
Nissan Leaf	Li	24	175	2010	80	PM
Ford Transit Connect EV	Li	28	129	2010	50	IM
Citroën C zero	Li	16	130	2010	49	PM
Gordon Murray T-27	Li	12	130	2010	25	
Wheego Whip LiFe	Li	30	161	2010	15	IM
Venturi Fétish	Li	54	340	2009	220	
Mini E	Li	35	195	2009	150	IM
BYD e6	Li	60	330	2009	115	PM
Mitsubishi i MiEV	Li	16	160	2009	47	PM
Subaru Stella EV	Li	9.2	80	2009	40	
Smart ED	Li	16.5	135	2009	30	PM
Citroën C1 ev'ie	Li	30	110	2009	30	IM
Zytel Gorila Electric	Pb	10.8	80	2009	17	
Micro-Vett Fiat Panda	Li	22	120	2009	15	IM
Micro-Vett Fiat 500	Li	22	130	2009	15	IM
Tazzari Zero	Li	19	140	2009	15	IM
Chana Benni	Pb	9	120	2009	10	
Tesla Roadster	Li	53	395	2008	215	IM
Th!nk City	Na	24	160	2008	34	IM
Th!nk City	Li	23	160	2008	34	IM
Lumeneo SMERA	Li	10	100	2008	30	PM
Stevens Zecar	Pb		80	2008	27	IM
REVAi	Pb	9.3	80	2008	13	IM
REVAi	Li	9.3	80	2008	13	IM
ZENN	Pb		64	2008		IM
AC Propulsion eBox	Li	35	250	2007	150	IM
ZAP! OBVIO! 828E	Li	39	386	2007	120	IM
Phoenix sut	Li	35	209	2007	100	
Phoenix sut	Li	70	403	2007	100	IM
Smart ED	Na	13.2	110	2007	30	PM
Kewet Buddy	Pb	8.4	40	2007	13	DC
The Kurrent	Pb		60	2007	4.1	
City Car	Li	7	120	2007		
ZAP Xebra	Pb	7.2	40	2006	5	DC
NICE Mega City	Pb	6.5	81	2006	4	DC
Commuter Cars Tango	Pb	16	100	2005	43	DC
Cree SAM	Li	7	100	2001	11.6	PM
G-Wiz	Pb	9.3	77	2001	4.8	DC
Dynasty IT	Pb	5	48	2001		
General Motors EV1	NiMH	26.4	225	1999	102	IM
Ford Ranger EV	NiMH	26	132	1999	67	IM
Peugeot Partner	NiCd	16.2	96	1999	28	DC
Hypermini	Li	15	115	1999	24	PM
Myers Motors NmG	Pb	8.6	64	1999	20	DC
Peugeot 106	NiCd	12	150	1999	20	DC
GM S-10	NiMH	29	113	1998	85	IM
Ford Ranger EV	Pb	20.6	100	1998	67	IM
Toyota RAV4 EV	NiMH	26	165	1998	50	PM
Renault Express Electr	Pb	22	100	1998	19	
GEM Car	Pb		48	1998	9	DC
CityCom Mini-El	Pb	3.6	96	1998	9	PM
GM S-10	Pb	16.2	76	1997	85	IM
Nissan Altra	Li	32	190	1997	62	PM
Honda EV Plus	NiMH	26.2	240	1997	49	DC
General Motors EV1	Pb	18.7	160	1996	102	IM
Citroën Berlingo	NiCd	16	100	1995	28	DC
Citroën Saxo	NiMH	17	100	1995	20	DC
Subaru minivan 200	Pb	15.6	70	1995	14	DC
Solectria Sunrise	NiMH	26	321	1994	50	IM
Chrysler TEVan	NiMH	32.4	80	1993	27	DC
Chrysler TEVan	NiMH	36	97	1993	27	DC
Citroën AX	NiCd	12	100	1993	20	DC
VW Golf CityStromer	Pb	17.2	90	1993	17.5	PM
Ford Ecostar	Na	37	151	1992	56	IM
Bertone Blitz	Pb		130	1992	52	DC
VW Golf CityStromer	Pb	11.5	50	1989	18.5	PM
City El	Pb	11.5	90	1987	4	DC
City El	Pb	8.6	80	1987	2.5	DC
Oka NEV ZEV				1987		
Lucas Chloride	Pb	40	70	1977	40	DC
Citicar	Pb			1974	2.5	DC
Enfield 8000	Pb	8	145	1969	10	DC

Legend: **Li:** based on lithium, **Pb:** lead-acid, **Na:** sodium nickel chloride Zebra batteries and sodium-sulphur in the Ford Ecostar, **IM:** Induction motor, **PM:** Permanent Magnet motor, **SB:** Synchronous Brushed motor.

Appendix C

Equipment Data-sheet

The equipment described in Section 2.1 is listed in Table C.1. These are the equipment specifications that will be found attached to this Appendix.

Table C.1: List of Equipment Specifications

Item	Equipment Specifications
1	GAIA Li-ion Battery Cell
2	Ametek Sorensen Power Supply
3	TDI Power WCL488 Water Cooled Electronic Load
4	National Instruments NI-PCIe6323 DAQ System
5	LABRepCo Low Temp Chest Freezer

Handling instructions for the lithium ion cell type HP 602030 NCA-45Ah/ 162Wh

Read the complete handling instructions. Not following them may be dangerous or illegal.

As of: 15-06-2009

Revision: 1

GAIA
Advanced Lithium Battery Systems

HP 602030 NCA
45 Ah/ 162 Wh
Lithium Ion Cell

Physical and mechanical characteristics	
Diameter	60 mm
Height	232 mm (203 mm without terminals)
Terminals	Positive terminal Al M12 L: 9 mm
	Negative terminal Cu M12 L: 9 mm
Weight	approx. 1500 g
Volume without terminals	0.57 l
Case material	Stainless Steel
Chemical characteristics	
Positve electrode	Lithium nickel cobalt oxide
Negative electrode	Graphite
Electrical characteristics*	
Nominal voltage	3.6 V
Nominal capacity at 0.2 C	45 Ah
Minimum capacity	42 Ah
AC Impedance (1 kHz)	≤ 0.4 mOhm
DC Resistance (ESR) (2 s pulse discharge @ 20 C/ 50% SOC)	≤ 1.2 mOhm
Specific energy at 0.2 C	108 Wh/kg
Energy density at 0.2 C	282 Wh/l
Specific power (2 s pulse discharge @ 27.8 C/ 100% SOC)	2080 W/kg
Power density (2 s pulse discharge @ 27.8 C/ 100% SOC)	5440 W/l
Operating conditions*	
Recommended charge method	Constant current - constant voltage
End of Charge	I ≤ C/100
Maximum charge voltage	4.2 V
Recommended charge current	up to 45 A (1 C)
Continuous charge current	up to 180 A (4 C)
Maximum pulse charge current (15 s) (Max. SOC 80 %, average current < 180 A)	270 A (6 C)
Recommended voltage limit for discharge	3 V
Lower voltage limit for discharge	2.7 V
Lower voltage limit for pulse discharge	2 V
Recommended discharge current	up to 90 A (2 C)
Maximum discharge current	up to 450 A (10 C)
Maximum pulse discharge current (2 s)	up to 1250 A (27.8 C)
Operating temperature	- 30℃ to + 60℃
Recommended charge temperature	0℃ to + 40℃
Storage and transport temperature	- 40℃ to + 60℃
Cycle life at 20℃ and 100% DOD	> 1000 cycles to 80% nominal capacity
(0.5 C charge; 0.5 C discharge)	> 2000 cycles to 60% nominal capacity

* Reference temperature 20℃

High Power

Doc HP 602030 NCA - 2009-06

GAIA
Advanced Lithium Battery Systems

GAIA Akkumulatorenwerke GmbH
Montaniastr. 17
99734 Nordhausen, Germany
www.gaia-akku.com

LTC Lithium Technology Corporation

Lithium Technology Corporation
5115 Campus Drive
Plymouth Meeting, PA 19462
www.lithiumtech.com

AMETEK®
PROGRAMMABLE POWER

Sorensen
SGI Series DC Power Supplies
Operation Manual

M550221-01 Rev AA

www.programmablepower.com

1.2 Specifications

The following subsections provide environmental, electrical, and physical characteristics for the SGI Series power supplies.

Note: *Specifications are subject to change without notice.*

Note: *The SGI Series power supplies are intended for indoor use only. Refer to Section 2.3 for use/location requirements.*

1.2.1 Environmental Characteristics

Parameter	Specification
Ambient Temperature	
Operating	0 to 50°C
Storage	-25° to 65°C
Cooling	Forced convection with internal, linearly-variable-speed fans; vents on front, sides and rear; units may be stacked without clearance above or below.
Humidity	95% maximum, non-condensing, 0 to 50°C; 45°C maximum wet-bulb temperature.
Altitude	5,000 ft (1,524 m) operating at full rated output power, derate 10% of full power for every 1,000 ft (3,048 m) higher; non-operating to 40,000 ft (12,192m)
Agency Approvals	CE Compliant: Certified to UL/CSA 61010 and IEC/EN 61010-1 by a NRTL; LVD Categories: Installation Category II, Pollution Degree 2, Class II Equipment, for Indoor Use Only; EMC Directive, EN 61326:1998; Semi-F47 Compliant

1.2.2 Electrical Characteristics

Note: *Output voltage accuracy, regulation, and stability specifications are valid at the point where the remote sense leads are connected.*

Parameter	Specification
Input Power	
Voltage	208/230 VAC ±10%, allowed range 187-253 VAC; 380/400 VAC ±10%, allowed range 342-440 VAC; 440/480 VAC ±10%, allowed range 396-528 VAC
Frequency	47 Hz to 63 Hz; 400 Hz at 208 VAC for 3U models; 400 Hz at 208 VAC for 6U models is an optional modification ("CV" in model number) and does not carry CE, UL or CSA markings
Configuration	3–phase, 3–wire plus ground; not phase rotation sensitive; neutral not used.

Parameter	Specification
Power Factor (at full rated load; 50/60Hz); contact factory for power factor of specific models	
PFC models: 10V-30V, 50V, 1000V, and models with optional modification, "PF"	0.90, typical, for all AC input ratings; with passive power factor correction (PFC)
Non-PFC models: 40V-800V	0.75, typical, for 208/230 VAC input; 0.72, typical, for 380/400 VAC input; 0.69, typical, for 440/480 VAC input; power factor is not solely determined by power supply input characteristics, but is dependent on the level of DC output power and interaction with the source impedance of AC mains.
Efficiency	87%, typical, at full load, nominal AC line
Hold-Up Time	1/2 cycle, typical, for loss of all three phases (6.4 ms, typical for 800V/1000V models); 3 cycle, typical, for loss of one phase; sustained missing phase will result in shutdown of the output.
Rated Output Power	4-15 kW for 3U chassis for10V-30V models; 5-15 kW for 3U chassis for 40V-1000V models; 20-30 kW for 6U chassis for 60V-600V models; maximum output power is the product of the rated output voltage and current; for specific values refer to Section 1.2.3.
Load Regulation (specified for ±100% rated load change, at nominal AC input voltage)	
Voltage	±0.05%, maximum, of rated output voltage for 10V- 30V models; ±0.02%, maximum, of rated output voltage for 40V-1000V models
Current	±0.1%, maximum, of rated output current
Line Regulation (specified for ±10% change of nominal AC line voltage, at constant load)	
Voltage	±0.05%, maximum, of rated output voltage for 10V-30V models; ±0.01%, maximum, of rated output voltage for 40V-1000V models
Current	±0.05%, maximum, of rated output current
Temperature Coefficient	
Voltage	±0.02%/°C, typical, of rated output voltage
Current	±0.03%/°C, typical, of rated output current
Stability	±0.05%, typical, of rated output voltage or current, over 8 hrs at fixed line, load, and temperature, after 30 min warm-up
Output Voltage Ripple/Noise	Refer to Ripple/Noise specifications in tables of Section 1.2.3.
Load Transient Response	1 ms, typical, to recover within 0.75% of rated output voltage for load step change of 50% of rated output current
Output Voltage Rise Time (with rated load, resistive; current rise time same)	10 ms, maximum, from 10-90% of programming change from zero to rated output voltage for 10V-30V models; 100 ms, maximum, from 5-95% of programming change from zero to rated output voltage for 40V-1000V models; contact factory for values of specific models

Parameter	Specification
Output Voltage Fall Time (with rated load, resistive; current fall time same)	10 ms, maximum, from 90-10% of programming change from rated output voltage to zero for 10V-30V models; contact factory for values of specific models
Output Voltage Fall Time (with no load)	50 ms, maximum, from 90-10% of programming change from rated output voltage to zero for 10V-30V models; 1.5 s, typical, from 100% to 10% of programming change from rated output voltage to zero for 40V-1000V models; contact factory for values of specific models
Front Panel Meter	
Display Resolution	4 digit
Voltage Accuracy (to actual output)	±(0.15% of rated output voltage + 0.1% of actual output + 1 digit) for 10V-30V models; ±(0.1%, maximum, of rated output voltage + 1 digit) for 40V-1000V models
Current Accuracy (to actual output)	±(0.4%, maximum, of rated output voltage + 1 digit)
Front Panel Programming	
Voltage	±(0.1% of rated output voltage + 0.1% of actual output voltage) for 10V-30V models; ±0.1%, maximum, of rated output voltage for 40V-1000V models
Current	±(0.4% of rated output current + 0.1% of actual output current) for 10V-30V models; ±0.4%, maximum, of rated output current for 40V-1000V models
Overvoltage Protection (OVP)	±1%, maximum, of rated output voltage
Remote Sensing	
Connection	Voltage accuracy/regulation specifications apply at the point where the remote sense leads are connected.
Line Drop	1 V, maximum per line for 10V-20V models; 1.5 V, maximum per line for 30V model; 5%, maximum of rated output voltage per line for models, 40V to less than 160V; 2%, maximum of rated output voltage per line for models greater than or equal to 160V; greater level of line drop is allowed, but output voltage regulation specifications no longer apply.
Line Drop Effect on Output Voltage	Rated output voltage applies at the rear panel output terminals, and line drop voltage subtracts from the voltage available at the load terminals
Remote Analog Interface	
Programming Accuracy	
Voltage	±0.25%, maximum, of rated output voltage for 0-5 VDC range, and ±0.5%, maximum, for 0-10 VDC range
Current	±1.0%, maximum, of rated output current for 0-5 VDC range, and ±1.2%, maximum, for 0-10 VDC range for 10V-30V models;

Parameter	Specification
	±0.8%, maximum, of rated output current for 0-5 VDC range, and ±1.0%, maximum, for 0-10 VDC range for 40V-1000V models
Overvoltage Protection (OVP)	±1%, maximum, of rated output voltage
Readback Monitor Accuracy	
Voltage (of actual output value)	±0.5%, maximum, of rated output voltage
Current (of actual output value)	±1%, maximum, of rated output current
Resistive-Control Programming	
Voltage	0–5 kΩ for 0-100% of rated output voltage
Current	0–5 kΩ for 0-100% of rated output current
Voltage-Control Programming	
Voltage	0–5 VDC or 0–10 VDC for 0-100% of rated output voltage
Current	0–5 VDC or 0–10 VDC for 0-100% of rated output current
Overvoltage Protection (OVP)	0.25–5.5 VDC for 5-110% or rated output voltage
Remote Control/Monitor Interface	On/Off control via contact closure, 6-120 VDC or 12-240 VAC, and TTL or CMOS gate; output voltage and current monitors; output voltage, current, and OVP programming; summary fault status
Output Isolation	
Output Float Voltage	
Negative Output Terminal	±300 V(PK), maximum, with respect to chassis ground; exceeding the limit will be detected as a fault by a protective supervisory monitor and shutdown of the output will be executed; this condition will be latched, requiring reset to resume normal operation.
Isolation of optional Isolated Analog Interface (J1) to output negative terminal	1000 V(PK), maximum; Isolated Analog Interface (J1 signals) are galvanically isolated from negative output terminal; operation of Isolated Analog Interface signals should be at SELV safety voltage conditions to chassis ground.
Reference of standard Non-Isolated Analog Interface (J1) to output negative terminal	The standard Non-Isolated Analog Interface (J1 signals) is connected to the negative output terminal and, therefore, is not isolated from the output.
Parallel Operation	
Parallel Group	Up to 5 units, of the same voltage rating, may be connected in parallel for additional output current; specifications apply as for single unit, with the exception that each additional paralleled unit will add 0.3% to the output current accuracy. Contact factory for applications requiring paralleling more than five units.
Series Operation	
Series Group	Up to 2 units, of the same current rating, may be connected in series for additional output voltage; see restrictions in Output Isolation section.

1.2.3 SGI Series Voltage and Current Specifications

The following tables present the specifications for rated voltage and current, and ripple/noise for the 10V-1000V models.

Rated Voltage, VDC	Rated Current, ADC						Ripple/ Noise** RMS, mV	Ripple/ Noise* PK–PK, mV
	4 kW	5 kW	8 kW	10 kW	12 kW	15 kW		
0-10††	0-400	N/A	0-800	N/A	0-1200	N/A	20	50
0-15††	0-267	N/A	0-534	N/A	0-801	N/A	20	50
0-20††	N/A	0-250	N/A	0-500	N/A	0-750	20	60
0-30††	N/A	0-167	N/A	0-334	N/A	0-501	20	60

Rated Voltage, VDC	Rated Current, ADC						Ripple/ Noise** RMS, mV	Ripple/ Noise* PK–PK, mV
	5 kW	10 kW	15 kW	20 kW	25 kW	30 kW		
0-40	0-125	0-250	0-375	0-500†	0-625†	0-750†	20	75
0-50	0-100	0-200	0-300	0-400†	0-500†	0-600†	20	75
0-60	0-83	0-167	0-250	0-333	0-417	0-500	20	75
0-80	0-63	0-125	0-188	0-250	0-313	0-375	20	100
0-100	0-50	0-100	0-150	0-200	0-250	0-300	20	100
0-160	0-31	0-63	0-94	0-125	0-156	0-188	25	150
0-200	0-25	0-50	0-75	0-100	0-125	0-150	25	175
0-250	0-20	0-40	0-60	0-80	0-100	0-120	30	200
0-300	0-17	0-33	0-50	0-67	0-83	0-100	30	200
0-330	0-15	0-30	0-45	0-61	0-76	0-91	30	200
0-400	0-12	0-25	0-38	0-50	0-63A	0-75	30	300
0-500	0-10	0-20	0-30	0-40	0-50	0-60	50	350
0-600	0-8	0-17	0-25	0-33	0-42	0-50	60	350
0-800	0-6.2	0-12.5	0-18.7	0-25†	0-31.2†	0-37.5†	80	500
0-1000	0-5	0-10	0-15	0-20†	0-25†	0-30†	100	650

* PK-PK ripple/noise, over 20 Hz to 20 MHz bandwidth, is measured across a 1 µF capacitor at the end of a 6' load cable with the supply operating at full load and nominal AC line voltage.

** RMS ripple/noise, over 20 Hz to 300 kHz bandwidth, is measured directly across the output terminals with the supply operating at full load and nominal AC input line voltage.

† Power level not available in 6U models, but could be produced with paralleled 3U units; up to 75 kW could be produced by paralleling up to five units. Paralleling will increase ripple/noise.

†† Models from 10V-30V are not available in 6U chassis.

1.2.4 Physical Characteristics

Dimensions	3U Models, 10V-30V	3U Models, 40V-1000V	6U Models, 60V-600V
Width	19.00 in (48.26 cm)	19.00 in (48.26 cm)	19.00 in (48.26 cm)
Depth	From inner surface of front panel to maximum protrusion of protective covers at rear panel; refer to installation drawings for chassis dimensions.		
	28.09 in (71.35 cm)	25.46 in (64.67 cm)	27.18 in (69.04 cm)
Height	5.25 in (13.34 cm)	5.25 in (13.34 cm)	10.5 in (26.67 cm)
Weight (nominal)	≤ 65 lb (29 kg), (4 kW, 10V, 15V) ≤ 65 lb (29 kg), (5 kW, 20V, 30V) ≤ 85 lb (39 kg), (8 kW, 10V, 15V) ≤ 85 lb (39 kg), (10 kW, 20V, 30V) ≤ 110 lb (50 kg), (12 kW, 10V, 15V) ≤ 110 lb (50 kg), (15 kW, 20V, 30V)	≤ 60 lb (27 kg), (5 kW) ≤ 75 lb (34 kg), (10 kW) ≤ 90 lb (41 kg), (15 kW)	≤ 140 lb (63 kg), (20 KW) ≤ 155 lb (70 kg), (25 kW) ≤ 170 lb (77 kg), (30 kW)
Shipping Weight	Contact factory for weights of specific models		

WCL488 Series Water Cooled Electronic Loads

Operation & Programming Manual

TDI-Dynaload® Division

Document Number 402828 — Revision B1

WCL488 Master 12KW

WCL488 Master

Series Specifications

OPERATION

Constant Current:	0 to selected full scale current
Prog. Accuracy:	±0.5% of selected full scale
Regulation:	±0.5% of selected full scale
Resolution:	1/4000 of selected full scale
Constant Resistance:	Constant Resistance mode operates in Amps/Volt, or entered in ohms
Prog. Accuracy:	±3% of selected full scale
Regulation:	±1% of selected full scale
Resolution:	1/4000 of selected full scale
Constant Voltage:	0 to selected selected full scale
Prog. Accuracy:	±0.5% of selected full scale
Regulation:	±0.2% of selected full scale
Resolution:	1/4000 of selected full scale
Constant Power:	0 to full scale power
Prog. Accuracy:	±3% of full scale
Regulation:	±3% of full scale
Resolution(IEEE):	0.25% of full scale power

ANALOG MODE

Ext. Prog:	0 to 10 Volts input yields 0 to selected full scale loading in all operating modes.
Input Impedance:	330k Ohms
Prog. Response:	Limited by internal adjustable slew rate limiter

PULSE MODE

Frequency:	0.06Hz to 3.33kHz
Accuracy:	0.1%
Duty Cycle:	0 - 100%(IEEE)
Accuracy:	0.1%
Adjustable Slew Rate:	
Max:	0 to full scale in 50µS
Min:	0 to full scale in 10mS

OUTPUT SIGNALS

Current Sample Output:	
Scaling:	10 Volts = selected full scale
Accuracy:	±0.5% of selected full scale
Sync Output:	
Timing:	Synchronous with pulse generator.
Output:	Sink with 10k pull up to +15V

PROGRAMMABLE PROTECTION

Current Limit:	
Range:	0 - 105% of selected full scale
Resolution:	0.5% of selected full scale
Voltage Limit:	
Range:	0 - 105% of selected full scale
Resolution:	0.5% of selected full scale
Power Limit:	
Range:	0 - 105% of full scale
Resolution:	50 Watts
Thermal:	Load disconnect at internal temperature of 70°C
Undervoltage:	Load inhibited at less than 0.5 Volt, when enabled

IEEE-488 READBACKS

Current:	
Resolution:	1/4000 of Selected Full Scale
Accuracy(Range):	±0.5% ±1 Digit
Voltage:	
Resolution:	1/4000 of Selected Full Scale
Accuracy(Range):	±0.5% ±1Digit
Power:	
Resolution:	3 Watts
Accuracy:	0.50%

MISCELLANEOUS

AC Input:	User Selectable 120VAC, 240VAC, ±10%, 48 - 62 Hz @ 350W Other voltages available. Consult Factory
Ambient Temp:	0°C to 40°C

WCL488 MASTER 12KW / WCS SLAVE 12KW

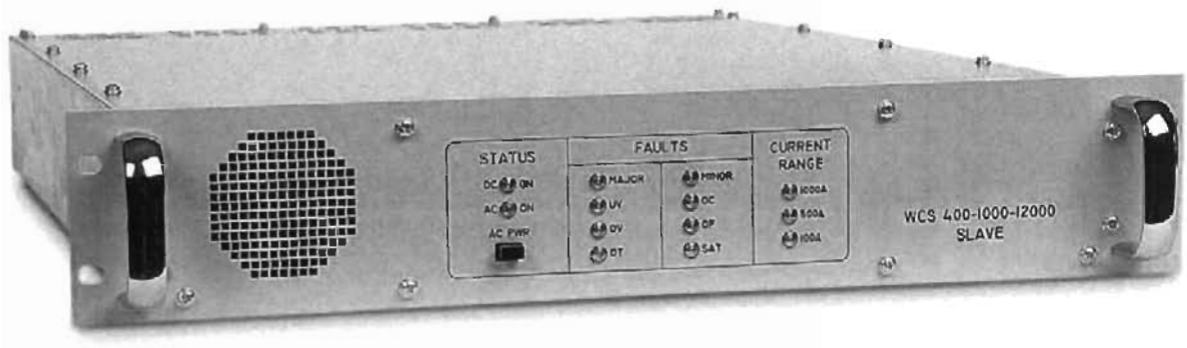

WCS Slave

UNIT SPECIFICATIONS

WCL488 50-1200-12000 (master) WCS 50-1200-1200 (slave)

OPERATING RANGES (FULL SCALES)
Voltage: 10 Volts, 20 Volts, 50 Volts
Current: 120 Amps, 600 Amps, 1200 Amps
Power: 12000 Watts
Short Circuit: 0.0002 Ohms max.
CONSTANT RESISTANCE RANGES
High Ohms Mode:

Range:	100A	500A	1000A
10V	0-5 A/V	0-25 A/V	0-50 A/V
20V	0-2.5 A/V	0-12.5 A/V	0-25 A/V
50V	0-1.0 A/V	0-5.0 A/V	0-10 A/V

Low Ohms Mode:

Range:	100A	500A	1000A
10V	0-50 A/V	0-250 A/V	0-500 A/V
20V	0-25 A/V	0-125 A/V	0-250 A/V
50V	0-10 A/V	0-20 A/V	0-100 A/V

METER RESOLUTION

	100A	500A	1000A
Ammeter:	10mA	100mA	100mA
	10V	20V	50V
Voltmeter:	10mV	100mV	100mV

Wattmeter: 1 Watt up to 9,999 Watts
(Autoranging) 100 Watts above 10,000 Watts
MECHANICAL - MASTER UNIT
Size: 19"W x 5.25"H x 24"D
483mm W x 133mm H x 610mm D
Rack Mountable
Weight: 55 lbs. / 24.95kg
MECHANICAL - SLAVE UNIT
Size: 19"W x 3.50"H x 24"D
483mm W x 89mmH x 610mm D
Rack Mountable
Weight: 55 lbs. / 24.95kg
INPUT CHARACTERISTICS: See chart (pg.5)

WCL488 100-1000-12000 (master) WCS 100-1000-1200 (slave)

OPERATING RANGES (FULL SCALES)
Voltage: 10 Volts, 50 Volts, 100 Volts
Current: 100 Amps, 500 Amps, 1000 Amps
Power: 12000 Watts
Short Circuit: 0.001 Ohms max.
CONSTANT RESISTANCE RANGES
High Ohms Mode:

Range:	100A	500A	1000A
10V	0-5 A/V	0-25 A/V	0-50 A/V
50V	0-1 A/V	0-5 A/V	0-10 A/V
100V	0-.5 A/V	0-2.5 A/V	0-5 A/V

Low Ohms Mode:

Range:	100A	500A	1000A
10V	0-50 A/V	0-250 A/V	0-500 A/V
50V	0-10 A/V	0-50 A/V	0-100 A/V
100V	0-5 A/V	0-25 A/V	0-50 A/V

METER RESOLUTION

	100A	500A	1000A
Ammeter:	10mA	100mA	100mA
	10V	50V	100V
Voltmeter:	10mV	100mV	100mV

Wattmeter: 1 Watt up to 9,999 Watts
(Autoranging) 10 Watts above 10,000 Watts
MECHANICAL - MASTER UNIT
Size: 19"W x 5.25"H x 24"D
483mm W x 133mm H x 610mm D
Rack Mountable
Weight: 55 lbs. / 24.95kg
MECHANICAL - SLAVE UNIT
Size: 19"W x 3.50"H x 24"D
483mm W x 89mm H x 610mm D
Rack Mountable
Weight: 55 lbs. / 24.95kg
INPUT CHARACTERISTICS: See chart (pg.5)

WCL488 400-1000-12000 (master) WCS 400-1000-12000 (slave)

OPERATING RANGES (FULL SCALES)
Voltage: 20 Volts, 200 Volts, 400 Volts
Current: 100 Amps, 500 Amps, 1000 Amps
Power: 12000 Watts
Short Circuit: 0.003 Ohms max.
CONSTANT RESISTANCE RANGES
High Ohms Mode:

Range:	100A	500A	1000A
20V	0-2.5 A/V	0-12.5 A/V	0-25 A/V
200V	0-.25 A/V	0-1.25 A/V	0-2.5 A/V
400V	0-.125 A/V	0-.625 A/V	0-1.25 A/V

Low Ohms Mode:

Range:	100A	500A	1000A
20V	0-25 A/V	0-125 A/V	0-250 A/V
200V	0-2.5 A/V	0-12.5 A/V	0-25 A/V
400V	0-1.25 A/V	0-6.25 A/V	0-12.5 A/V

METER RESOLUTION

	100A	500A	1000A
Ammeter:	10mA	100mA	100mA
	20V	200V	400V
Voltmeter:	10mV	100mV	100mV

Wattmeter: 1 Watt up to 9,999 Watts
(Autoranging) 10 Watts above 10,000 Watts
MECHANICAL - MASTER UNIT
Size: 19"W x 5.25"H x 24"D
483mm W x 133mm H x 610mm D
Rack Mountable
Weight: 55 lbs. / 24.95kg
MECHANICAL - SLAVE UNIT
Size: 19"W x 3.50"H x 24"D
483mm W x 89mm H x 610mm D
Rack Mountable
Weight: 55 lbs. / 24.95kg
INPUT CHARACTERISTICS: See chart (pg.5)

WCL488 Input Characteristics

WCL488 50-1200-12000
(Low Voltage Operation)

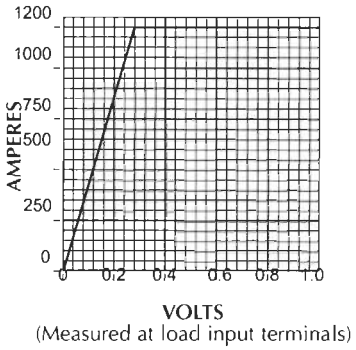

VOLTS
(Measured at load input terminals)

WCL488 100-1000-12000
(Low Voltage Operation)

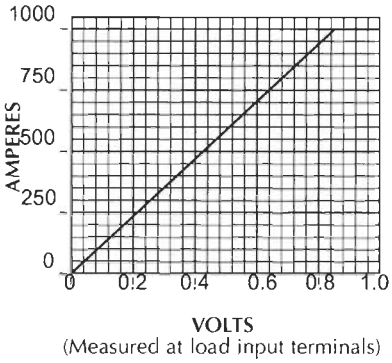

VOLTS
(Measured at load input terminals)

WCL488 400-1000-12000
(Low Voltage Operation)

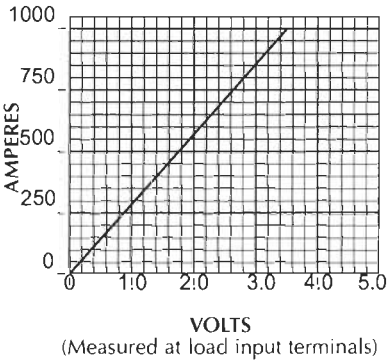

VOLTS
(Measured at load input terminals)

WCL488 Master Outline

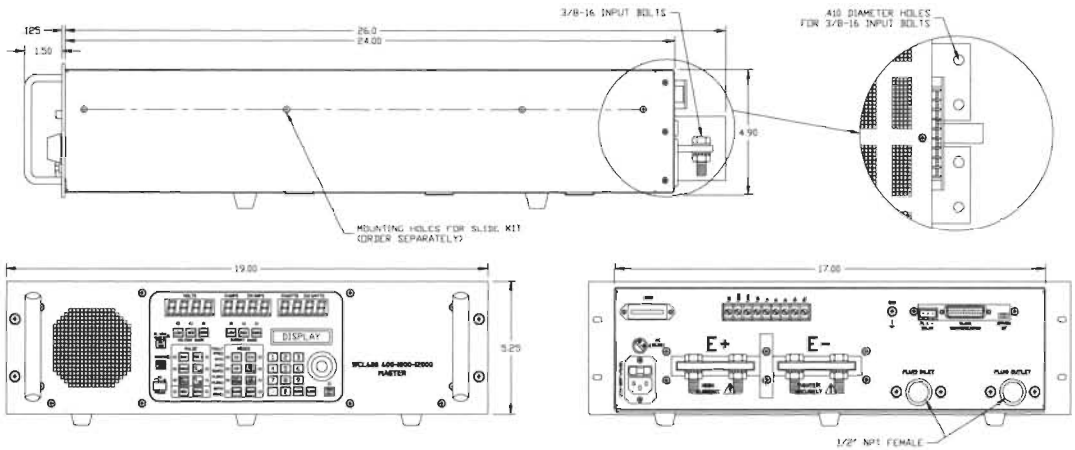

WCS Slave Outline

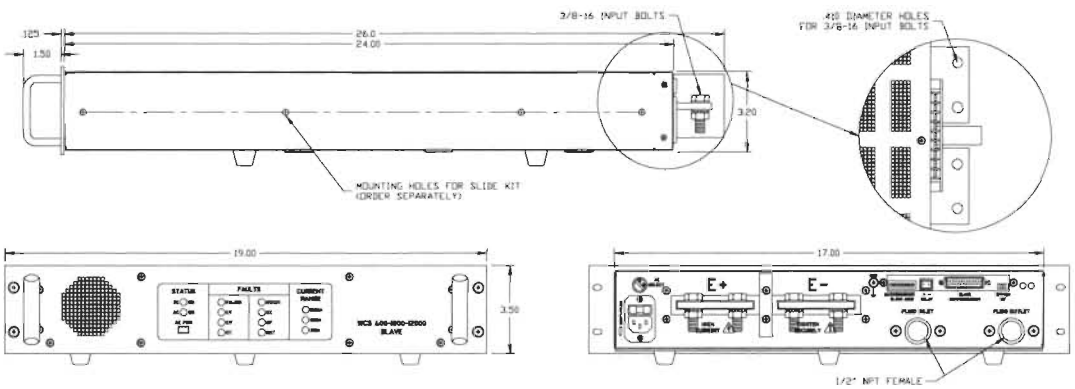

DEVICE SPECIFICATIONS

NI 6323

X Series Data Acquisition: 250 kS/s, 32 AI, 48 DIO, 4 AO

The following specifications are typical at 25 °C, unless otherwise noted. For more information about the NI 6323, refer to the *X Series User Manual* available at *ni.com/manuals*.

Analog Input

Number of channels	16 differential or 32 single ended
ADC resolution	16 bits
DNL	No missing codes guaranteed
INL	Refer to the *AI Absolute Accuracy* section.
Sample rate	
Single channel maximum	250 kS/s
Multichannel maximum (aggregate)	250 kS/s
Minimum	No minimum
Timing resolution	10 ns
Timing accuracy	50 ppm of sample rate
Input coupling	DC
Input range	±0.2 V, ±1 V, ±5 V, ±10 V
Maximum working voltage for analog inputs (signal + common mode)	±11 V of AI GND
CMRR (DC to 60 Hz)	100 dB
Input impedance	
Device on	
AI+ to AI GND	>10 GΩ in parallel with 100 pF
AI- to AI GND	>10 GΩ in parallel with 100 pF

NATIONAL INSTRUMENTS

Device off	
AI+ to AI GND	1,200 Ω
AI- to AI GND	1,200 Ω
Input bias current	±100 pA
Crosstalk (at 100 kHz)	
Adjacent channels	-75 dB
Non-adjacent channels	-90 dB
Small signal bandwidth (-3 dB)	700 kHz
Input FIFO size	4,095 samples
Scan list memory	4,095 entries
Data transfers	DMA (scatter-gather), programmed I/O
Overvoltage protection for all analog input and sense channels	
Device on	±25 V for up to two AI pins
Device off	±15 V for up to two AI pins
Input current during overvoltage condition	±20 mA max/AI pin

Settling Time for Multichannel Measurements

Accuracy, full-scale step, all ranges	
±90 ppm of step (±6 LSB)	4 µs convert interval
±30 ppm of step (±2 LSB)	5 µs convert interval
±15 ppm of step (±1 LSB)	7 µs convert interval

Analog Output

Number of channels	4
DAC resolution	16 bits
DNL	±1 LSB
Monotonicity	16 bit guaranteed
Maximum update rate	
1 channel	900 kS/s
2 channels	840 kS/s per channel
3 channels	775 kS/s per channel
4 channels	719 kS/s per channel
Timing accuracy	50 ppm of sample rate
Timing resolution	10 ns
Output range	±10 V
Output coupling	DC
Output impedance	0.2 Ω
Output current drive	±5 mA
Overdrive protection	±15 V
Overdrive current	15 mA
Power-on state	±20 mV
Power-on/off glitch	2 V for 500 ms
Output FIFO size	8,191 samples shared among channels used
Data transfers	DMA (scatter-gather), programmed I/O
AO waveform modes	Non-periodic waveform, periodic waveform regeneration mode from onboard FIFO, periodic waveform regeneration from host buffer including dynamic update
Settling time, full-scale step, 15 ppm (1 LSB)	6 µs
Slew rate	15 V/µs
Glitch energy	
Magnitude	100 mV
Duration	2.6 µs

Device Pinout

Figure 6. NI PCIe-6323 Pinout

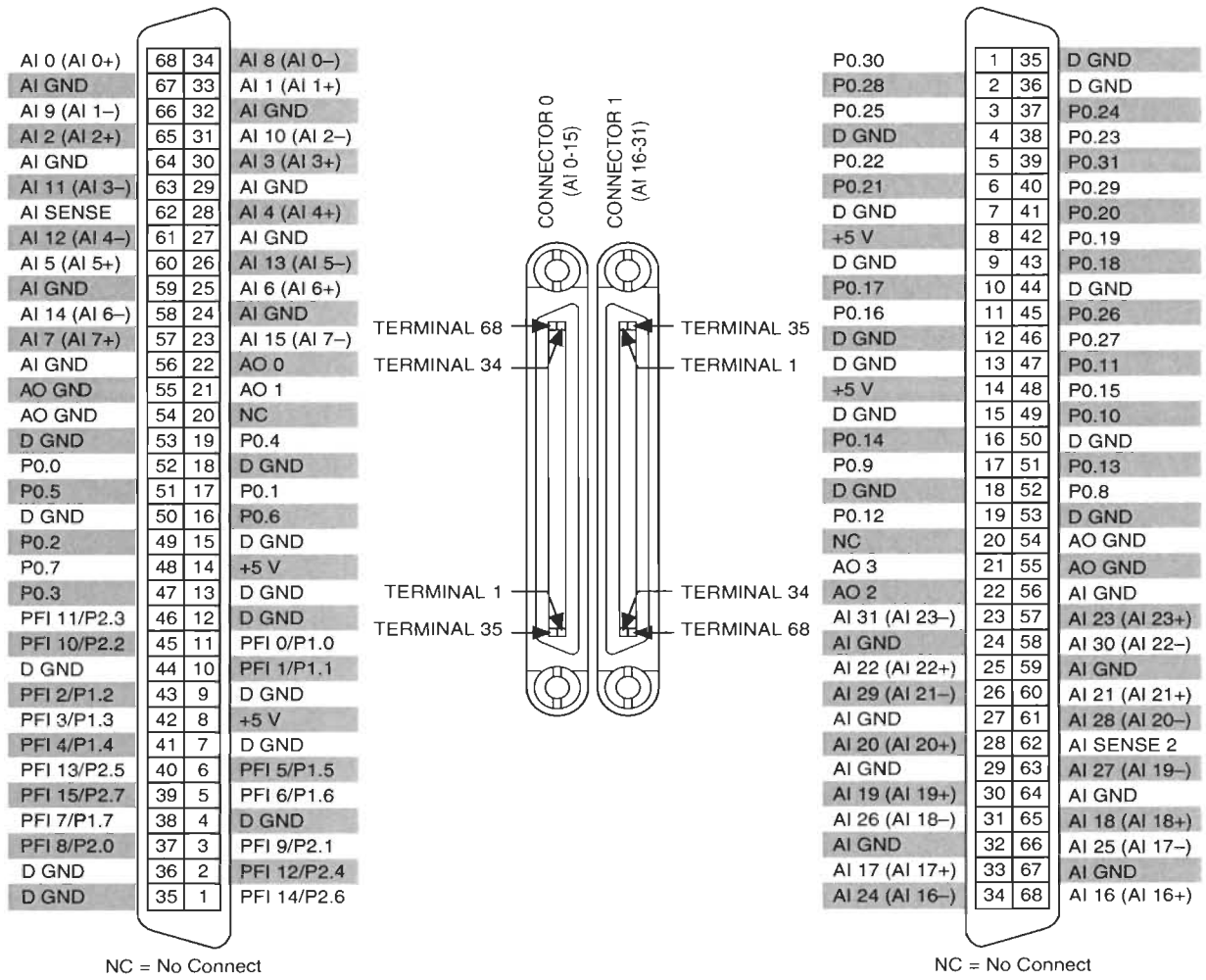

Futura -40°C

Low Temp Chest Freezers

Our **FUTURA PLUS+ Series** low temperature manual defrost chest freezers are designed for applications in the standard research and clinical market requiring more rigorous temperature control and construction features.

LABL-5-CT45

Standard Product Features:

- Manual defrost
- 5.0, 9.0 & 13.0 cu. ft. capacities
- -40°C, -43°C & -45°C temperature ranges
- Digital control with two temperature displays. One display shows the set temperature, the other shows the actual temperature in the freezer.
- Battery operated alarm system will emit an audible and visual signal when there is a mechanical or electrical failure. The alarm has an over and under temperature setting, alarm silencing switch, and battery test switch.
- Single-stage type refrigeration system with hermetic motor compressor
- Four heavy duty, swivel casters allow for convenient mobility
- White interior and exterior with hinged solid door
- 115V operation
- ETL electrical approved
- Warranties: 1 year parts and 90 days labor

Optional Features:

- Chart recorder
- Alarm relay contacts

LABL-13-CT40

LABRepCo

One Company • Many Solutions

101 Witmer Road, Suite 700 Horsham, PA 19044 / www.labrepco.com / (800) 521-0754 / sales@labrepco.com

Specifications and Ordering Information:

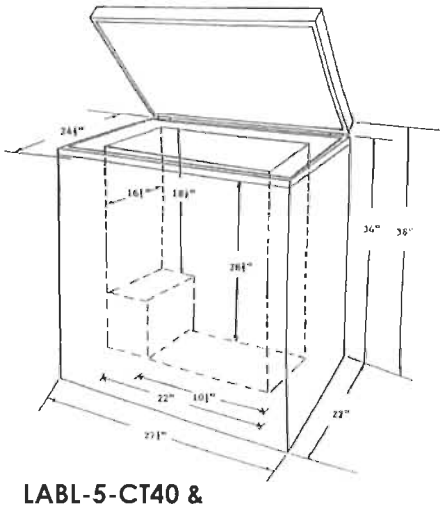

LABL-5-CT40 &
LABL-5-CT45

Models	*LABL-5-CT40*	*LABL-5-CT45*	*LABL-9-CT43*	*LABL-13-CT40*
Overall Height in.	39	39	38 1/2	38 1/2
Overall Width in.	28 1/2	28 1/2	42	43
Overall Depth in.	22	22	24 1/2	31
Interior Height in.	27 1/2	27 1/2	28 1/2	28 1/2
Interior Width in.	23	23	36	37 1/2
Interior Depth in.	15	15	16 1/2	22
Interior cu. ft.	5.0	5.0	9.0	13.0
Number of Casters	4	4	4	4
Temperature	0° to -40°C	0° to -45°C	0° to -43°C	0° to -40°C
Voltage	115V, 1PH, 60Hz	115V, 1PH, 60Hz	115V, 1PH, 60Hz	115V, 1PH, 60Hz

Specifications subject to change without notice.

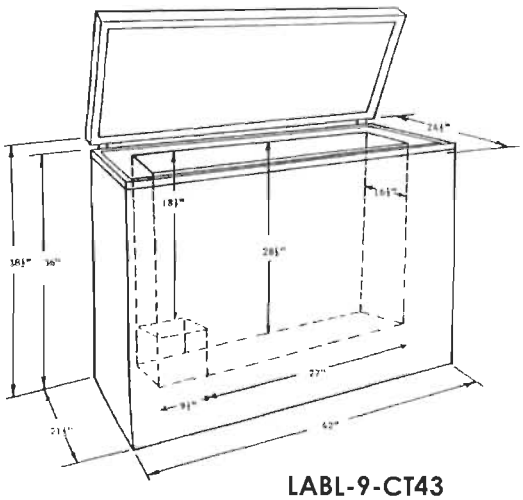

LABL-9-CT43

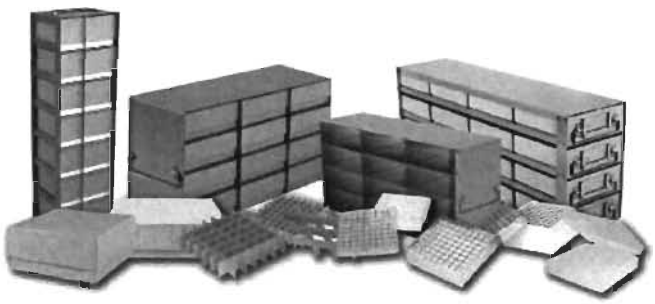

Maximize Freezer Space
Please visit labrepco.com or speak with your local representative for inventory rack information.

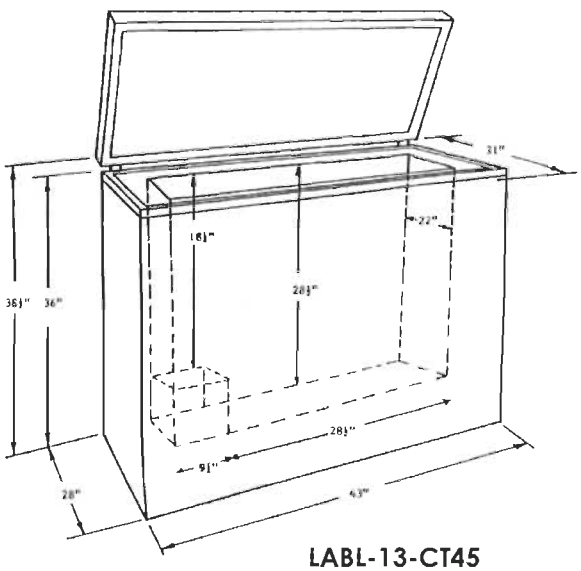

LABL-13-CT45

LABRepCo
One Company • Many Solutions
Revision Date: 10/3/2013

Efficient Internal Resistance and Specific Heat Identification of Li-ion Battery at Low Temperature Conditions

D. Herrera Vega*‡, S. Kelouwani†‡, L. Boulon*‡
*Department of Electrical and Computer Engineering
†Department of Mechanical Engineering
‡Institut de Recherche sur l'Hydrogène
Université du Québec à Trois-Rivières
3351 boul. des Forges, C.P. 500, Québec G9A 5H7, Canada.
E-mail: loic.boulon@uqtr.ca - sousso.kelouwani@uqtr.ca

***Abstract*—The operating temperature has a significant impact on the performance of electrochemical systems such as batteries. The amount of energy stored inside depends largely on the temperature (especially under 0°C). To maintain a good energy performance of the electric vehicle, it is necessary to know the parameters that characterize the battery to allow a better approximation of the amount of remaining energy in the battery. This document presents an approximated battery model and shows the effect of the low temperature on the parameters of the battery. The objective of this document is to show a simple method to identify the internal resistance and the specific heat of the battery by measuring the open circuit voltage through time, this will allow to know how to manage the energy of the battery that is required to perform the cold start of an electric vehicle.**

***Index Terms*—Battery, Batteries, Electric Vehicles, Lithium batteries, Resistance, Temperature.**

I. Introduction

Electric vehicles (EVs) use electric motors to obtain propulsion and there are three main different types of EVs: First, there are Hybrid Electric Vehicles (HEVs) that have both an internal combustion engine (ICE) and an electric motor for propulsion, which can be configured in series, parallel or both series/parallel. In this vehicles the battery is recharged by conversion of breaking energy; Second, there are Plug-in Hybrid Electric Vehicles (PHEVs) that are like the HEVs but the only difference is that the battery is rechargeable by external power sources; and Third, Battery Electric Vehicles (BEVs) that have only electric propulsion and a rechargeable battery pack [1].

The location of HEVs and BEVs in transport systems for geographic areas where the winter season is very long and very cold (Quebec's weather for example, TABLE I), requires the development of solutions reliable and effective for the cold start and for reducing the risk of irreversible damage.

There are different types of batteries for the EVs and among them exist the Lead-acid batteries, Ni-Cd batteries, Ni-Mh batteries and Lithium-ion batteries. This last one is the most recent used technology, and so, it is interesting to study how it behaves at different temperature conditions. When the lowest temperature is reached (-40°C), the battery performance falls down rapidly. Thus, autonomy and dynamic performances of vehicles are greatly diminished [3]–[5]. It is important to master the problem of cold start of the battery in freezing conditions because, as it will be shown in further sections, the effect of the cold on the battery will generate a bigger voltage drop when current is requested from the battery. In real applications, car manufacturers like Honda or Toyota take preventive measures by implementing mechanisms to assist in starting through auxiliary heating system to minimize degradation of the battery [6], [7].

TABLE I
1981 TO 2010 CANADIAN TEMPERATURES, TROIS RIVIERES, QUEBEC [2]

	Jan	Feb	Mar	Apr	May	Jun	Jul	Aug	Sep	Oct	Nov	Dec
Daily Average (°C)	-12.1	-9.7	-3.6	4.8	12.3	17.6	20	18.9	14.2	7.4	0.5	-7.4
Extreme Minimum (°C)	-44.4	-38.6	-36	-17.2	-6.1	-1.5	3.5	1.1	-7.2	-10.6	-29.6	-35.6

Indeed, exposure of the battery to temperatures below zero degrees for a considerable period of time without operation will cause that the internal temperature of the battery gets down slowly or quickly depending on the characteristics of thermal insulation layers implanted on it [8]–[10].

Besides the thermal insulation, there exists different methods to heat up the batteries while they are exposed to cold weather conditions. In previews work has been proved that convective heating requires the least heating time, while mutual pulse heating can consume the least battery capacity. Mutual pulse heating has the additional advantage of uniform internal heating and is free of convective heat transfer system [11].

The literature tells us that Lithium-ion battery performance characteristics are sensitive to the cell operating temperature. The recoverable power and capacity can be reduced significantly when these batteries are operated or stored at low temperatures [3]. Those low temperatures also lead to increase

978-1-4673-7637-2/15/$31.00 ©2015 IEEE

This document was made with LaTeX using document class "report.cls" and it was modified to comply with UQTR memory document requirements and standards.

report.cls:

"Copyright 1993-2014

The LaTeX3 Project and any individual authors listed elsewhere in this file.

This file was generated from file(s) of the LaTeX base system.

It may be distributed and/or modified under the conditions of the LaTeX Project Public License, either version 1.3c of this license or (at your option) any later version. The latest version of this license is in http://www.latex-project.org/lppl.txt and version 1.3c or later is part of all distributions of LaTeX version 2005/12/01 or later."